

Alma Mater Studiorum - Università degli Studi di Bologna

**DOTTORATO DI RICERCA IN
SCIENZE FARMACEUTICHE**

Ciclo XXII

Settore scientifico disciplinare di afferenza: **CHIM/06**

**PROGRESS IN THE CHARACTERIZATION
OF SUPRAMOLECULAR SYSTEMS
BY EPR SPECTROSCOPY**

Presentata da: Dott.ssa Elisabetta Mileo

**Coordinatore Dottorato
Prof. Maurizio Recanatini**

**Relatore
Prof. Marco Lucarini**

Esame finale anno 2010

SUMMARY

CHAPTER 1

SUPRAMOLECULAR CHEMISTRY

1.1	Introduction	5
1.2	Molecular recognition.....	6
1.3	Self-assembly.....	8
1.4	Self-assembly with covalent modification.....	12
1.5	Into the 21st century.....	12
1.6	Conclusion	15

CHAPTER 2

USE OF NITROXIDES RADICALS TO INVESTIGATE SUPRAMOLECULAR ASSEMBLIES

2.1	Introduction.....	16
2.2	Historical background.....	18
2.3	Dinamic aspects in Host- Guest interaction.....	21
2.4	Study of exchange of different solutes between micellar and water phase	30
2.5	Measuring the rate of distribution of organic substrate between cyclodextrins, micelles and water	32
2.6	References	39

CHAPTER 3
CUCURBITURIL HOSTS

3.1	Introduction.....	40
3.2	Cucurbit[n]urils (n=5, 7-10)	41
3.3	EPR studies of 2,2,6,6 tetramethyl piperidyl-N-oxyl (TEMPO)	49
3.4	EPR studies of 4-amino-2,2,6,6 tetramethyl piperidyl-N-oxyl (tempamine)	51
3.5	References.....	56

CHAPTER 4
PARAMAGNETIC SUPRAMOLECULAR ARCHITECTURES
DERIVED FROM GUANOSINE

4.1	Introduction	57
4.2	Recent studies on the molecular self-assembly of lipophilic guanosine analogues	58
4.3	Lipophilic guanosine assemblies not templated by ions	60
4.4	Guanosine derivatives functionalised with open-shell units	61
4.5	Self-assembled hexadecanitroxide	66
4.6	References	71

CHAPTER 5

RESORCINARENE MOLECULAR CAPSULES

5.1	Introduction	73
5.2	Hexamer assembly in organic solvents	74
5.3	Probing the inner space of resorcinarene molecular capsules with nitroxide guest	75
5.4	NMR investigation on the interaction of nitroxides probes with resorcinarene molecular capsules	82
5.5	Experimental section	87
5.6	References	88

CHAPTER 1

SUPRAMOLECULAR CHEMISTRY

1.1 Introduction

Molecules that can recognize other molecules or ions, mixtures of molecules that can self-assemble into racks, rosettes or ribbons, molecular machinery, and molecules that can mimic life by self-replicating may sound like science fiction, but are actually examples of the progress made in the area of *supramolecular chemistry* in the last 30 years. Familiar molecules such as methane (CH₄) and carbon dioxide (CO₂) are made up of atoms joined together by strong chemical interactions called covalent bonds. Molecular chemistry is concerned with making and breaking covalent bonds to form new molecules. Supramolecular chemistry *is different* because it deals with synthetic molecular systems that are held together by weaker non-covalent interactions, such as electrostatic forces, hydrogen bonds, π - π stacking interactions, van der Waals forces, or hydrophobic effects. These non-covalent interactions taken individually are weak, but when several are used together, very stable molecular ensembles or complexes may result. Jean-Marie Lehn encapsulated these ideas succinctly when he described supramolecular chemistry as 'chemistry beyond the molecule'.

Early work concentrated on molecular recognition, which is the selective binding of a particular substrate (or **guest**) by a receptor molecule (or **host**) using non-covalent interactions. This can be achieved by the careful design and synthesis of the receptor molecule so that it is complementary to the desired guest. For example, a problem in environmental chemistry might be the removal of pollutant metal ions from a river. A supramolecular coordination chemist may be able to design a receptor that is complementary to the metal ion, i.e. its size and the position of its binding sites matches the binding requirements of the metal-ion guest. The receptor may then form a strong complex with the metal ion, removing it from the environment. Some interactions, such as hydrogen bonds and metal-ligand coordinate bonds, are directional. Chemists have learned how to use these interactions to 'programme' information

into molecular subunits so that they self-assemble into potentially useful supramolecular superstructures. This self-assembly process, when combined with traditional synthetic covalent modification, gives us access to new molecules (e.g. molecular knots and chains) that previously could not be made.

1.2 Molecular recognition

The birth of supramolecular chemistry can be traced back to the pioneering work of Charles Pedersen, an industrial chemist who worked for DuPont. Pedersen was interested in finding ways to prevent the oxidative degradation of petroleum products and rubber, which is caused by trace amounts of metal-ion impurities, such as copper and vanadium. To do this, he developed a series of compounds known as 'metal deactivators'. These molecules bind the metal ions, converting them into inactive complexes. The catalytic activity of the metal ions is therefore suppressed. In 1960, while attempting to synthesize one of these compounds, he isolated some white crystals in very low yield. His curiosity was piqued by the fibrous, silky quality of the crystals. Even more interestingly, they were soluble in alcohols when sodium cations were present but insoluble in their absence. Elemental analysis and mass spectrometry showed that the crystals were a cyclic polyether **1** (Figure 1.1a) that had formed due to the presence of a small amount of catechol (Figure 1.1b) impurity in his reaction mixture (Pedersen 1967). Pedersen observed from a space filling model that a sodium ion is held in the cavity of this macrocycle by attractive electrostatic ion-dipole interactions between the cation and the six oxygen atoms in the polyether ring. This binding mode accounted for the interesting solubility properties of the compound. It was later found that the metal ion acts as a template during the formation of the macrocycle by causing the reactants to wrap around it and orienting them in a favourable way to form the 18-membered ring, **1**. Because the model of compound **1** looked like a crown, Pedersen called this class of compound the 'crown ethers'. This particular compound was named dibenzo- [18]crown-6. The [18] refers to the number of atoms in the macrocycle and 6 to the number of oxygen atoms in the ring. This is much easier to remember than the systematic name of compound **1** which is 2,3,11,12-dibenzo-1,4,7,10,13,16-hexaoxacyclooctadecane. Many different sizes of crown ether have now been synthesized and coordination studies have shown that a relationship exists between the cavity size, cationic

radius and stability of the resulting complex. In short, the better the fit of the cation into the crown, the stronger the complex formed. This phenomenon is referred to as optimal spatial fit. Although Pedersen's discovery was serendipitous (Pedersen 1988), it demonstrated that selectivity could be introduced into synthetic receptors by making them complementary to the desired guest. In 1969, improving on the cation binding ability of the crown ethers, Lehn and his co-workers at the Universite Louis Pasteur in Strasbourg reported a new class of 'three-dimensional' cation receptors called cryptands (Dietrich et al. 1969, 1973a, b). These materials are cage-like bicyclic molecules that contain three polyether strands strung between two nitrogen bridgehead atoms (Figure 1.1g). The cryptands have been found to complex group 1 and 2 metal cations with stability constants much higher than those of analogous crown ethers. For example, in methanol, [2.2.2] cryptand (**5**) is selective for potassium cations (with a diameter of 2.66 Å), binding them with a stability constant ($\log K$) of 10.4, which is over four orders of magnitude higher than [18]crown-6. The crystal structure of this complex is shown in Figure 1.1h. By changing the length and number of oxygen atoms in each polyether strand, Lehn found that he could tune the receptor to be selective for smaller cations. For example, [2.1.1] cryptand (**3**) is selective for lithium cations (with a diameter of 1.36 Å) and [2.2.1] cryptand (**4**) is selective for sodium (with a diameter of 1.94 Å). Both the crown ethers and the cryptands require some degree of rearrangement in order to form a complex with a metal cation. Recognizing this, Donald Cram reasoned that rigid receptors with binding sites fixed in an octahedral arrangement around an enforced cavity would show enhanced binding over flexible receptors. With the help of molecular models, he designed a new class of receptor, the spherands, that contains an enforced spherical cavity (compound **6** in figure 1.1i). Spherands bind sodium and lithium cations very strongly (compound **6** forms complexes with sodium with a stability constant $K=1.2 \times 10^{14} \text{ M}^{-1}$ in chloroform-*d* saturated with water). Cram formalized these observations with the principle of preorganization, which states 'the more highly hosts and guests are organized for binding and low solvation prior to their complexation, the more stable will be their complexes' (Cram 1988).

The pioneering work of Pedersen (1988), Lehn (1988) and Cram (1988) ignited interest in supramolecular chemistry and was recognized with the award of the 1987 Nobel prize for

chemistry. Since then, the field of molecular recognition has grown with the development of receptors for a wide range of cationic, anionic and neutral guests as well as for more complex biomolecules.

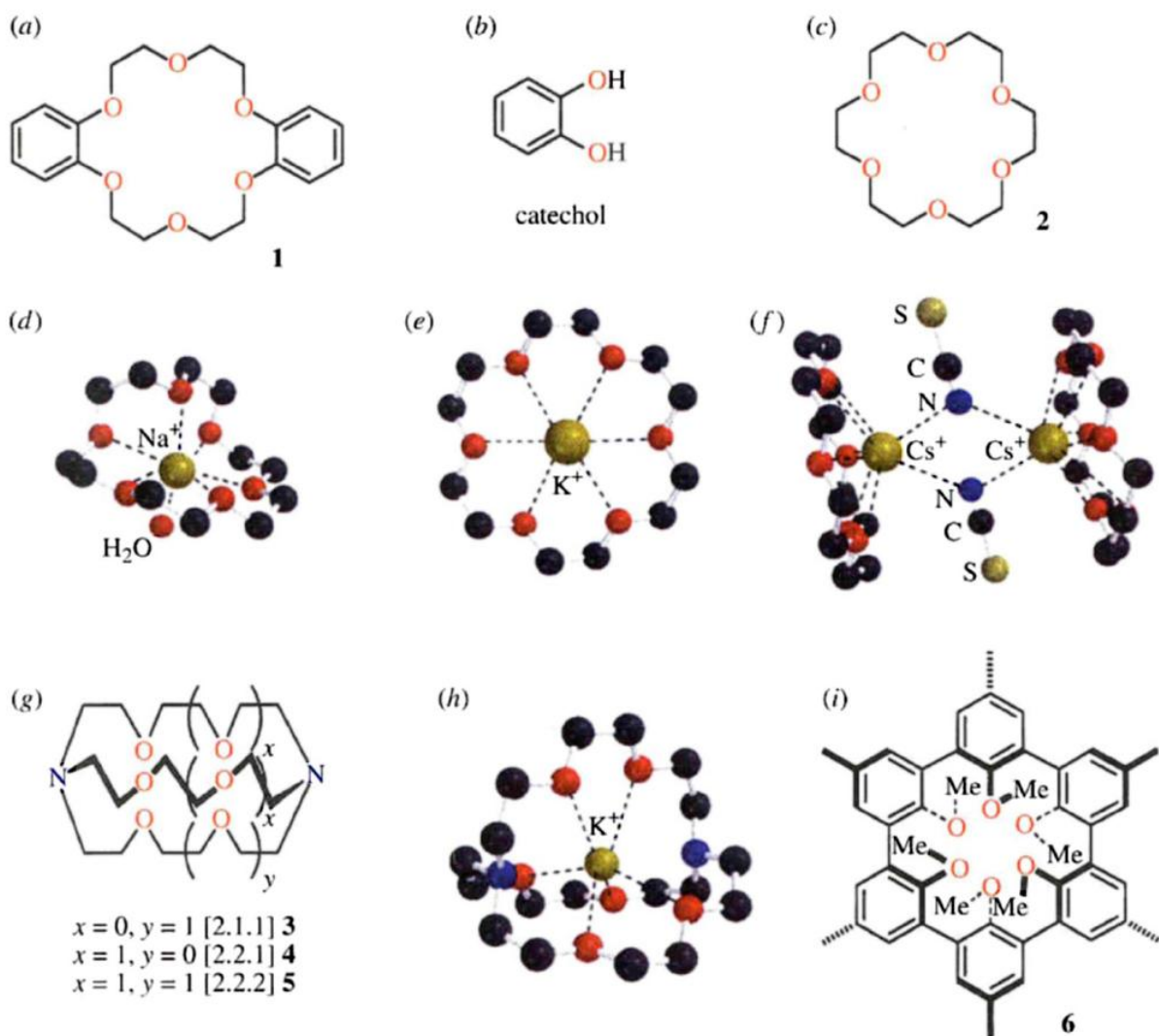


Figure 1.1: The chemical structures of the cation binding agents (a) dibenzo[18]crown-6 **1** and (b) 18-crown-6 **2**, with the crystal structures of the sodium (c), potassium (d) and caesium (e) cation complexes of [18]crown-6. The chemical structure of [2.1.1], [2.2.1] and [2.2.2]cryptands (**3**, **4** and **5**, respectively) is shown in (f) with the crystal structure of the potassium complex of [2.2.2] crypt and (g), and (h) spherand **6**. Cations are yellow, oxygen is red and nitrogen is blue.

1.3 Self-assembly

The formation of the DNA double helix from two complementary deoxyribonucleic acid strands is a particularly striking example of self-assembling biological systems. The

thermodynamically stable double helical structure forms spontaneously and reversibly as the strands are mixed together under the right conditions and hydrogen bonds form between complementary base pairs. The rapid reversibility of the process ensures that any errors that may have occurred during assembly can be corrected. Chemists can use self-assembly to access new non-covalently linked molecular architectures by combining appropriately designed yet simple subunits. These molecular components contain within them the information required to construct the self-assembled architecture in terms of the position and directionality of their binding sites, the distribution of electron density over their surfaces, or their oxidation states. This information is accessed when the components are mixed together and 'read out' as the self-assembled structure. Hydrogen bonds have been used to direct the assembly of many different types of non-covalently linked molecular architectures. One early example is the formation of a 'rosette-like' insoluble complex **14** between melamine and cyanuric acid discovered by Whitesides and co-workers (Mathias et al. 1994).

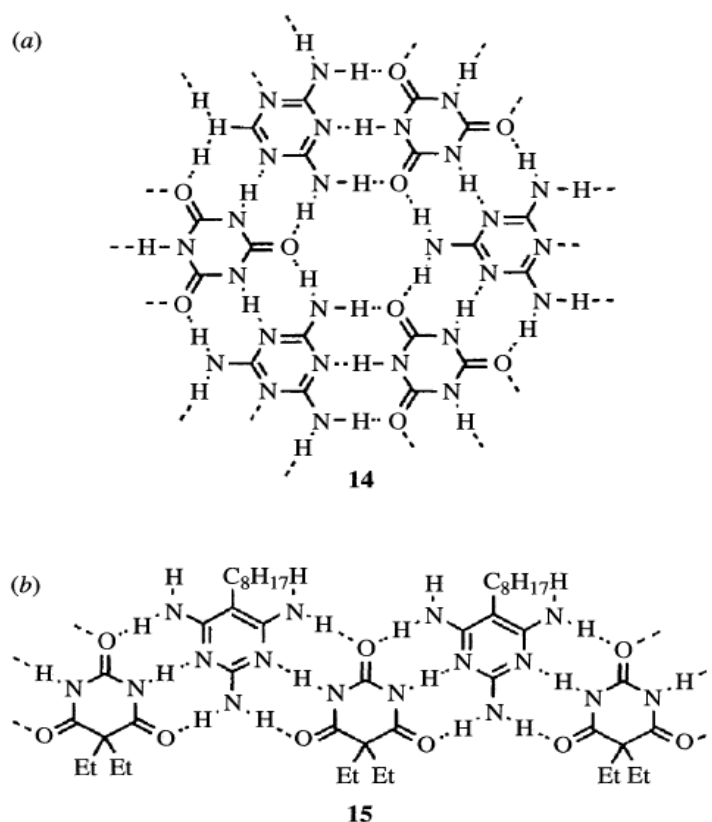


Figure 1.2: Melamine and cyanuric acid form an insoluble 'rosette-like' complex **14** (a), whereas sterically hindered analogues form a molecular ribbon **15** (b).

Melamine can be regarded as having three faces, each of which can donate two hydrogen bonds from the amine groups and accept one from the aromatic nitrogen atom. In contrast, cyanuric acid can accept two hydrogen bonds and donate one from each of its 'faces'. When mixed together, the two compounds form an insoluble hexagonal network resembling a rosette, as shown in Figure 1.2*a*. Lehn and co-workers adapted this hydrogen-bonding motif by blocking one face of each of the subunits with alkyl chains (Lehn et al. 1990). Steric interactions cause these compounds to form a linear molecular ribbon **15**, which is a non-covalently linked polymer (Figure 1.2*b*).

Self-assembled molecular arrays that contain large interior cavities have the potential to bind large guest species or act as 'molecular reaction vessels' in which reactions may be catalysed by increasing the effective concentration of the reactants. The molecular subunits required to construct these cavities need not be complex. Indeed, MacGillivray & Atwood (1997) have shown that six molecules of commercially available (and easy to make) C-methylcalix[4]resorcinarene (**16**) self-assemble with eight water molecules to form a chiral spherical molecular assembly held together by 60 hydrogen bonds (**17**). This remarkable structure contains an internal cavity of ca. 1375 Å³ (a side view of the capsule is shown in Figure 1.3).

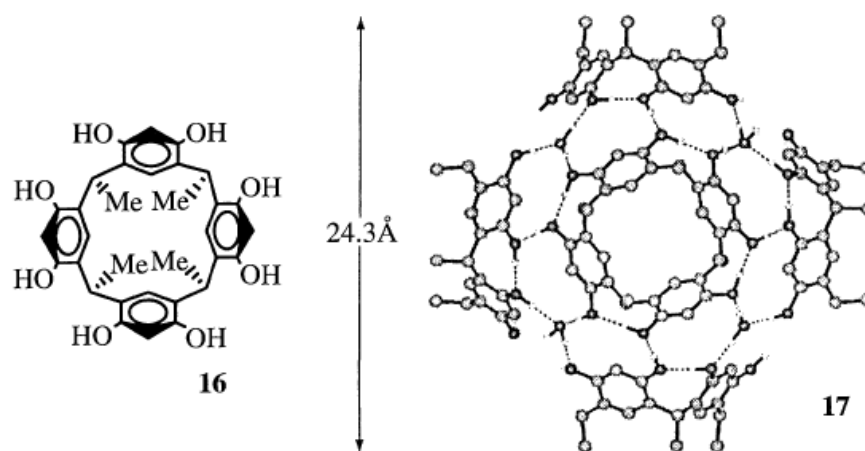


Figure 1.3: The cross-sectional view of the self-assembled capsule **17** showing part of the hydrogen-bond network that holds this complex together.

The chirality of this assembly arises from the complex network of hydrogen bonds holding it together. Molecular-modelling studies suggest that **17** is large enough to encapsulate

coordination compounds (ML-octahedra) or fullerenes. Nuclear magnetic resonance experiments in benzene- d_6 suggest that the cage structure persists in solution. This introduces the exciting possibility of using these C-methylcalix[4]resorcinarene cages as chiral catalysts.

In cell membranes, proteins such as gramicidin A form channels that allow the passage of protons and alkali metal cations across the lipid bilayer. They do this by forming a β -helix (this type of helix contains a central channel) in which amide (N-H) groups from the peptide backbone alternatively point up and down, forming hydrogen bonds with amide carbonyl oxygen atoms. Two gramicidin A helices, assembled in a head-to-head arrangement, are required to span the membrane. A supramolecular approach to the formation of synthetic ion channels has been pioneered by Ghadiri and his research group at the Scripps Research Institute in California (Hartgerink et al. 1998). These researchers use cyclic β -peptides and cyclic D,L- α -peptides to form self-assembled peptide nanotubes. The cyclic peptides adopt conformations wherein the peptide NH and CO bonds point up and down in a similar fashion to the hydrogen bonds of the gramicidin A helix. This allows the formation of multiple hydrogen bonds between cyclic peptides and drives the formation of the peptide nanotube. The opening and closing of this channel can be monitored using conductance techniques, which reveal sharp opening and closing corresponding to either conformational changes in the assembly or to a dynamic assembly-disassembly processes occurring in the membrane. Larger versions of these channels have been shown to transport bigger molecules, such as glucose, across membranes (Granja & Ghadiri 1994).

Transition metals can also be used to direct the assembly of non-covalently linked molecular ensembles. Although metal-ligand bonds are not non-covalent interactions, they are commonly used by supramolecular chemists because, although they are thermodynamically strong interactions, they have varying degrees of lability. This means that the bonds may persist for a long time or may be short lived, continuously breaking and remaking in a reversible, dynamic process. This reversibility allows a type of 'error checking' in the assembly process that will consistently lead to the thermodynamically most stable assembly. Additionally, due to ligand field effects, transition-metal ions often have very specific coordination geometry requirements, which afford very precise control of the structure of the molecular assembly. By

changing the oxidation state of the transition metal in an assembly, it may be possible to alter its preferred coordination geometry and so electrochemically switch the assembly between two different states.

1.4 Self-assembly with covalent modification

When a strategy of self-assembly is used in concert with covalent modifications, previously inaccessible molecular topologies may be obtained. Stoddart and co-workers have employed electron-rich and electron-poor aromatic components that self-assemble primarily via a charge-transfer interaction to produce a wide variety of self-assembled structures, including catenanes (molecular chains). This work stemmed from Stoddart's discovery that bisparaphenylene[34]crown-10 (an electron-rich crown ether) will bind the positively charged and electron-poor paraquat dication to form the charge-transfer complex **20** (Figure 1.4a). Catenanes can be synthesized from precursors similar to this complex. One example, the [5]catenane **21** ([5] designates the number of interlocked rings) is shown in Figure 1.4b. This compound is called 'Olympiadane' because of its similarity to the five interlinked Olympic rings (Amabilino et al. 1994, 1998).

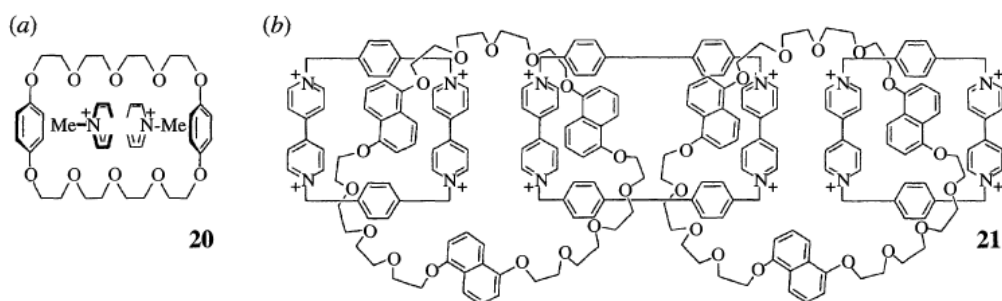


Figure 1.4: (a) A paraquat dication threaded through a bisparaphenylene-[34]crown-8 forming a charge transfer complex **20**; and (b) the chemical structure of the [5]catenane, olympiadane **21**.

Perhaps the most ambitious chemical goal that has been reached so far, using self-assembly techniques, is the synthesis of a molecular knot. Sauvage and his research team at the Universite Louis Pasteur, Strasbourg, are pioneers in this area of chemistry (Dietrich-Buchecker et al. 1994). Sauvage used a transition metal (in this case copper (I), an ion that prefers to adopt a tetrahedral coordination environment) to direct the assembly of a double

helical complex. Again, it should be emphasized that the synthesis of this remarkable material would be practically impossible without self-assembly strategies.

1.5 Into the 21st century

The future may hold for supramolecular assemblies new catalysts, self-replicating molecular systems, complexes that might be used for data storage, and even the creation of molecular motors. In the coming years, we can expect to see the use of custom-designed supramolecular catalysts that solve specific problems in mainstream organic synthesis. We have already seen that self-assembled structures can enhance the rate of a chemical reaction by increasing the effective concentration of the reactants. A more controlled approach to catalysis is to stabilize the transition state of the reaction product relative to the starting materials, which thus enhances the forward reaction rate (Sanders 1998). Sanders and co-workers have synthesized porphyrin trimer molecules that are capable of coordinating to pyridine-containing reactants via the porphyrin-bound zinc metal ions, and then catalysing the reaction between them.

The development of chemical systems that can self-replicate by catalysing their own formation may, in the future, provide us with insights into how our own ecosystem arose from the pre-biotic chemical soups on the early Earth (Rebek 1994). Self-replicating systems developed over the last few years have increased in complexity. In an important paper (Lee et al. 1996), Ghadiri and co-workers have shown that peptides can self-replicate. Unlike simple nucleic acid base pairing interactions that provide a clear basis for establishing complementary molecular recognition and, therefore, the transfer of genetic information, polypeptide-polypeptide interactions are much more complex. Nevertheless, these workers have shown that certain α -helical peptides are capable of self-replication and have, therefore, demonstrated that peptide self-replication may have been involved in the early evolution of life (Lee et al. 1997).

Lehn has suggested that spectacular complexes such his 3x3 molecular grid **32** may be used in the future for the storage of information. The grid self-assembles when six equivalents of the linear ligand **31**, which contains three binding sites, are mixed with nine silver (I) metal ions (Figure 1.5; see Baxter et al. (1994)). One could imagine that each metal ion corresponds to a 'bit' of information, with one oxidation state corresponding to a 1 and another to a 0. Such

arrays would allow the storage of very large amounts of information at the molecular level, in very small volumes of material.

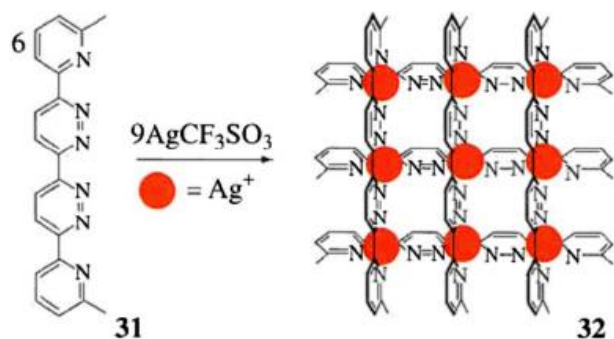


Figure 1.5: Six equivalents of compound **31** and nine silver (I) cations self-assemble to form a 3 x 3 molecular grid **32**.

Rotaxanes are composed of a macrocyclic ring through which an axle is threaded. The ends of the axle are blocked by bulky groups that prevent the macrocycle from slipping off. These systems also have potential uses for the storage of information. Sauvage and co-workers have produced the rotaxane **37** (Figure 1.6), which acts as an abacus-like molecular shuttle (Gavina & Sauvage 1997). The complex was produced using transition-metal-directed self-assembly to thread the macrocycle onto the axle with subsequent covalent modification of the axle by the introduction of blocking groups. The axle contains a 1,10-phenanthroline moiety containing two nitrogen atoms and a terpyridine group containing three nitrogen atoms. The macrocycle also contains a 1,10-phenanthroline group, and, in the presence of copper (I), the metal ion coordinates to both the phenanthroline groups (complex **37** in Figure 1.6). Copper (II) requires a higher number of coordinated groups than copper (I). When the copper ion is oxidized to +2 oxidation state, it jumps to the 3-coordinate terpyridine group, so increasing its coordination sphere to five, forming complex **38** (Figure 1.6). The position of the macrocycle is, therefore, dependent on the oxidation state of the copper ion. The synthesis of the molecular shuttle **37/38**, and others like it, may come to be viewed as the genesis of molecular machinery, i.e. the generation of molecular-sized devices such as gears, switches and motors built by chemical and supramolecular chemical techniques from the ground up (Chambron & Sauvage 1998; Sauvage 1998).

1.6 Conclusion

The supramolecular systems described illustrate the great creativity of the researchers involved in this interdisciplinary area of science. As supramolecular chemistry moves into the third millennium, we can look forward with great excitement to the development of new

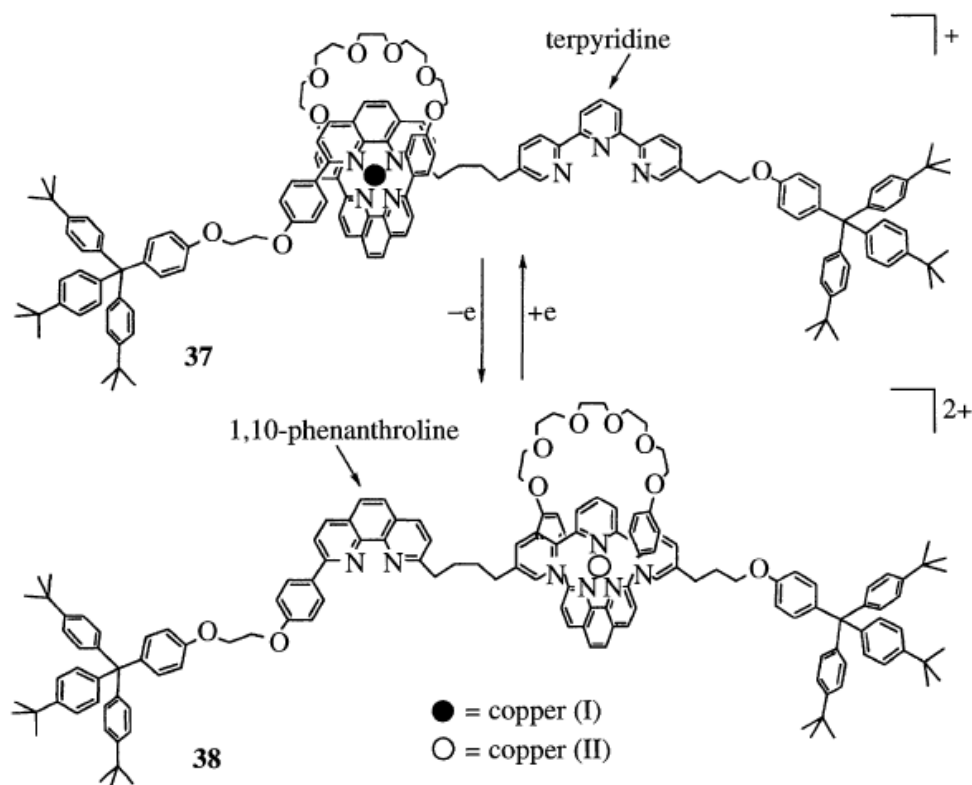


Figure 1.6: An electrochemically controlled molecular shuttle 37/38.

supramolecular drug delivery systems, pharmaceuticals, smart materials, molecular machinery and logic gates, and catalysts. There can be no doubt that more esoteric complexes, with uses that can now only be dreamt of in the pages of science fiction novels, will emerge in the coming years.

CHAPTER 2

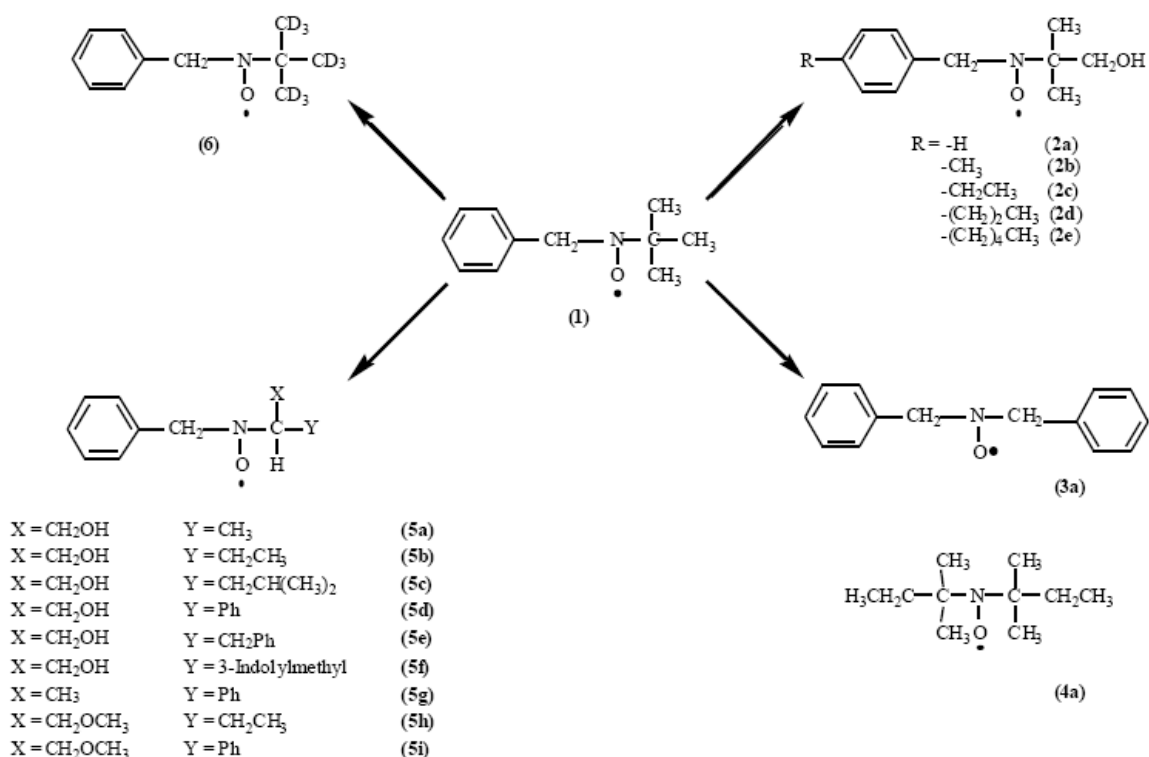
USE OF NITROXIDE RADICALS TO INVESTIGATE SUPRAMOLECULAR ENTITIES

2.1 *Introducción*

Supramolecular chemistry, broadly the chemistry of “multicomponent” molecular assemblies in which the structural units are typically held together by a variety of weak (non covalent) interactions, has developed rapidly over recent years¹. Supramolecular processes are also those occurring in the interaction between receptors and substrates. These are known as molecular recognition and are responsible for many basic principles of life as regulation, transport and catalysis. The weak interactions that hold together the *host-guest* complexes, include hydrogen bonding, π - π stacking, dipolar interactions, van der Waals and London dispersion forces. In water solution these enthalpic attractions are supplemented by hydrophobic forces, which give rise to desolvation of host and guest changing the organized solvent molecules into randomly oriented molecules. This randomization of solvent provides entropic driving forces for complexation, which partially compensate for the entropically expensive process of freezing out degrees of freedom of host and guest molecules². These thermodynamically unstable complexes are also kinetically labile; consequently only a few methods are suitable for measuring the kinetics of association and dissociation processes, which occur in the microsecond and submicrosecond time range³. One of the most useful tools for the study of supramolecular entities is represented by NMR spectroscopy; since, however, the equilibration between host and guest in solution is a dynamic process taking place at rates higher than the differences in the NMR frequencies, in most cases the experimental NMR spectra appeared as averages of those from the free and complexed species, allowing to obtain the only information on the equilibrium of association⁴. Actually, despite the large number of binding constant values reported in the literature, only few reports deal with the determination of the kinetics of complexation^{3,5}. On the other hand, when radicals are involved, EPR spectroscopy, being characterized by a shorter time scale, allows to detect different signals from the complexed and uncomplexed radicals: the radical used as guest shows an “environmental” sensitivity, with a subsequent change of the spectroscopic parameters upon complexation.

In our studies on inclusion phenomena of radical species in different host-systems⁶⁻¹¹, we have found benzyl *tert*-butyl nitroxide (**1**) to be a particularly suitable spin probe for studying both the equilibrium association constants and the rate constants for the association and dissociation processes of the complexes in aqueous solution. In order to extend the use of this technique to various supramolecular systems, we have recently designed, synthesized and tested the nitroxidic probes, shown in scheme 1.1, that are based on structural modification of **1**.

Benzyl *tert*-butyl nitroxide (**1**) is the parent of a large family derived to study the dynamic aspects in the host-guest interactions. In particular, with **1** we investigated host systems such as cyclodextrins⁶, calix[4]arenes⁷ and micelles⁸.



Scheme 2.1

Nitroxides **2a-2e** is a family of *para*-substituted benzyl hydroxyalkyl nitroxides particularly useful to investigate the exchange of different solutes between micellar phases⁸ or the ligand shell of protected gold nanoparticles⁹ and water.

Nitroxides, **3a-4a**, two symmetric compounds used to study cyclodextrin complexes with a stoichiometry other than 1:1¹⁰.

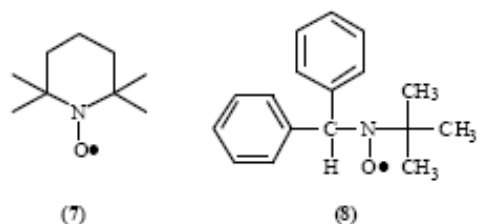
Nitroxides, **5a-5i**, a series of chiral benzyl nitroxides, which have been conveniently employed to study the factors governing the enantiodiscrimination by methylated cyclodextrins¹¹.

Nitroxide **6**, a deuterated probe, which shows a better separation of the component spectra due to the sharper EPR lines.

2.2 Historical background

The inclusion of nitroxide radicals by host systems (especially by cyclodextrins) has been studied from time to time by EPR spectroscopy during the last 30 years, but all reports have been concerned with very persistent species such as sterically-protected nitroxides¹². In particular, using 2,2,4,4-tetramethyl-oxazolidinyl-3-oxy radical¹³ as guests of β -cyclodextrin (β -CD), the free and included species show separated high field EPR lines.

The spectrum with the smaller nitrogen hyperfine splitting, a_N , was assigned to the complexed radical which resides in a less polar environment than pure water. On the other hand, by using a commonly employed nitroxide spin probe such as 2,2,6,6-Tetramethyl-1-piperidyloxy radical (TEMPO, **7**) no clear distinction between the free and included species can be observed as shown in



Scheme 2.2

Scheme 2, for studying complexation by CDs¹⁴.

The EPR spectrum of **8**, recorded in the presence of β -CD, showed three different signals, assigned to the radical in water and to the radical included in the cavity of the CD either from the phenyl side or from the *tert*-butyl side. It was also found that ENDOR spectroscopy is able to distinguish the diastereomers formed by the inclusion from the phenyl side of **8** by β -CD¹⁵. However, it must be emphasized that when using **8** as radical probe in the presence of host different from CDs, such as the calixarene **14**, the EPR spectrum of the included species is almost identical to that observed in water, except for a little broadening of the high field lines, as shown in Figure 2.1.

radical (TEMPO, **7**) no clear distinction between the free and included species can be observed as shown in Figure 2.1.

Kotake and Yanzen largely employed the diphenylmethyl *tert*-butyl nitroxide (**8**), shown in

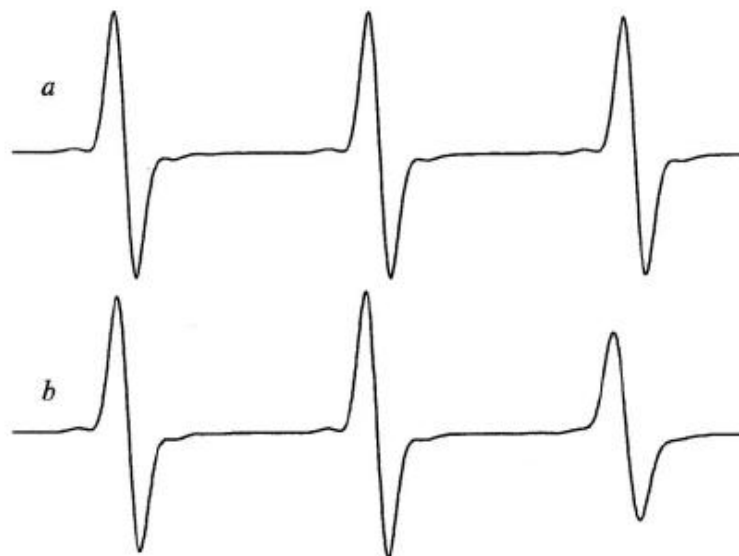
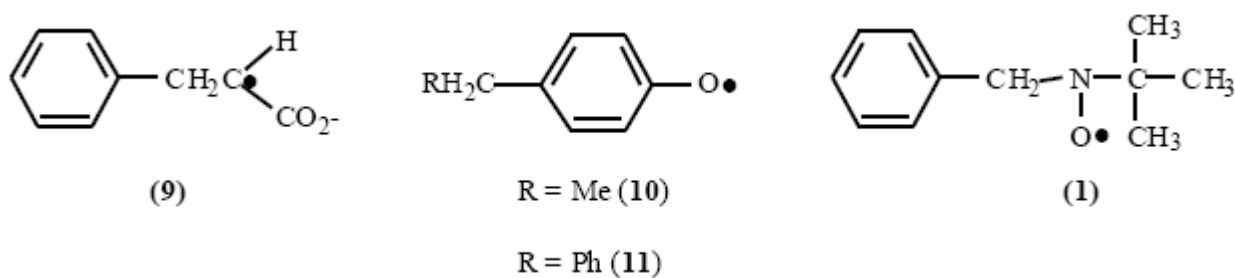


Figure 2.1: Experimental EPR spectra of TEMPO in water (a) and in the presence of β -CD= 3×10^{-3} M (b).

Recently, spin trapping in the presence of a cyclodextrin has also been investigated. Luo *et al.* reported the trapping of carbon centered radicals with nitroso compound stabilized by cyclodextrins¹⁶. Tordo and co-workers showed that when the trapping of superoxide with nitrones was carried out in the presence of β -cyclodextrin, inclusion complexes were formed between the resulting nitroxide spin adduct, and the cyclodextrin¹⁷. The inclusion of these spin adducts resulted in a dramatic increase of their half-life. Also molecular recognition of different host receptors, besides cyclodextrins, has been investigated by EPR spectroscopy. One of the few examples reported is concerned with the equilibrium complexation between TEMPO derivatives, employed as EPR probes, and water soluble cryptophane¹⁸, which was found slow in the EPR time scale. Jansen and co-workers extended the investigation by using α -substituted benzyl *tert*-butylnitroxide to find recognition ability of a water-soluble octamethoxy-*p*cyclophane¹⁹.

EPR spectroscopy has also been utilized to obtain useful information on the interaction of free radical species in micellar environments; both paramagnetic surfactants and radical solubilizates were examined²⁰. Recently, the intercalation of a series of stable β -phosphorylated cyclic aminoxy radicals with sodium dodecyl sulphate micelles has been studied²¹.

Lucarini's group interest in the use of EPR for studying supramolecular chemistry started in 1996 (in collaboration with Professor B. P. Roberts from the University of London)²² when trying to test whether transient radicals such as **9**, **10**, **11** (Scheme 2.3) would show significant conformational changes when included in modified CDs such as hydroxypropyl- β -CD (Hp- β -CD) and dimethyl β -CD (DM- β -CD).



Scheme 2.3

These radicals were generated in aqueous solution, using the flow technique²³, in which the solution passes through the microwave cavity about 60 milliseconds after mixing the reagents. In the presence of CDs, the spectra of all considered radicals showed additional signals, which were assigned to the species included in CD. In all cases by increasing the concentration of CD, the spectra of the included radicals became dominant, thus allowing an accurate determination of the spectral parameters of the radical inside the hydrophobic cavity of CD (see Table 2.1).

Radical	Host	<i>g</i> -factor	Hyperfine splitting ^a / G
9	None	2.0033	20.28 (1H _a), 23.08 (2H _b)
	Hp- β -CD ^b	2.0033	20.3 (1H _a), 26.2 (2H _b)
		2.0033	20.2 (1H _a), 27.9 (2H _b)
10	None	2.0044	10.33 (2H), 6.13 (2H _o), 1.39 (2H _m)
	Hp- β -CD	2.0045	9.7 (2H), 6.2 (2H _o), 1.5 (2H _m)
11	None	2.0044	9.71 (2H), 6.19 (2H _o), 1.47 (2H _m)
	Hp- β -CD	2.0045	10.3 (2H), 6.3 (2H _o), 1.6 (2H _m)

^a Nuclei indicated in parentheses; ± 0.05 for unbound radicals, ± 0.1 for included radicals.

^b The radical **9** is included bimodal into the Hp- β -CD cavity, although the detailed modes of inclusion remain to be established.

Table 2.1: EPR parameters for unbound and included short lived alkyl radicals **9-11** in aqueous media at 293 K.

Inspection of this table shows that the values of the benzyl proton splitting, $a_{2H\beta}$, of the included and free species are considerably different in all the examined cases. These data demonstrate that the inclusion leads to changes in the conformation adopted by the radical as

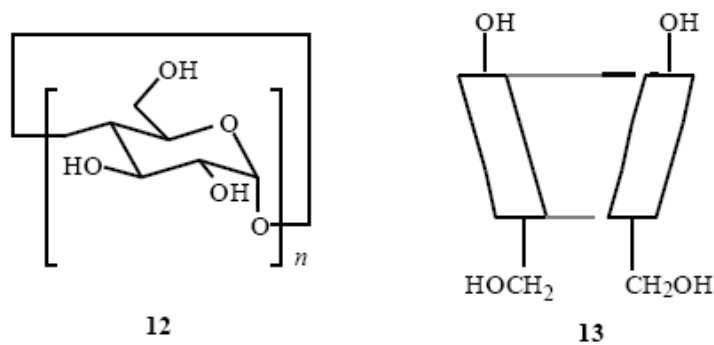
reflected by the change of the hyperfine splitting of the hydrogen β atoms to the radical center, whose magnitude depends on the conformation adopted by the radical, according to the Heller Mc-Connell relationship²⁴.

On the basis of the reported results, we looked for a more persistent radical in which a combination of polar and conformational effects might give rise to large differences in the resonance frequencies of the included and free species. A good candidate was benzyl *tert*-butylnitroxide (**1**); this, in the presence of different hosts, afforded easily including complexes as indicated by the moderate decrease of the nitrogen hyperfine splitting, a_N (due to the less polar environment of the host cavities), and from the strong change of the coupling to the benzyl protons, $a_{2H\beta}$ (due to conformational changes upon complexation). Moreover, inclusion created a significant difference in the resonance field of the wing lines of each β -proton triplet ($MI(H_\beta) = \pm 1$) of the included and free species with all kind of host systems so far investigated, and in many cases the EPR spectra of **1** showed a strong linewidth dependence on temperature, indicating that the lifetime, t , of formation and dissociation of the supramolecular complexes is in the range characteristic of the EPR spectroscopy. This favorable feature enabled us to measure, for the first time by EPR, the rate constants for the exchange process by analysing of the line shape variations. Finally, although benzyl *tert*butylnitroxide (**1**) had decayed faster than related sterically protected nitroxides, continuous flow was not necessary for its generation since steady-state concentrations large enough could be obtained for tens of minutes by oxidation of the parent amine.

2.3 *Dinamic aspects in Host-Guest interactions*

2.3.1 *The investigated Host Systems*

Among the very large number of known organic compounds, very few have a molecular cavity able to accommodate guest molecules; cyclodextrins being the most studied. α -, β - and γ -cyclodextrins (CDs) **12** are cyclic oligosaccharides made up of 6, 7, or 8 D-glucose units, respectively, bonded through α -(1-4)-linkages (see Scheme **4**). The oligosaccharide ring forms a torus, with primary OH groups of the glucose residues positioned at the narrower end of these



Scheme 2.4

tube-shaped molecules (see **13**), while the secondary glucopyranose OH groups are located around the wider opening. The chiral internal cavity of a CD is hydrophobic, while the external surface of the torus is hydrophilic. In aqueous solution, CDs form a broad range of complexes with guest molecules fitting, at least partially, into the hydrophobic cavity²⁵. For this reason, CDs are regarded as practical enzyme models and have found applications in the pharmaceutical science as well as in the area of separation science^{26,27}.

Nitroxide **1** and a family of related nitroxide were also used to investigate micellar solutions, *i.e.* media more similar to biological systems. For many years there has been a keen interest in the dynamics of micellar solutions that has been studied by stopped flow, pressure jump, and ultrasonic relaxation techniques²⁸. All of these techniques provided evidence for two distinct relaxation-times: a short one, characteristic of a process occurring on a time scale of microseconds and a longer one, of the order of milliseconds to seconds²⁸. The faster relaxation is attributed to an association-dissociation process involving the exchange of individual surfactant molecules between the micelles and the water phase, while the slower process is identified as the rearrangement of the system involving the creation and destruction of micelles²⁹. When the micelles contain hydrophobic solutes, another type of dynamic process becomes important, namely, the exchange of solute molecules between the micellar and the water phases^{28,30}. We studied the latter process by investigating the behavior of our spin probe in the presence of the anionic surfactant sodium dodecyl sulfate (SDS), the cationic surfactant hexadecyltrimethylammonium bromide (HTAB) and the non-ionic surfactant polyoxyethylene(6) decanol (C₁₀E₆)⁸.

2.3.2 Geometry analysis of the complexes

The EPR spectrum in water at 298 K of benzyl *tert*-butyl nitroxide (**1**), produced by reacting the magnesium salt of monoperoxyphthalic acid (5.0×10^{-4} M) with benzyl *tert*butylamine (5.0×10^{-4} M), has been shown in Figure 2.2. The spectrum can be straightforwardly interpreted on the basis of the coupling of the unpaired electron with the nitrogen atom and with the two benzyl protons whose hyperfine splitting constants have been reported in Table 2.2.

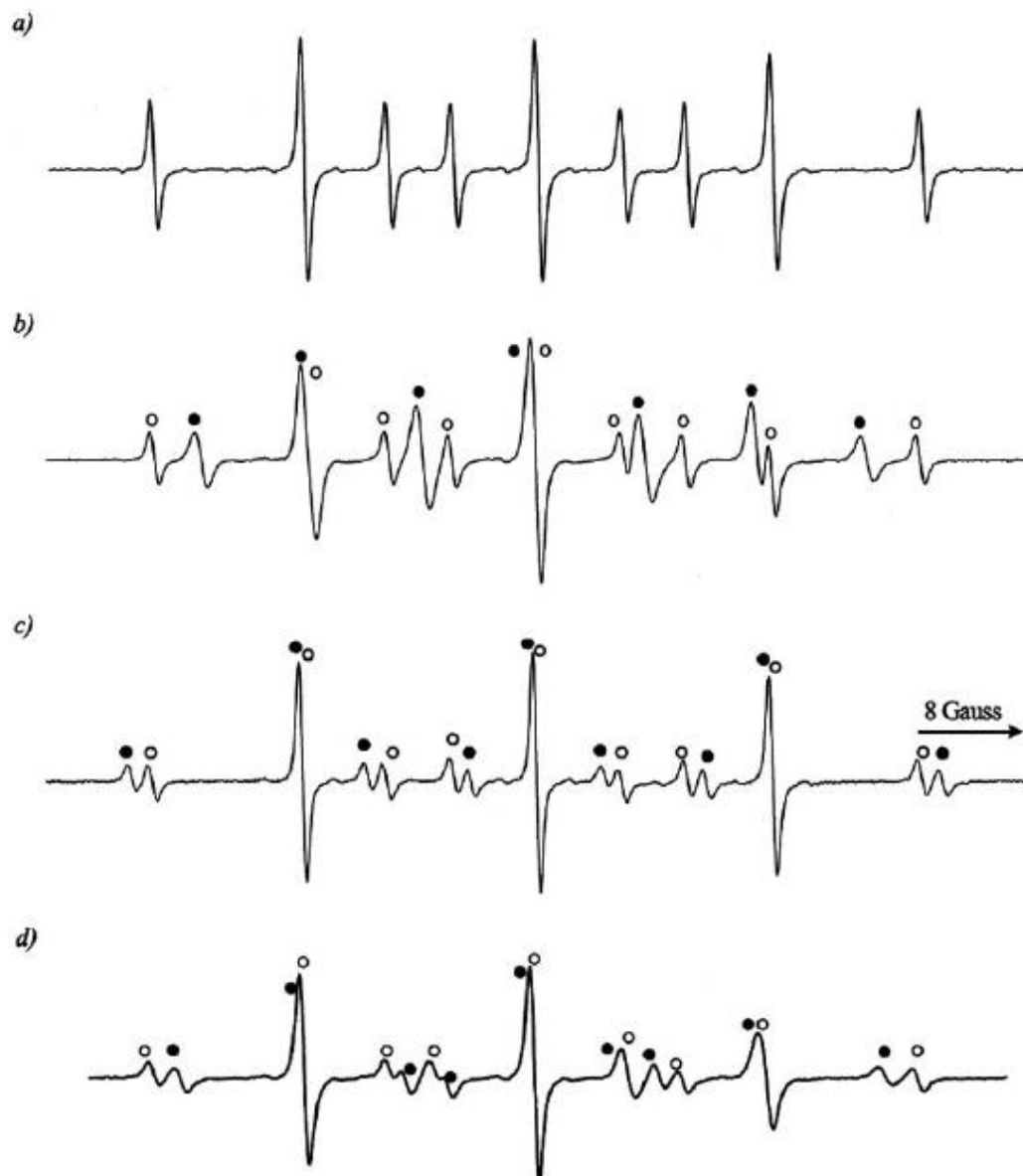
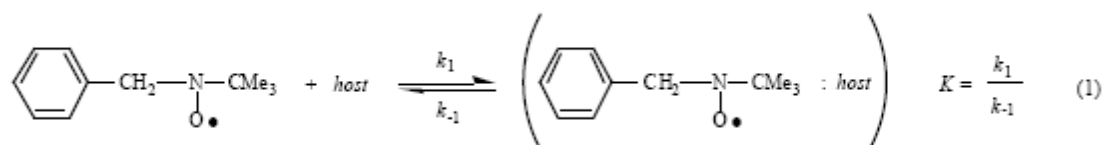


Figure 2.2: EPR spectra of radical **1** in water at 298 K (a), in the presence of β -CD 1.3×10^{-3} M (b), in the presence of calixarene **14** 5.2×10^{-2} M (c), in the presence of SDS 3.3×10^{-2} M (d). Empty (\circ) and full symbols (\bullet) indicate the lines of the free and included radicals, respectively.

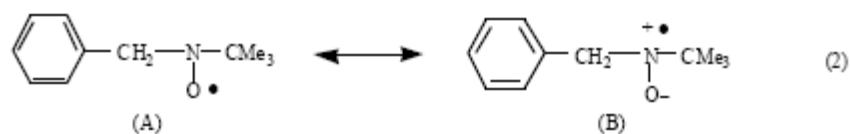
Host	$a(\text{N})/\text{G}$	$a(2\text{H}_\beta)/\text{G}$	$g\text{-factor}$	T/K
none	16.69	10.57	2.0056	298
α -CD	16.56	9.44	2.0058	298
β -CD	15.74	7.88	2.0058	298
γ -CD	15.97	8.02	2.0058	294
DM- β -CD	15.60	7.80	2.0058	298
TM- β -CD	15.70	8.27	2.0058	294
Calix[4]arene 14	16.86	12.11	2.0056	294
SDS	16.04	8.84	2.0057	300
HTAB	15.88	8.74	2.0057	300
C_{10}E_6	15.82	8.23	2.0057	300

Table 2.2: EPR parameters for nitroxide 1 included in different hosts in aqueous media.

In the presence of the investigated host systems the spectra showed additional signals [Figure (2b), (2c), (2d)] that were assigned to the radical included in the host in equilibrium with the free species [Eq. (1)]:



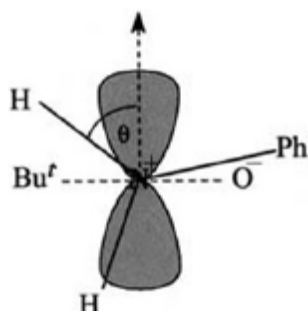
when the absolute concentration of the host was increased, the ratio between included and free nitroxide varied linearly until the spectrum of the complexed radical became dominant. The spectroscopic parameters for these latter species also have been reported in Table 2.2. As two main resonance structures can be derived for the nitroxide radical 1, see Eq. (2),



with the charged form, B, prevailing in polar solvents, so the magnitude of a_{N} , reflecting the spin density on the N-atom, is sensitive to the polar environment and provides information on the depth of inclusion. Actually the significantly smaller nitrogen hyperfine coupling found with β - and γ -CD with respect to water suggests that the N-O group is deeply included in the cavity of the CDs; this being consistent with the large internal diameter of β - and γ -CD (~ 6.6 and 8.4 \AA respectively). On the other hand, with α -CD (internal diameter $\sim 5.2 \text{ \AA}$) the very similar value of a_{N} observed for the free and bound nitroxides indicates that also in the included radical the N-O group is exposed to the bulk water ⁶.

A more detailed picture of the solution geometry of the host-guest complex can be obtained by measuring intermolecular nuclear Overhauser effects (NOE) by NMR spectroscopy, in the assumption that the geometry of the nitroxide-CD complex and the amine-CD complex is similar. We performed 2D NOESY spectra of benzyl *tert*-butyl amine, *i.e.*, the diamagnetic precursor of **1**. In the presence of *heptakis*-(2,6-O-dimethyl)- β -CD (DM- β -CD), which have been shown to behave similarly to the unmodified β -CD³¹, the aromatic protons gave rise to intense cross peak only with the methoxyl protons at 6' position, at the narrower end of the cavity. This demonstrates not only the full involvement of the molecule in the complexation but also the inter-proton distance between the aromatic protons and the protons of the 6-OMe group is very short. Thus, it was concluded that the complexation occurs with the phenyl ring embedded in the smaller rim of the cavity.

On dissolving the nitroxide probe **1** in a micellar phases³², a reduction of a_N was observed similarly to what had been reported in previous studies carried out with different nitroxide radicals. This effect has been attributed to a greater weight of the nitroxide mesomeric form (B, Eq. 2), in media of low polarity, in which the unpaired electron is rather located on the oxygen than on the nitrogen atom. The magnitude of $a_{2H\beta}$ provides information on the preferred conformations adopted by radical **1** in the various conditions. The hyperfine splitting constant of hydrogens in β -position of a radical center (the nitrogen atom in the present case) is



Scheme 2.5

determined both by the spin density ρ on the α -atom and the dihedral angle θ (see Scheme 2.5) between the symmetry axes of $2p_z$ orbital containing the unpaired electron and the N-C-H plane, via the well-known [24] Heller-Mc-Connell equation (Eq. 3):

$$a_{H\beta} = \rho_N (B_0 + B_2 \langle \cos^2 \theta \rangle) \quad (3)$$

Here B_0 is small and usually neglected and $\rho_N B_2$ can be obtained by the hydrogen splitting ($a_H = 14.33$ G) at the methyl protons in methyl *tert*-butyl nitroxide where $\langle \cos^2 \theta \rangle$ is 0.5 for symmetry reasons. The calculated values of θ indicate that the rotation about the C-N bond of the radical **1** is relatively free in water, is more hindered in the α -CD complex, and is strongly

hindered in the β - and γ -CD complexes. The fact that in the latter two cases the barrier to the internal rotation is higher than in the former two is consistent with a structure where the nitroxide is deeply included inside the cyclodextrin cavity.

The reduction of the β -proton splitting of **1** was also observed in the presence of a micellar phase. Differently to what occurs in the previously described case, this effect is due mainly to polarity changes rather than to conformational changes.

2.3.3 Kinetic and thermodynamic analysis for the inclusion reaction

Due to the remarkable differences in the resonance fields of the EPR lines of the complexed and free nitroxide **1**, the determination of their relative concentrations and therefore of the association constants, K_1 , could be done easily by simulating the EPR spectra. When the host concentration is in large excess with respect to that of the radical probe, quantitative information on host-radical guest equilibrium can easily be obtained by using the following equation:

$$K_1 = \frac{x_{host}}{x_{water} \cdot [host]_0} \quad (4)$$

where $[host]_0$ denotes the initial concentrations of the host, which for practical purposes coincides with the actual concentration, and x_{host} and x_{water} are the relative amounts of the bound and the free radical species. At room temperature, good simulations of the composite spectra were obtained, while the EPR spectra observed at higher temperatures could not be correctly simulated. Actually, on increasing the temperature a marked linewidth broadening became apparent; this was particularly evident on the outer lines of the proton triplets, as is shown in Figure (2.3a-d) as an example the spectra of nitroxide **1** recorded at different temperatures in the presence of β -CD 3.25 mM. Similar effects were observed in the EPR spectra of radicals undergoing intra or intermolecular dynamic exchanges. In the present case, line broadening is due to rapid exchange of the nitroxide radical between the two different environments, i.e., bulk water and the cavity of the complexing species, which modulates the nitrogen and proton hyperfine splitting constants. Changing the experimental conditions, i.e.

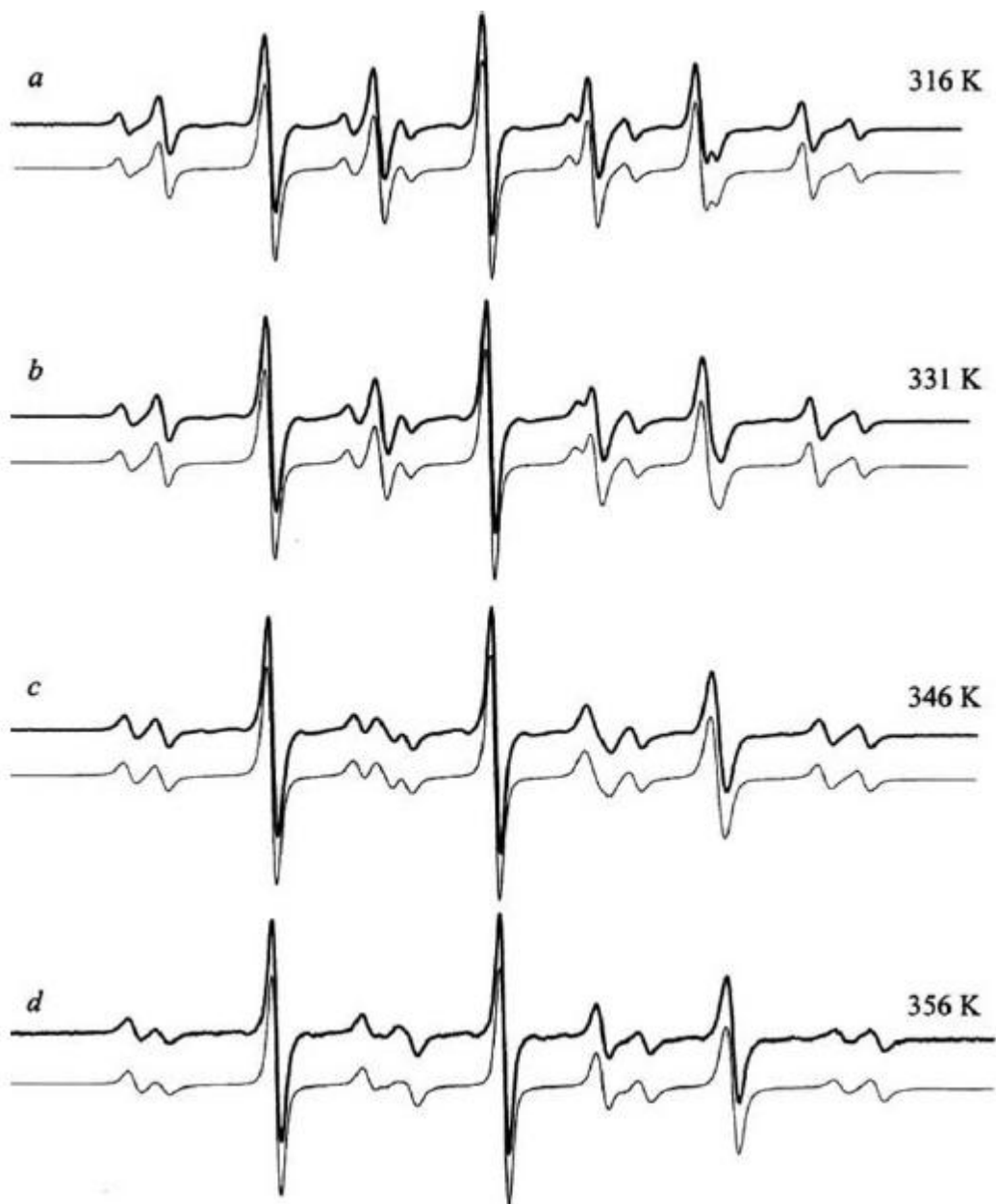


Figure 2.3: EPR spectra of radical **1** recorded in water in the presence of β -CD 3.25×10^{-3} M at different temperatures. Thin lines represent the corresponding theoretical simulations (*a*, $k_1 = 1.0 \times 10^9 \text{ M}^{-1} \text{ s}^{-1}$, $k_{-1} = 1.6 \times 10^6 \text{ s}^{-1}$; *b*, $k_1 = 1.6 \times 10^9 \text{ M}^{-1} \text{ s}^{-1}$, $k_{-1} = 2.9 \times 10^6 \text{ s}^{-1}$; *c*, $k_1 = 2.0 \times 10^9 \text{ M}^{-1} \text{ s}^{-1}$, $k_{-1} = 5.1 \times 10^6 \text{ s}^{-1}$; *d*, $k_1 = 2.3 \times 10^9 \text{ M}^{-1} \text{ s}^{-1}$, $k_{-1} = 8.7 \times 10^6 \text{ s}^{-1}$). As an examples the spectrum *b* was reproduced considering one species present at 37% in the bulk aqueous phase (g -factor: 2.0056, line width: 0.29 G, $a(9\text{H})$: 0.18 G, $a(\text{N})$: 16.59 G, $a(2\text{Hb})$: 10.31 G), and the other, corresponding to the nitroxide located inside the cyclodextrin (g -factor: 2.0058, line width: 0.31 G, $a(9\text{H})$: 0.18 G, $a(\text{N})$: 15.84 G, $a(2\text{Hb})$: 8.02 G), present at 63 %.

the temperature and host concentrations, affects the spectral shape, thus providing information about the mean life time t of the individual species.

The rate constants k_1 and k_{-1} for the exchange process can be determined at each temperature point by simulating the experimental EPR spectra using the density matrix theory³³ i. e. a two-jump model as exemplified in Eq. (1). The best fitting to the experimental spectra was obtained by a Monte Carlo least-square procedure³³. Fig. (4a-d) shows the quality of the fitting obtained.

The rate constants and the ΔH^0 and ΔS^0 parameters for the activated complexes have been presented in Table 3, while the thermodynamic parameters for the inclusion reaction have been reported in Table 4. The activation parameters (Table 2.3), for association and dissociation of the inclusion complexes of the spin probe with β -CD and DM- β -CD in water, present some interesting features. At room temperature the enthalpic contribution (ΔH^0_{\ddagger} , $\Delta H^0_{-\ddagger}$) to the Gibbs energy term, ΔG^0 , is larger than that of the entropic one. Moreover the appreciable enthalpies of activation for the association process (3.55 and 4.55 kcal mol⁻¹ for β -CD and DM- β -CD, respectively) indicate that the rate constants approach, but not reach, the limit for a diffusion-controlled process.

Host	$k_1/\text{M}^{-1}\text{s}^{-1}$	k_{-1}/s^{-1}	$\Delta H^0_{\ddagger}/$ kcal mol ⁻¹	$\Delta S^0_{\ddagger}/$ cal mol ⁻¹ K ⁻¹	$\Delta H^0_{-\ddagger}/$ kcal mol ⁻¹	$\Delta S^0_{-\ddagger}/$ cal mol ⁻¹ K ⁻¹
α -CD	1.1×10^8	7.7×10^6				
β -CD	6.8×10^8	5.3×10^5	3.55	-6.0	8.38	-3.8
γ -CD	3.8×10^8	7.6×10^6				
DM- β -CD	6.5×10^8	6.1×10^5	4.55	-2.7	8.98	-1.5
TM- β -CD	1.2×10^8	5.7×10^6				
Calix[4]arene 14	4.4×10^7	3.5×10^6	3.66	-11.32	7.58	-3.21
SDS ^e	1.2×10^{10}	3.9×10^6				
HTAB ^e	7.4×10^9	2.5×10^6				
C ₁₀ E ₆ ^e	2.6×10^{10}	5.3×10^6				
SDS ^d	7.0×10^9	2.0×10^6	4.68	2.30	6.69	-7.31

^e Estimated uncertainty: 10%.

^b estimated uncertainties: ΔH^0_{\ddagger} , ± 0.5 kcal mol⁻¹, ΔS^0_{\ddagger} , ± 2 eu.

^c Values obtained by using aggregation numbers of 64, 61 and 73 for SDS, HTAB and C₁₀E₆, respectively.

^d Values obtained by using nitroxide 2a as spin probe and 64 as aggregation number of SDS.

Table 2.3: Rate constants^a (294 K) and activation parameters^b for the inclusion reaction of nitroxide 1 with different hosts.

The factors governing the magnitude of the entropy of activation are more difficult to be appreciated conceptually. Since ΔS^0_{\ddagger} and $\Delta S^0_{-\ddagger}$ related to a change in randomness on passing from reactants and products to the transition state, respectively, it may be inferred that the following three terms contribute to the activation entropy: (a) freezing of motional freedom of

the guest molecule, (b) desolvation around the guest molecule and reorganization of water, (c) release of water molecules from the CD cavity and conformational changes of the CD ring. While the first term is negative, the other two are expected to contribute positively to the activation entropy. In the present case the experimental activation entropy for association is only slightly negative, indicating that the negative entropy due to the freezing of the motional freedom is almost completely compensated by the factors contributing positively to DS^\ddagger_1 . The entropy of activation for the dissociation process, DS^\ddagger_{-1} , is also negative, but its value is smaller than DS^\ddagger_1 ; thus, the enthalpy term, DH^\ddagger_{-1} , provides the dominant contribution to the free energy of activation for the dissociation process, leading to exothermicity for the inclusion process.

In the presence of SDS micelles, instead, we found a clearly positive entropic term essentially determined by the hydrophobic effect for the solubilization of the probe in micelles (i.e. desolvation of the nitroxide by bulk water). Moreover, differently from what was observed in the presence of CD, where the host-guest complexes were stabilized primarily by the favorable enthalpic change ($\Delta H^\circ < 0$), partially cancelled by the negative entropy change ($\Delta S^\circ < 0$), the major driving factor to the solubilization of the probe in micelles is the positive entropy change ($\Delta S^\circ > 0$) accompanied by a minor stabilizing ($\Delta H^\circ < 0$) enthalpic contribution.

Finally, the effect on inclusion of the host size was also investigated, in particular of the cyclodextrins size. Inspection of Table 4 reporting the affinity constant, K_1 , indicates that β -CD is more suitable a host for **1** than α - and γ -CD. This better steric selectivity of β -CD indicates that α - and γ -CD have cavities too small and too large, respectively, to accept **1** as a guest. On examining the rate constants for the inclusion process, reported in Table 2.3, the difference in the affinity constants of β -CD and γ -CD appears mainly due to an increase in the rate of dissociation for the latter, since the rates of association are comparable. With α -CD, both the smaller association rate constant and the larger dissociation rate constant contribute to the lower affinity of guest **1** for the CD, this being consistent with a weak interaction between the radical and the small α -CD cavity.

2.4 Study of exchange of different solutes between micellar and water phases

The factors governing the exit, k_{OFF} , and entrance, k_{ON} , rates of probes from and into the micelles have been extensively discussed in the literature³⁴. For the case where the kinetic barrier is low, the rates of the process are controlled by diffusion. Viewing the entrance process as a sequence of jumps over free-energy barriers between adjacent equilibrium positions in the liquid, the following equation has been derived for a diffusion-controlled process:

$$k_1 = 4\pi N (R_{\text{micelle}} + R_{\text{probe}}) (D_{\text{micelle}} + D_{\text{probe}}), \quad (5)$$

where D 's are the diffusion coefficients of the probe and the micelle in water, R_s are the corresponding hydrodynamic radii and N is the Avogadro number. In the present case, where diffusion of a small molecule to a relative larger sphere occurs, the equation can be simplified to the form:

$$k_1 = 4\pi N R_{\text{micelle}} D_{\text{probe}} \quad (6)$$

Using $D \gg 7 \times 10^{-6} \text{ cm}^2/\text{s}$ for the diffusion coefficient in water for the probe studied (substituted aromatic compounds have D values in the range $4\text{-}9 \times 10^{-6} \text{ cm}^2/\text{s}$ ³⁵ and $R = 24 \text{ \AA}$) one obtains:

$$k_1 = 1.3 \times 10^{10} \text{ mol}^{-1} \text{ s}^{-1} \quad (7)$$

The experimental value of k_1 obtained from the study of nitroxide **1**, i.e. $1.2 \times 10^{10} \text{ mol}^{-1} \text{ s}^{-1}$, indicates that the association reaction is very close to being controlled by diffusion, while the experimental value of k_1 obtained at 298 K for the nitroxide **2a** (see Scheme 1.1) is significantly lower ($7.0 \times 10^9 \text{ mol}^{-1} \text{ s}^{-1}$). Although, in principle, this reduction might be due to a decrease of the probe diffusion coefficient, in the present case this explanation seems quite unlikely and we prefer to attribute this difference in the k_1 value to electrostatic effects. Actually, the barrier that the probe should overcome when passing from the aqueous phase to the interior of the micelle can be imagined to reflect the search for a suitable spot on the surface among head groups, counterions, and hydration water; this being more difficult for nitroxides containing a polar OH group as **2a**.

As far as the exit rate, k_{OFF} , is concerned, it is known that its magnitude approximately parallels the solubility of the probe in water. Actually, an inverse linear dependence of the $\log k_{-1}$ vs. the

number of aliphatic carbons has been reported for sodium alkyl sulphates, N-alkylpyridinium bromides and 10-(4-bromo-1-naphthyl) alkylammonium bromides.

In order to check whether the EPR technique also gives similar results, nitroxides **2a-2e** obtained by substituting one of the methyl groups of the *tert*-butyl substituent in **1** with a hydroxymethyl group and by introducing in the *para* position of the benzyl group alkyl substituents of increasing length and therefore lipophilicity were investigated. It should be mentioned that the surfactant concentration was kept higher than the critical micelle concentration CMC and the nitroxide/micelle ratio was low enough to avoid possible anomalous effects due to multiple occupancy of micelles.

The EPR spectral parameters reported in Table 5 indicate that also with nitroxides **2a-2e** the values of hyperfine splitting constants in water and in the micelles differ considerably, resulting in a great difference between the resonance fields for the triplet outer lines of the radical in the two phases. It is worth pointing out that with increases the alkyl chain length of the probe in the value of a_N in the micellar phase remains approximately constant, while the value of $a_{2H\beta}$ decreases significantly. This indicates that polarity of the environment around the nitroxide function is similar for all the radicals, **2a-2e**: in other words, the N-O group is deeply inside the micelle irrespective of the alkyl chain length. The decrease of the β -proton splitting, on the other hand, implies that the motional freedom of the substituted benzyl group experiences some change. Since the magnitude of $a_{2H\beta}$ suggests that the minimum energy conformation in these nitroxide radicals is the one where the aryl group is eclipsed with respect to the symmetry axis of the $2p_z$ orbital on the nitrogen atom, it seems that due to increase in the alkyl chain length the aryl group is more rigidly held in this position.

Nitroxide	R	$a(N) / G$	$a(2H\beta) / G$	<i>g</i> -factor	$k_t / M^{-1} s^{-1}$	k_d / s^{-1}
2a	-H	16.17	10.26	2.0056	2.1×10^{10}	11.0×10^6
		15.83	9.31	2.0057		
2b	-CH ₃	16.17	10.18	2.0056	1.9×10^{10}	5.7×10^6
		15.85	9.16	2.0057		
2c	-CH ₂ CH ₃	16.18	10.11	2.0056	2.2×10^{10}	2.8×10^6
		15.83	8.97	2.0057		
2d	-(CH ₂) ₂ CH ₃	16.19	10.10	2.0056	1.9×10^{10}	1.4×10^6
		15.78	8.80	2.0057		
2e	-(CH ₂) ₄ CH ₃	16.25	10.14	2.0056	2.2×10^{10}	0.45×10^6
		15.82	8.62	2.0057		

Table 2.4: EPR spectral parameters in water (normal) and in SDS micelles (bold) and rate constants k_1 and k_{-1} at 343 K for the entrance and exit processes for the dialkyl nitroxides 2a-2e.

The rate constants at 343 K obtained by analyzing the EPR line shape variations as function of surfactant concentration are also reported in Table 2.4. Inspection of the experimental data reveals that the dynamics of probe association with the host micelles is clearly dependent on the probe hydrocarbon chain length. In particular, while k_1 is almost independent of the length of the para-alkyl group, k_{-1} decreases significantly by increasing the lipophilicity of the probe. Figure 2.4, reporting the measured $\log k_{-1}$ values as function of the number of aliphatic carbons in the alkyl chain nitroxides 2a-2e. This result is similar to that one found in previous studies using luminescence quenching techniques.

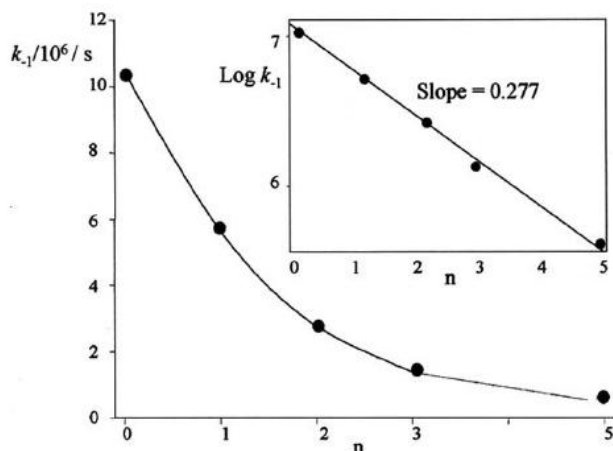


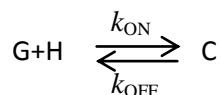
Figure 2.4: The dependence of the exit rate for the probe 2a-2e as a function of number of aliphatic carbons in the hydrocarbon tail R.

We may therefore conclude that the solubilization rate of a given guest in micelle is controlled only by diffusion independently on the structure of the probe, while the rate of escape from the micelles is determined by the size of the hydrophobic chain, i.e., by the lipophilicity of the molecule.

2.5 Measuring the rate of distribution of organic substrates between cyclodextrin, micelles and water

Mixed organized media represent an intriguing system because of the possibility for a given guest to interact selectively with a single binding site.¹ When a substrate is added to such

system the noncovalent binding of the guest (G) with the different hosts (H) to form a guest–host complex (C) is observed:



where k_{ON} and k_{OFF} are the rate constants of complex formation and dissociation, respectively. The stability of the complex is generally described in terms of the equilibrium dissociation constant, $K_d=k_{\text{OFF}}/k_{\text{ON}}$. In order to understand the chemistry of this system, it is vital to know the rate at which an organic molecule is partitioned between the different phases.²

One of the most studied system is the cyclodextrin–micelle mixed system, because of its application in separation-based affinity methods (i.e. capillary electrophoresis),³ as a reaction medium⁴ and in supramolecular devices.⁵ While rates of solubilization into surfactant solutions⁶ and of the inclusion complexation by cyclodextrins⁷ (CDs) of specific probes have been extensively investigated using a variety of methods, the direct measure of individual binding events between analyte molecules and a mixture of both CD and micelle is still challenging.

EPR spectroscopy is characterised by a peculiar timescale which is comparable to that of many complexation processes. Here we introduce and describe an EPR method that allows, for the first time, direct and simultaneous measurement of the concentration of an organic spin probe in three different “pseudo-phases” (namely SDS micelles, CDs and water), if it exceeds the limit of detection. This new method allows the determination of all thermodynamic and kinetic parameters, K_d , k_{ON} , and k_{OFF} , in a single experiment that requires only a minute amount of substrates. This has the potential for significantly augmenting the arsenal of methods available for studying the partitioning of a given substrate in different pseudo-phases.

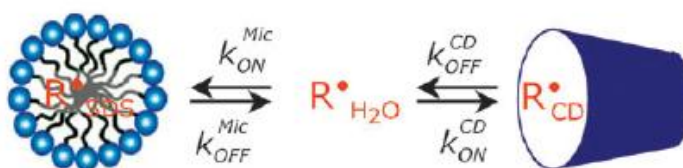
	$a(\text{N})/\text{G}$	$a(2\text{H}_\beta)/\text{G}$	g -factor
Water	16.69	10.57	2.0056
SDS	16.04	8.84	2.0057
DM- β -CD	15.60	7.80	2.0058

Table 2.5: EPR parameters of tert-butyl benzyl nitroxide (1 G =0.1 mT)

The method is based on the significant differences in the EPR parameters shown by tert-butyl benzyl nitroxide (**1**) when it experiences water,⁸ cyclodextrin cavity⁹ or micellar

environments¹⁰ (see Table 2.5). The partitioning of nitroxide probes in the hydrophobic environment of SDS micelle gives rise to a reduction of the value of both nitrogen and β -protons splittings, with the result that the resonance fields for the $MI(2_{H\beta}) = \pm 1$ lines of the free and included species are significantly different from those of the nitroxide dissolved in water. These differences are even more pronounced when **1** is included in the cavity of CD's due to both polar and conformational changes occurring upon complexation. The EPR spectra also show a strong linewidth dependence on temperature both in the presence of SDS micelle and CD, indicating that the lifetime of the radical in the associated and free form is comparable to the EPR timescale. Because of this favorable feature, the analysis of the line shape makes it possible to measure the rate constants for the partition of the probe in the pseudo-phases.

The EPR spectra at 298 K of **1**, produced by reaction of the magnesium salt of monoperoxyphthalic acid with tertbutyl benzyl amine in the presence of heptakis-(2,6-O-dimethyl)-CD (DM- β -CD) 5.3 mM or SDS 33 mM are shown in Figure 2.5a and 2.5b, respectively. The spectra show in both cases two sets of signals due to the radical in the aqueous phase and to that included in the CD cavity (Figure 2.5a) or solubilised in the micellar pseudo-phase (Figure 2.5b). In the presence of a mixture of CD and SDS at the same concentration as above, the EPR spectrum differs significantly from the previous ones.



Scheme 2.6

All the spectra can be correctly reproduced only by assuming the kinetic scheme reported in Scheme 2.6 in which the radical probe is exchanging, with a rate comparable to the EPR time scale, between the water phase and both the CD cavity and the micellar pseudo-phase.

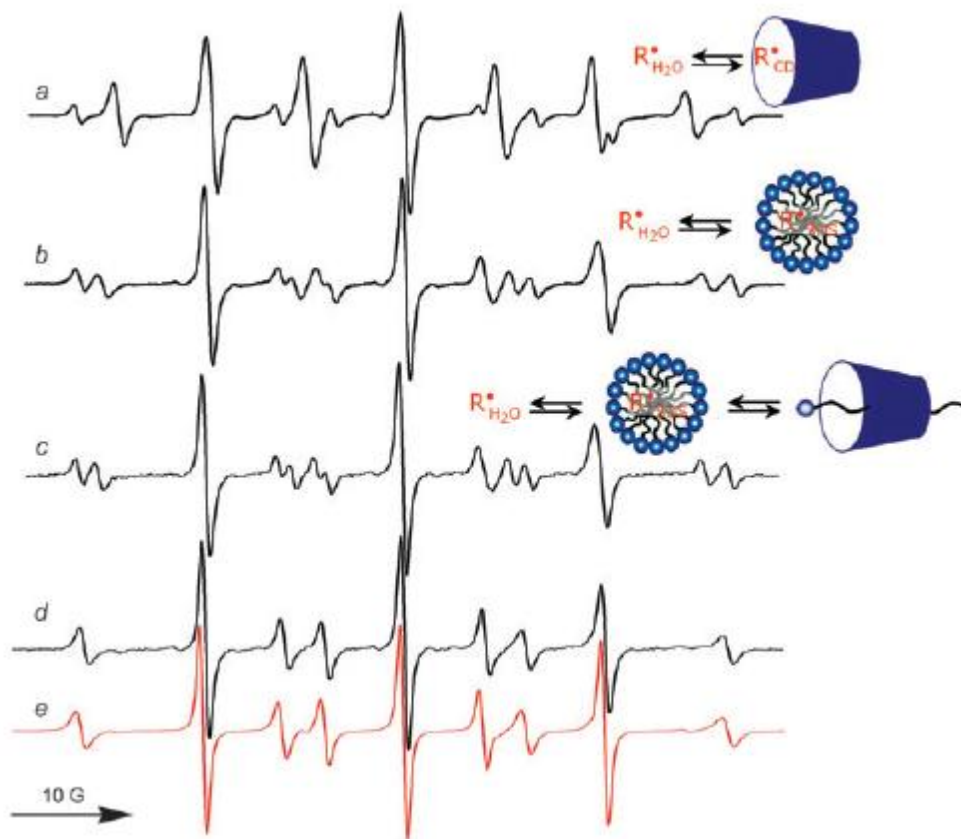


Figure 2.5: EPR spectra of 1 recorded in water at 298 K. (a) DM- β -CD 5.3 mM; (b) SDS 33 mM; (c) β -CD 16 mM and SDS 49 mM; (d) DM- β -CD 16 mM and SDS 49 mM. (e) Theoretical simulation of spectrum (d) obtained with the rate constant reported in Table 1, entry 11.

Simulation of the exchange-broadened EPR spectra, by using well established procedures based on the density matrix theory¹¹ and assuming a three-jump model as illustrated in Scheme 2.6, led to the determination of the residence time (τ_X) of the paramagnetic species in the three different pseudo-phases which are related to rate constants (see Table 2.6) of the exchange processes by the following expressions:

$$\tau_{CD} = 1/k_{OFF}^{CD} \quad \tau_{MIC} = 1/k_{OFF}^{MIC} \quad \tau_{H2O} = 1/k_{ON}^{CD} + 1/k_{ON}^{MIC}$$

Entry	[SDS]/mM	Cyclodextrin (mM)	$k_{\text{ON}}^{\text{CD}}/\text{s}^{-1}$	$k_{\text{OFF}}^{\text{CD}}/\text{s}^{-1}$	$k_{\text{ON}}^{\text{MIC}}/\text{s}^{-1}$	$k_{\text{OFF}}^{\text{MIC}}/\text{s}^{-1}$
1	—	β -CD (5.3)	3.6×10^6	5.3×10^5	—	—
2	—	DM- β -CD (5.3)	3.4×10^6	6.1×10^5	—	—
3	3.4	DM- β -CD (5.3)	1.7×10^6	6.5×10^5	—	—
4	5.0	DM- β -CD (5.3)	3.4×10^5	7.0×10^5	—	—
5	33	—	—	—	6.2×10^6	3.9×10^6
6	26	β -CD (16)	6×10^4	5.3×10^5 ^a	8.0×10^5	3.9×10^6
7	33	β -CD (16)	$<3 \times 10^4$	5.3×10^5 ^a	3.0×10^6	3.9×10^6
8	49	β -CD (16)	$<3 \times 10^4$	5.3×10^5 ^a	6.2×10^6	3.9×10^6
9	33	DM- β -CD (5.3)	$<4 \times 10^4$	6.1×10^5 ^b	5.5×10^6	7.8×10^6
10	33	DM- β -CD (20)	8.0×10^4	6.1×10^5 ^b	1.6×10^7	4.7×10^7
11	49	DM- β -CD (16)	4.0×10^4	6.1×10^5 ^b	1.5×10^7	2.8×10^7
12	105	DM- β -CD (20)	$\ll 4 \times 10^4$	6.1×10^5 ^b	1.5×10^7	1.0×10^7
13	73	DM- β -CD (40)	8.0×10^4	6.1×10^5 ^b	2.2×10^7	2.8×10^7
14	53	TM- β -CD (20)	—	—	1.5×10^7	2.4×10^7

^a Assumed equal to that of entry 1. ^b Assumed equal to that of entry 2.

Table 2.6: Selected EPR rate constants at 298 K for the partition of **1** in the micellar and CD locations

By recording the corresponding EPR spectra it is possible, therefore, to obtain the distribution of the radical probe in the different environments at different concentrations of surfactant and cyclodextrin. As an example, in Figure 2.6 is reported the variation of the molar fraction of **1**

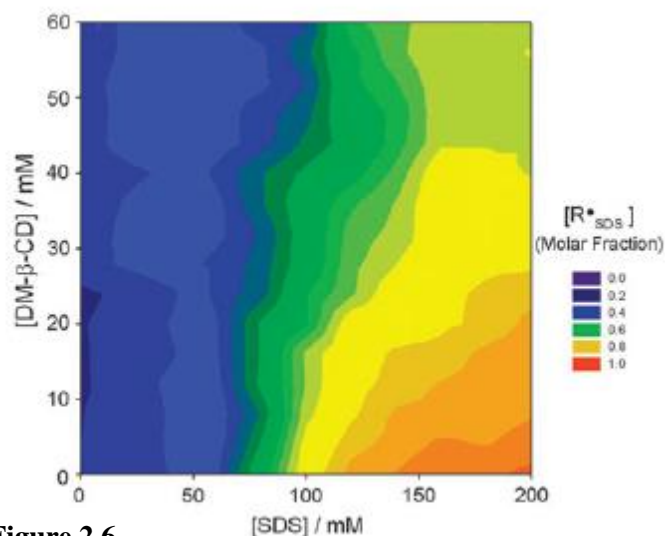


Figure 2.6

partitioned in the micellar phase in the presence of different DM- β -CD/SDS concentrations.

Depending on the relative amount of CD and SDS we can distinguish different regimes:

$[\text{SDS}] \leq [\text{CD}]$: Under this condition the amount of radical included in the CD cavity decreases proportionally to the amount of surfactant present in the

solution. This effect is attributed to complexation of the surfactant monomer by CD and release of the probe into the bulk aqueous medium giving rise to an increase in the residence time of the probe in the water phase (entries 3–4). According to the fact that in this condition the free dissolved SDS monomer concentration is well below the critical micelle concentration (cmc) no EPR signals due to the radical partitioned in the SDS phase are observed.

[SDS] > [CD]: The formation of SDS–CD complex increases the concentration of surfactant required for micellization,¹² and the critical micelle concentration of a micellar system in the presence of a cyclodextrin (cmc_{app}) is equivalent to the combined concentrations of surfactant monomers complexed to the CD, and of free dissolved monomer in equilibrium with the micellized surfactant, cmc_{real} . Once micellization starts, the system behaves like a typical micellar system. Analysis of EPR data shows that this is actually the case when β -CD (see Entries 5–8) is employed as the macrocyclic host. As an example Fig. 1c shows the EPR spectrum recorded in the presence of SDS 49 mM and β -CD 16 mM which perfectly matches that one recorded in the presence of SDS 33 mM (Figure 2.5b). A change in the nature of the macrocyclic host has, however, a dramatic effect on the partitioning behaviour of the radical probe. In the presence of a small amount of methylated cyclodextrins (DM- β -CD or TM- β -CD) the EPR spectra are characterised by an increased broadening of the external lines, indicating that the exchange rate of the probe between water and the micellar pseudo-phase is becoming faster (see entries 9–10). Further addition of methylated cyclodextrins in the solution results in a dramatic decrease of the life time of the probe in the SDS micelles. Nevertheless, when the concentration of DM- β -CD is so much so that $([\text{CD}] + \text{cmc}_{\text{real}}) > [\text{SDS}]$, the EPR spectrum can be correctly simulated by admitting that a sizeable fraction of the probe is still experiencing a hydrophobic environment. While the dramatic reduction of the residence time of the radical guest in the micelle suggests that the micellar structure is altered significantly in the presence of methylated cyclodextrins, the existence of radicals dissolved in an hydrophobic aggregate for concentration of SDS below cmc_{app} ($\text{cmc}_{\text{app}} = \text{cmc}_{\text{real}} + \text{CD}$) indicate that this altered micelle is still able to solubilise the probe. According to recent findings by Dreiss and coworkers¹³ we can suppose that the presence of methylated cyclodextrins results in a lowering of the aggregation number, and in an increase of solvent penetration and polydispersivity of the micelle.

From an applicative point of view we checked if the residence time of the probe in each environment determined by EPR could be employed to predict the electrophoretic behaviour of a given analyte. Capillary electrophoretic (CE) analysis of neutral solutes in CD-micellar systems is based on the differences in the mobility of the analytes in the homogeneous phase.

The anionic SDS micelle acts as a carrier and the inclusion of the solutes into the neutral CD cavity is a process in competition with the partitioning into the micelle. When the residence time of the probe in the cyclodextrin is long compared with the residence time in the micelle, the mobility of the neutral probe approaches to zero; this condition is also observed when surfactant concentration is below the critical micelle concentration. CE experiments were performed by analyzing the electrophoretic behaviour of tert-butyl benzyl ketone, the diamagnetic analogue of **1**, in the presence of either β -CD and DM- β -CD at 16 and 20 mM, respectively. SDS was supplemented as a micelle separation carrier in a wide concentration range (15–165 mM) and the effective electrophoretic mobility (μ_e) of the probe was plotted against the SDS concentration (Fig. 3).

As expected, in the absence of cyclodextrin only small mobility variations were observed in the investigated SDS range, while, in the presence of β -CD, the mobility variation profile shows a marked break point which corresponds to a surfactant concentration below cmc_{app} ($[\beta\text{-CD}] + \text{cmc}_{\text{real}} = 24 \text{ mM}$). In the presence of DM- β -CD the effective mobility of the carbonyl probe is significantly reduced. According to EPR data this should be attributed to the reduced residence time of the probe in the micellar pseudo-phase. Conversely to that found with β -CD, in the presence of SDS between 20 and 28 mM, that is below the hypothetical cmc_{app} ($[\text{DM-}\beta\text{-CD}] + \text{cmc}_{\text{real}} = 28 \text{ mM}$) the transport ability of the micellar carrier is still maintained with DM- β -CD, this being an indication that a modified micellar carrier is present in the solution as predicted by EPR measurements.

In conclusion, the combined use of selected nitroxide and EPR spectroscopy has been proved to be suitable for studying the partitioning rate of a given substrate in CD–micelle systems. On the condition that the spectroscopic parameters of the probe are sufficiently different to distinguish the different environment experienced by the radical, EPR data can be employed to predict the partitioning behaviour of non radical analytes in mixed organised systems. We foresee the potential role of EPR in extending the utility of this technique by using probes characterized by a different lipophilicity or containing a chiral centre.

2.6 References:

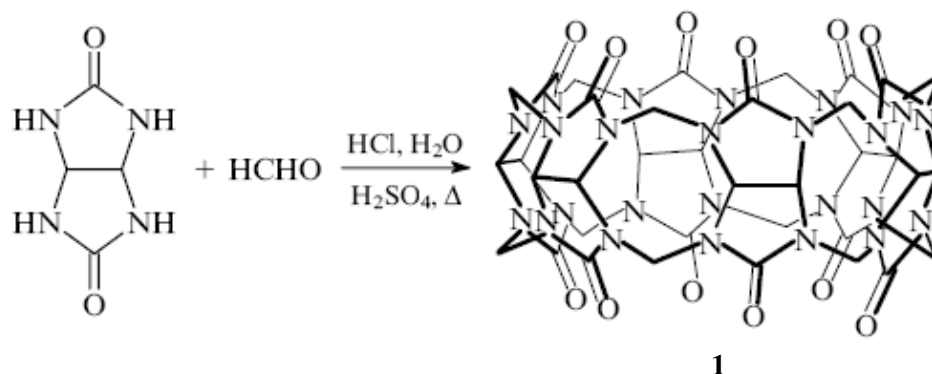
1. For example, see: a) Lehn, J. M., Nobel Lecture, *Angew. Chem. Int. Ed. Engl.*, **1988**, *112*, 90. b) *Comprehensive Supramolecular Chemistry*, Eds. Atwood, J. L.; Davies, J. E. D.; MacNicol, D. D.; Vögtle, F. Pergamon, Oxford, **1996**, vol. *11* and preceding volumes. c) Lehn, J. M. *Supramolecular Chemistry: Concepts and Perspectives*, VCH, Weinheim, **1995**. d) Stoddart, J. F.; Philip, D. *Angew. Chem., Int. Ed. Engl.*, **1996**, *35*, 1154.
2. a) Sahyun, M. R. V. *Nature*, **1966**, *209*, 613. b) Hymes, A. J.; Robinson, D.A.; Canady, W.J. *J. Biol. Chem.*, **1965**, *240*, 134.
3. a) Eigen, M. *Pure Appl. Chem.*, **1963**, *6*, 97-115. b) Nau, W. M.; Wang, X. *ChemPhysChem*, **2002**, *3*, 393.
4. Schneider, H. J.; Hacket, F.; Rüdiger, V. *Chem. Rev.*, **1998**, *98*, 1755 and references therein.
5. For examples, see: a) Cramer, F.; Saenger, W.; Spatz, H. *J. Am. Chem. Soc.*, **1967**, *89*, 14. b) Yoshida, N.; Fujimoto, M. *Chem. Lett.*, **1980**, 231. c) Yoshida, N.; Fujimoto, M. *Bull. Chem. Soc. Jpn.*, **1982**, *55*, 1039. d) Hersey, A.; Robinson, B.H. *J. Chem. Soc., Faraday Trans. 1*, **1984**, *80*, 2039. e) Clarke, R. J.; Coates, J.H.; Lincoln, S. F. *Carbohydr. Res.*, **1984**, *127*, 181. f) Yoshida, N.; Seiymana, A.; Fujimoto, M. *J. Inclusion Phenom.*, **1984**, *2*, 573.
6. Lucarini, M.; Luppi, B.; Pedulli, G. F.; Roberts, B.P. *Chem. Eur. J.*, **1999**, *5*, 2048.
7. Franchi, P.; Lucarini, M.; Pedulli, G.F.; Sciotto, D. *Angew. Chem. Int. Edn.*, **2000**, *39*, 263.
8. Brigati, G.; Franchi, P.; Lucarini, M.; Pedulli, G.F.; Valgimigli, L. *Res. Chem. Intermed.*, **2002**, *28*, 131-141.
9. Lucarini, M.; Franchi, P.; Pedulli, G. F.; Pengo, P.; Scrimin, P.; Pasquato L. *J. Am. Chem. Soc.*, **2004**, *126*, in the press.
10. Franchi, P.; Lucarini, M.; Pedulli, G.F. *Angew. Chem. Int. Edn.*, **2003**, *42*, 1842-1845.
11. Franchi, P.; Lucarini, M.; Mezzina, E.; Pedulli G.F. *J. Am. Chem. Soc.*, **2004**, *126*, 4343.
12. a) Atherton, N. M.; Strach, J. *J. Chem. Soc., Faraday Trans. 1*, **1975**, *71*, 357. b) Motozato, Y.; Nishihara, T.; Hirayama, C.; Furuya, Y.; Kosugi, Y. *Can. J. Chem.*, **1982**, *60*, 1959. c) Okazaki, M.; Kuwata, K. *J. Phys. Chem.*, **1984**, *88*, 3163. d) Okazaki, M.; Kuwata, K. *J. Phys. Chem.*, **1984**, *88*, 4181. e) Jeunet, A.; Nickel, B.; Rassat, A. *Nouv. J. Chim.*, **1986**, *10*, 123. f) Eastman, M. P.; Freiha, B.; Hsu, C. C.; Lum, K. C.; Allen Chang, C. *J. Phys. Chem.*, **1987**, *91*, 1953. g) Eastman, M. P.; Freiha, B.; Hsu, C. C.; Allen Chang, C. *J. Phys. Chem.*, **1988**, *92*, 1682. h) Petr, A.; Dunsch, L.; Koradecki, D.; Kutner, W. *J. Electroanal. Chem.*, **1991**, *300*, 129.
13. Martinie, J.; Michon, J.; Rassat, A. *J. Am. Chem. Soc.*, **1975**, *97*, 1818.
14. Janzen, E. G.; Kotake, Y. *J. Am. Chem. Soc.*, **1988**, *110*, 3699. b) Janzen, E. G.; Kotake, Y. *Chem. Phys. Lett.*, **1988**, *150*, 199. c) Janzen, E. G.; Kotake, Y. *J. Am. Chem. Soc.*, **1989**, *111*, 7319. d) Janzen, E. G.; Kotake, Y. *J. Am. Chem. Soc.*, **1992**, *114*, 2872.
15. Janzen, E. G.; Kotake, Y. *J. Am. Chem. Soc.*, **1988**, *110*, 7912.

CHAPTER 3

CUCURBITURIL HOSTS

3.1 Introduction

Cucurbituril with composition $C_{36}H_{36}N_{24}O_{12}$ [cucurbit[6]uril, **1**] consisting of six methylene-linked glycoluril fragments has been studied the most. This compound is the first example of cucurbiturils. It was prepared by Behrend et al.¹ in 1905 by condensation of formaldehyde with glycoluril (condensation product of urea and glyoxal) in acidic medium. At that time, however, the procedures available did not allow one to determine correctly its composition and structure. In 1981, Freeman, Mock and Shih² reproduced the synthesis developed by Behrend and obtained a colourless crystalline compound whose structure was established by X-ray diffraction analysis.



Cucurbituril **1** is a barrel-shaped macrocyclic cavitand containing carbonyl oxygen atoms (portals) at the top and bottom of the barrel. This cavitand received its trivial name for the visual similarity of its molecular shape to Cucurbitaceae (pumpkin family). Hereinafter, cucurbiturils consisting of n glycoluril fragments will be abbreviated to CB n or referred to as cucurbit[n]uril.

The dimensions of the inner cavity of cucurbit[6]uril **1** (the height is 6 Å and the inner diameter is 5.5 Å) allow the molecule to accommodate small guest organic molecules or ions and the portals formed by the carbonyl groups (the diameters of the portals are 4 Å) can bind cations. The structure determination of CB6 gave impetus to investigations of its ability to act as a macrocyclic cavitand. Cucurbit[6]uril **1** whose cavity is similar in size to those of α -cyclodextrin and 18-crown-6 has higher negative charges on the donor oxygen atoms resulting

in the enhancement of stability of its adducts with positively charged ions.^{3, 4} Yet another difference between cucurbituril CB6 and other cavitands is its structural rigidity. Thus, this cucurbituril virtually retains its shape upon the inclusion of different guests and, consequently, exhibits higher selectivity in the formation of inclusion compounds.³ Cucurbit[6]uril **1** is a colourless crystalline compound, which is insoluble in water and organic solvents but is readily soluble in some mineral acids (HCl, H₂SO₄, CF₃SO₃H), carboxylic acids (for example, HCOOH) and aqueous solutions of alkali salts.

Cucurbit[6]uril serves as a convenient starting compound for the preparation of various supramolecular compounds due to its unique structure, the simplicity of the synthesis procedure and thermal stability (it does not decompose upon heating to 400 °C)⁵. Presently, cucurbit[6]uril is a readily available reagent.

The presence of the rather rigid inner cavity is responsible for the ability of cucurbit[6]uril **1** to accommodate small guest molecules. The formation of inclusion compounds was established by crystallographic methods as well as by different physicochemical methods because absorption, fluorescence and NMR spectra of guests are changed as the guest molecules go from the solvent environment (generally, from weakly acidic aqueous solutions) to the non-polar cavity of cucurbituril. Cucurbit[6]uril **1** forms stable inclusion compounds with amines, diamines, alkylammonium ions, benzylammonium ions and dye molecules.

3.2 Cucurbit[*n*]urils (*n*=5, 7 - 10)

In addition to the above-considered macrocyclic cavitand cucurbit[6]uril **1** consisting of six methylene-bound glycoluril fragments, there are also cucurbiturils, which are composed of a smaller or larger number of these fragments and have the shape of barrels with smaller or larger diameters. Crystals of the cyclic pentamer were first prepared by the reaction of dimethylglycoluril with formaldehyde and structurally characterised in 1992.⁶ The decamethylcucurbit[5]uril has a slightly distorted symmetry D_{5h} and its methyl groups are located at the periphery of the molecule. In the cited study, the nomenclature for cucurbiturils was proposed by analogy with that used for calixarenes. According to this nomenclature, the

number of glycoluril (or substituted glycoluril) fragments is denoted by the figure in brackets and the number of substituents is represented by the prefix.

In 2000, K. Kim and coworkers⁷ performed the reaction of glycoluril with formaldehyde in 9 M sulfuric acid and obtained a mixture of cyclisation products (n=5 - 11) from which five-, seven- and eight-membered homologues of cucurbituril were isolated in very low yields. These compounds were structurally characterised. A comparison of their structural parameters (Table 3.1) demonstrates that the diameters of the cavity and portals of cucurbiturils increase as the number of glycoluril fragments in the rings is increased. A two fold increase in the inner diameter of the cavity on going from cucurbit[5]uril to cucurbit[8]uril leads to more than a fivefold increase in the volume of the cavity.

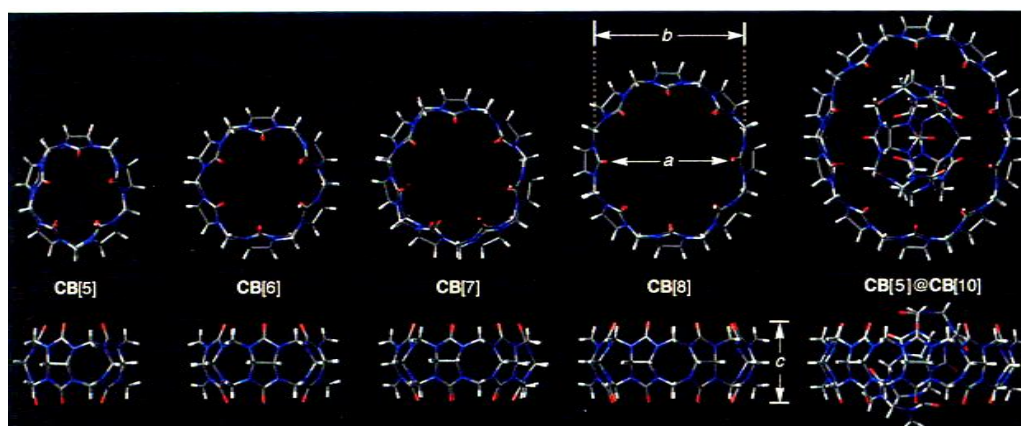


Figure 3.1: X-Ray structure of CB_n .

Day et al.⁸ studied the reactions of glycoluril with formaldehyde in H_2SO_4 , HCl or HBF_4 solutions by electrospray mass spectrometry and ^{13}C NMR spectroscopy and established the existence of cucurbit[n]urils with n=5 - 16 in solution. Based on the results of investigations into the effects of the nature of acid and its concentration, the concentrations of other reagents and the reaction temperature, a mechanism for the formation of different cucurbit[n]urils was proposed and the procedure for their synthesis optimised. Cucurbit[n]urils with n=5 - 10 were isolated in pure form (the yields were 8%, 46%, 24%, 12%, 85% and 5%, respectively). Individual cucurbit[n]urils with larger numbers of glycoluril fragments are presently unavailable. According to the results of theoretical calculations (density functional theory),⁹ compounds containing six or seven glycoluril fragments are the most stable homologues of cucurbiturils, and decamethylcucurbit[5]uril is the most stable methyl-substituted derivative.

These results agree with both the above described experimental data and the distortions of the NCN angles at the carbon atoms of the bridging methylene groups that link the glycoluril fragments upon assembly.

Cucurbit[n]uril	Portal diameter /Å	Cavity diameter /Å	Cavity volume /Å ³	Molecule height /Å
<i>n</i> = 5	2.4	4.4	82	9.1
<i>n</i> = 6	4.0	5.5	164	9.1
<i>n</i> = 7	5.4	7.3	279	9.1
<i>n</i> = 8	6.9	8.8	479	9.1

Scheme 3.1

The presence of the hydrophobic cavity along with the polarised carbonyl groups at the portals of cucurbit[6]uril **5** are responsible for the formation of numerous inclusion compounds. The smaller cavity in cucurbiturils allows small molecules to be encapsulated and securely held, whereas larger-size molecular containers can accommodate bulkier guest molecules. Besides, an increase in the number of the oxygen atoms at the portals is favourable for the formation of a large number of hydrogen bonds and, correspondingly, more stable supramolecular compounds.

Decamethylcucurbit[5]uril can accommodate a molecule of nitric acid. Due to the fact that the molecular size of nitric acid matches the volume of the cavity, this guest molecule can form rather short contacts and be held in the cavity through both Coulombic interactions with the carbon atoms and hydrogen bonding with the carbonyl oxygen atoms of the macrocycle.¹⁰ It was proved by electrospray mass spectrometric study of the ammonium acetate-decamethylcucurbit[5]uril system that the N₂, O₂, methanol and acetonitrile molecules can be included into the cavity, held in the cavity through the formation of the NH₄⁺ lids and released upon the removal of these lids. This ability of the rather rigid macrocycle to accommodate small molecules is of interest for purification or separation of gas mixtures.¹¹

The cavity volume of cucurbit[5]uril is insufficient for the inclusion of aromatic molecules. According to the results of X-ray diffraction analysis, the terminal ammonium groups of 1,6-

diaminohexane are involved in hydrogen bonds with the portal oxygen atoms of the adjacent macrocycles to form chains.

The water solubility of cucurbit[5]uril and decamethylcucurbit[5]uril as well as the solubility of cucurbit[6]uril are substantially increased upon the addition of salts of ammonium, alkali and alkaline earth metals due to formation of complexes with cations,¹² decamethylcucurbit[5]uril giving alkali metal complexes with composition 1:1.¹³

Due to the larger cavity volumes in cucurbiturils consisting of seven or eight glycoluril fragments, these compounds can encapsulate bulky molecules whose sizes are too large to be included into compounds of CB6. Thus, CB7 forms inclusion compounds with *o*-carborane,¹⁴ with the 2,3-diazabicyclo[2.2.2]oct-2-ene molecule, whose size matches excellently the cavity size and fills virtually the entire cavity resulting in a stable supramolecular compound.¹⁵

The cavity sizes of cucurbit[n]urils (n=8, 10) allows smaller macrocycles to be included giving rise to rather rare compounds. Heating of an aqueous solution of CB8 with 1,4,7,10-tetraazacyclododecane (cyclen) and 1,4,8,10-tetraazacyclotetradecane (cyclam) afforded inclusion compounds, which have been structurally characterised. These compounds are stabilised primarily through van der Waals interactions between the inner macrocycle and the cavity of the outer macrocycle.¹⁶ The small and large macrocycles are inclined to one another (the angle between the equatorial planes is $\sim 38^\circ$). The ability of tetraazamacrocycles to coordinate transition metal ions (these complexes are known as catalysts, for example, of epoxidation or DNA hydrolysis) was used in the reactions of the resulting inclusion compounds with Cu^{2+} and Zn^{2+} salts. The compound containing $[\text{Cu}(\text{cyclen})\cdot(\text{H}_2\text{O})]^{2+}$ in the cavity of CB8 was studied by X-ray diffraction analysis. In this compound, the macrocycles are virtually parallel to each other (Fig. 21) and the copper atom present in the inner macrocycle additionally coordinates the water molecule, which is located in the plane of the portal of CB8 and can be replaced by other ligands. It should be noted that the cyclen coordinated by the metal atom is not encapsulated into cucurbit[8]uril because the formation of the complex with the metal atom enhances its conformational rigidity and hinders its inclusion into the cavity of CB8.

Recently, the unique compound of cucurbit[5]uril encapsulated into cucurbit[10]uril was prepared and characterised by X-ray diffraction analysis (Fig. 3.2).¹⁷ The molecules of the macrocycles are inclined to each other (the angle between their equatorial planes is 64°).

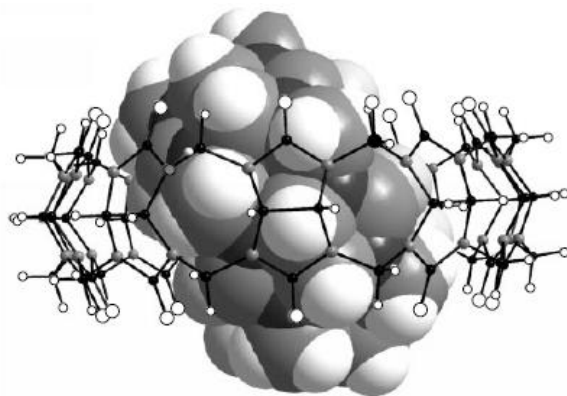


Figure 3.2: Structure of the inclusion compound of cucurbit[5]uril in cucurbit[10]uril.

This fact along with the ¹H and ¹³C NMR spectroscopic data provide evidence that the macrocycles in solution undergo free rotation with respect to each other (molecular analogue of a gyroscope). The cavity of CB5 contains the chloride anion and there is a system of hydrogen bonds between the portal oxygen atoms of both macrocycles and water molecules serving as the lids of the inner pentamer (see Fig. 3.2). It is believed that CB5 serves as a template for the assembly of larger- size cucurbiturils. Cucurbituril CB10 is as yet unavailable as an individual compound.

Like cucurbit[6]uril, larger macrocycles form stable inclusion compounds with organic molecules whose protonated nitrogen atoms are linked to the polarised oxygen atoms at the portals through Coulombic interactions. Due to the larger sizes of the cavities, such bulky molecules as 2,6-bis(4,5-dihydro-1H-imidazol-2-yl)naphthalene can be accommodated in these macrocycles. Inclusion compounds with compositions 1 : 1 and 2 : 1 were prepared with cucurbit[7]uril and cucurbit[8]uril, respectively. The results of quantum-chemical calculations (density functional theory) of the former compound demonstrated that not only van der Waals interactions and the hydrophobic effect but also hydrogen bonding between the protonated dihydroimidazole substituents and the portal oxygen atoms of CB7 play an important role in the formation of inclusion compounds.²¹ Two such bulky molecules are located in an even larger inner cavity of CB8.

According to the X-ray diffraction data, the imidazole substituents are located outside and are bound to the portals of CB8. Two naphthalene rings within the cavity are located parallel to each other at a distance of 3.4 Å, which is indicative of π - π interactions between these rings.

The encapsulation of two or more guest molecules into the cavity of the macromolecule is of great interest in view of the unique possibility of studying new types of stereoisomerism, bimolecular reactions and the behaviour of the molecules in the microenvironment. The CB8 molecule possessing a very large cavity provides rich possibilities for investigating such interactions. K. Kim and coworkers²² were the first to study the selective encapsulation of two different guests into the cavity of one host.

Interactions between two guests are the driving forces for the formation of supramolecular compounds. Two organic molecules, viz., the electron-deficient molecule A and molecule B acting as the electron donor, are accommodated in the cavity of CB8 [A is the *N,N'*-dimethyl-4,4'-bipyridinium cation (methylviologen $\text{MeN}^+\text{C}_{10}\text{H}_8\text{N}^+\text{Me}$) and B is 2,6-dihydroxynaphthalene or 1,4-dihydroxybenzene]. It should be noted that inclusion compounds with only either molecules A or molecules B were not obtained. The data from ^1H NMR, emission and UV spectroscopy are unambiguously indicative of strong charge-transfer interactions between the guest molecules due to their tight contact within the cavity. This interaction is much stronger than the interaction between these guest molecules if they are not encapsulated in the cavity of the cavitand. The resulting inclusion compounds are rather stable, which enables one to isolate and structurally characterise these compounds. For instance, the structure of the compound of CB8 with the unsymmetrical guest, viz., the cation of carboxybenzylviologen $\text{CH}_3\text{N}^+\text{C}_{10}\text{H}_8\text{N}^+\text{CH}_2\text{C}_6\text{H}_4\text{CO}_2\text{H}$, was established by X-ray diffraction analysis (Fig. 3.3). The methylpyridine fragment of this cation and the naphthalene ring of 2,6-dihydroxynaphthalene serving as the electron donor are located in the cavity virtually parallel to each other at a distance of 3.4 Å. This confirms the occurrence of a strong interaction, which was found by spectroscopic methods.

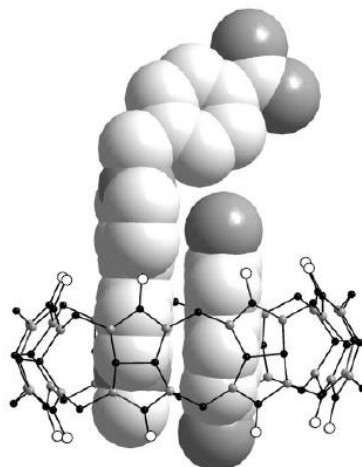
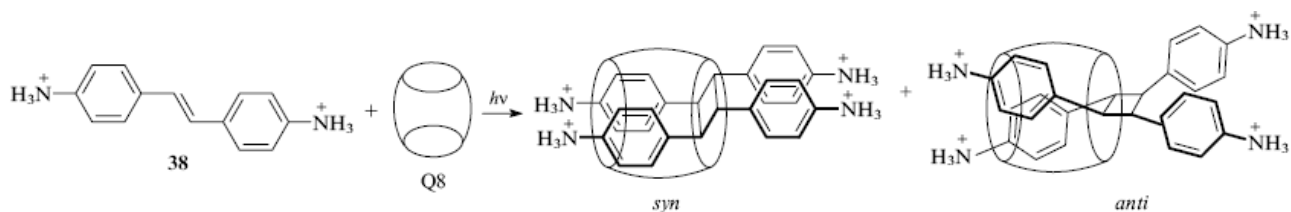


Figure 3.3: Encapsulation of 'heteroguests', viz., electron-deficient (carboxybenzylmethylviologen) and electron-donating (2,6-dihydroxynaphthalene) molecules in cucurbit[8]uril.

The ability of cucurbit[8]uril to accommodate two closely spaced guests located in particular orientations allows one to use this compound as the synthetic molecular container in which bimolecular reactions between specially selected guests can proceed with high regio- and stereoselectivity. Thus, photodimerisation between two molecules of 4,4'-diammonio stilbene dichloride **2** encapsulated into the cavity of CB8 proceeded with a much higher rate and high stereoselectivity (0.5 h, the ratio *syn* : *anti* > 95 : 5) as compared, for example, with this reaction in the presence of γ -cyclodextrin (72 h, the ratio *syn* : *anti* ~ 4 : 1). According to the ^1H NMR spectroscopic data, CB8 forms a stable inclusion compound with two molecules **2** in solution even if the starting reagents are taken in a ratio of 1 : 1. In this case, the guests can occupy only particular positions, viz., with the parallel orientation of the alkene groups involved in photodimerisation (Scheme 3.2).



Scheme 3.2

Owing to rather rigid structures and the ability to include various molecules and ions, cucurbiturils are very attractive compounds both as synthetic receptors and convenient building

blocks for the construction of supramolecular materials. The detailed study of supramolecular compounds based on the known cucurbiturils is hindered, in particular, by their very low solubilities in water and organic solvents. Because of this, the most promising line of investigation of the chemistry of these compounds is the development of procedures for the preparation of soluble derivatives by the insertion of substituents containing different functional groups. One approach to the solution of this problem involves the synthesis of cucurbiturils by condensation of substituted glycolurils whose bridging CH groups contain either alkyl or aryl substituents instead of hydrogen atoms. However, decamethylcucurbit[5]uril containing peripheral methyl groups, which was synthesised from dimethylglycoluril, also appeared to be a poorly soluble compound. The synthesis of cucurbiturils consisting of five or six cyclohexanoglycoluril fragments is the first success after years of failed attempts. The resulting compounds were reliably characterised by different methods, among them X-ray diffraction analysis. The cyclohexane fragments formed by two carbon atoms of glycoluril and four methylene units are located at the periphery of cucurbiturils. The sizes of the cavities and portals are only slightly different from those in the unsubstituted analogues. These compounds are readily soluble in water, methanol and DMSO and moderately soluble in ethanol, DMF and acetonitrile. Good solubility in organic solvents enables one to use cyclohexanocucurbit[n]urils ($n=5, 6$) as membrane ion-selective electrodes. Cyclohexanocucurbit[6]uril dissolved in water can be used for highly selective isolation of acetylcholine (neurotransmitter).²³

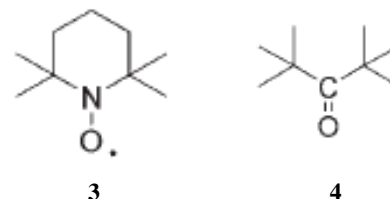
As we have shown in chapter 2, the formation of a host–guest complex can be studied very conveniently with EPR spectroscopy by the use of an appropriate radical probe. Benzyl tert-butyl nitroxide and related dialkyl nitroxides were found to be very suitable probes to investigate host–guest interactions in cyclodextrins,[20] calixarenes,[21] micelles[22] and protected nanoparticles.[23] Evidence for the formation of paramagnetic complexes between these radicals and the host systems was provided by large spectral changes caused by the different environments experienced by the radical guest, and to conformational changes occurring upon complexation. In most cases, the EPR spectra also showed a strong linewidth dependence on temperature, indicating that the lifetime of nitroxides in the associated and free

form is comparable to the EPR timescale; this enabled us to measure the rate constants for the association and dissociation processes.

On this basis, we decided to employ EPR spectroscopy to explore the binding properties of the cucurbit[7]uril host.

3.3 EPR studies of 2,2,6,6-tetramethyl piperidine-N-oxyl (TEMPO, **3**)

When CB7 is added to a solution of TEMPO **3** in water, the high-field line in the EPR spectrum splits into two well-separated components that we assign to the free and complexed radical exchanging slowly on the EPR



timescale (Figure 3.4). The complexed guest showed distinctly smaller nitrogen hyperfine splitting (16.20 G) and larger g -factor (2.0064) values than the corresponding free species (a_N 017.30 G, g =2.0056). Although this effect is expected because of the less polar environment experienced by the NO group within the CB7 cavity,²⁴ the spectral resolution of the signals due to the free and included radical is much higher than that generally observed in water with other macrocyclic host, such as cyclodextrins or calixarenes.²⁵

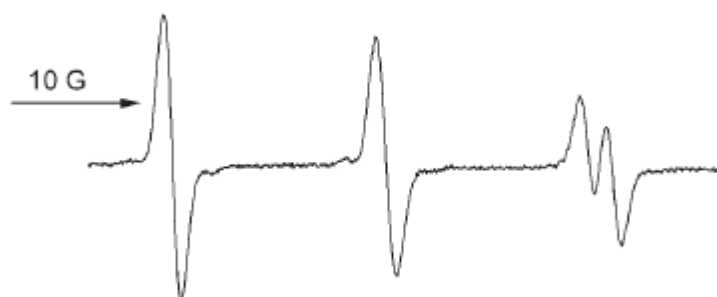


Figure 3.4: EPR spectrum of **3** (0.1 mM) recorded in the presence of CB7 (0.20 mM) at 298 K.

This observation can be justified by assuming that the NO group of the nitroxide is deeply immersed in the CB7 cavity, thus experiencing the hydrophobic environment of the inner part of the cavity. In fact, calculated molecular models for the CB7@**3** complex (AMBER Force Field as provided in the Macromodel 7.0 package) show that the guest is inserted in a symmetrical fashion with the NO group lying on the plane passing through the equatorial

carbon–carbon bonds of the host and with the geminal methyl groups pointing toward the carbonyl portals (Figure 3.5).

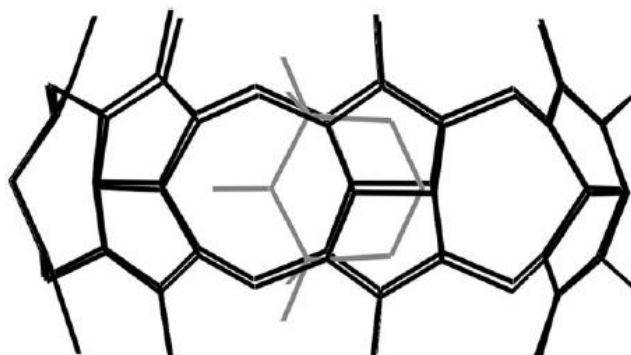


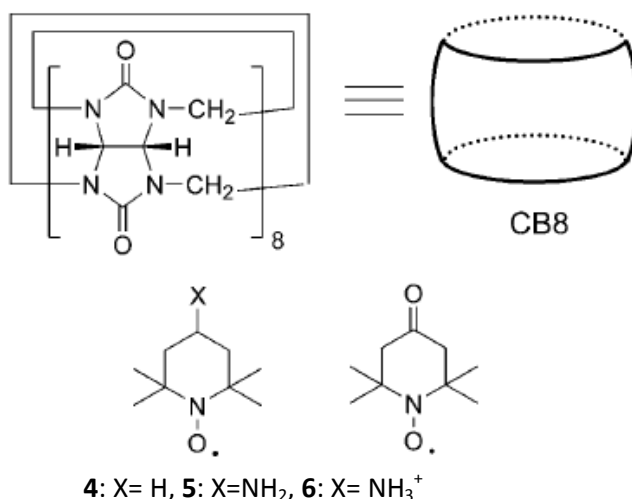
Figure 3.5: Molecular mechanics-minimised structure of the CB7@3 complex. Hydrogen atoms have been omitted for clarity.

Further evidence for the correct assignment of the geometry of the CB7@3 complex is obtained by measuring NOE interactions in the complex formed by CB7 and di-tert-butyl ketone **4**, an alicyclic sterically hindered diamagnetic analogue of TEMPO. ROESY spectra of aqueous solutions of **4** containing a large excess of CB7 show significant NOE interactions of the methyl protons of the tert-butyl groups of the guest molecule with the methylene hydrogen of the macrocyclic host pointing toward the carbonyl portals and resonating at $\delta=5.77$ ppm. This demonstrates that the guest is lodged in the host cavity with the methyl groups very close to the carbonyl rims.

Simulation of the EPR spectra recorded at different concentrations of the macrocyclic host provides a value of $25\,000 \pm 2000\text{ M}^{-1}$ for the binding constant K_1 for TEMPO complexation (Table 2). This is one order of magnitude larger than that measured for the same guest with β -cyclodextrin (2950 M^{-1}).²⁶ The huge enhancement of the affinity constant should be attributed to the larger equatorial width of CB7 that allows total inclusion of the paramagnetic guest inside the internal cavity as previously discussed. On the other hand, the narrower internal cavity of β -CD cannot easily accommodate the radical guest with the N-O bond perpendicular to the long axis of the macrocyclic ring, thus leaving the N-O group in the complexed radical exposed to bulk water.

3.4 EPR studies of 4-amino-2,2,6,6-tetramethyl piperidine-N-oxyl (tempamine, **6**)

CB8 is known to be essentially insoluble in water.²⁷ Because of this, mixing an aqueous solution containing **4**, **6** or benzyl tert-butyl nitroxide, generated in situ by oxidation of the parent amine,²⁸ with CB8 did not give rise to any EPR signal from the radical included in the macrocycle ligand, which remained as an undissolved solid.



Scheme 3.2

On the other hand, complete solubilisation of CB8 was observed when CB8 was dissolved in an aqueous solution containing **6**.²⁹ In practice, a powder of CB8 (6.6 mg, 5×10^{-3} mmol) was suspended in a solution of **6** (1 mg, 5.0×10^{-3} mmol) in H₂O (1.0 mL) and stirred for 1 h at room temperature. After filtration the solution was diluted with H₂O (9 mL) and used for EPR spectroscopy measurements. The EPR spectrum of this solution, given in Figure 3.6a, was nicely simulated by assuming the presence of three different species.

The first species is characterised by the coupling of the unpaired electron with a nitrogen nucleus with a hyperfine splitting constant (*hfsc*) of 16.97 G ($g=2.0056$) and is due to the radical dissolved in bulk water (**6**_{water}). The second species shows three lines with $a_N=16.47$ G and $g=2.0058$, which indicates that the nitroxide is experiencing a less polar environment than water. This species was identified as the inclusion complex of the radical with the macrocyclic CB8 with a 1:1 stoichiometry (**6**_{CB8}), in equilibrium with the free nitroxide. It is very likely

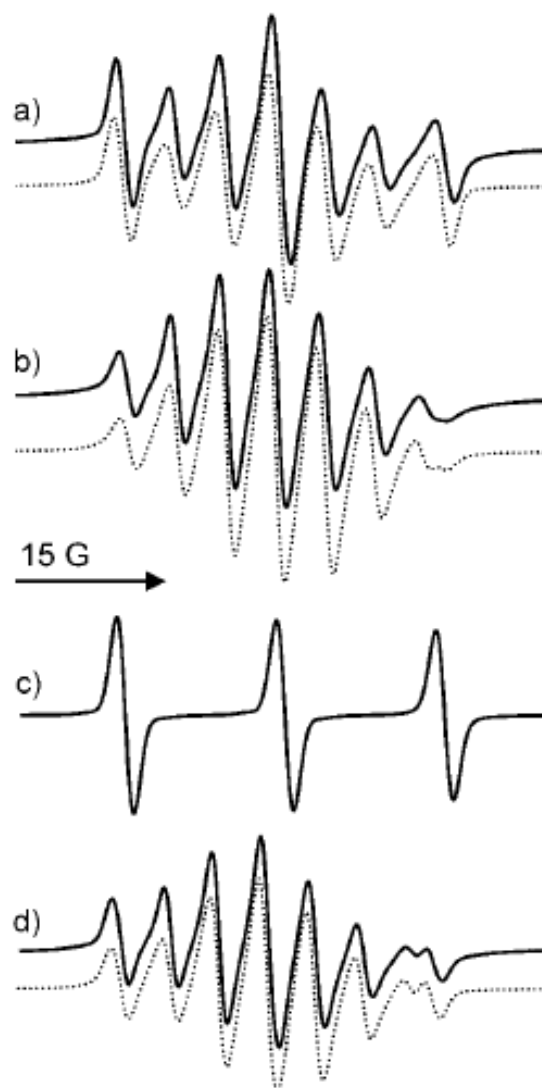


Figure 3.6: Experimental (solid lines) and simulated (dotted lines) EPR spectra of **6** in the presence of CB8: a) initial solution; b) fibres redissolved in water containing 1 mM NaCl; c) in the presence of anilium chloride at pH 3 and d) at pH~7. The simulations were obtained by using the reported relative amounts of nitroxidic species.

this complex is much more soluble than free CB8, thereby “pulling” CB8 into solution.

The formation of a strong complex between nitroxide **6** and CB8 is expected on the basis of the strong interaction between the ammonium site and the carbonyl oxygen atoms of CB8, as already found with protonated amines.³⁰

We have previously shown that in the presence of CB7, radical **4** is forced to be inserted symmetrically inside the macrocycle with the NO group lying on the plane passing through the equatorial carbon–carbon bonds of the host and with the geminal methyl groups pointing toward the carbonyl portals.³¹ Evidence for this was obtained from the strong reduction of the

nitrogen splitting (0.9 G) observed when passing from water to the complex. In the present case, the smaller difference between a_N for the free and included radical indicates that the nitroxide moiety is experiencing a more polar environment than in the complex 4@CB7. Moreover, the larger size of the cavity and the presence of a strong interaction between the ammonium cation and the carbonyl groups should favour a geometry in which the longer axis of the nitroxide is parallel to the short principal axis of the macrocycle (Figure 3.7).

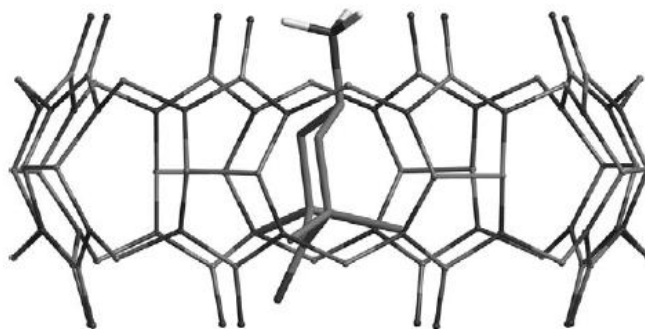


Figure 3.7: Plausible geometry of the complex 6@CB8.

All these observations suggest that a plausible geometry of the complex might be that shown in Figure 3.7.

The signals due to the third species were instead completely unexpected and consisted of seven equally spaced hyperfine lines separated by 5.1 G ($g=2.0063$) with a relative intensity of 1:3:6:7:6:3:1. It should be noted that this species has never been observed with the smaller macrocycle CB7. We assign this spectrum to a nitroxide triradical in which each electron divides its time equally between the three nitrogen nuclei (6_{trimer}). The a_N hyperfine coupling line separation of 5.1 G = $a_N/3$, that is, $a_N=15.3$ G is similar to the value generally measured for a sterically hindered nitroxide experiencing a hydrophobic environment.

The spectral shape also indicates an exchange-coupled nitroxide triradical with an exchange interaction greater than a_N , $|J/g\mu_B| \gg |a_N|$. Since the three radicals are not directly linked through a C=C π -system framework, we assume that the spin exchange between the three nitroxide units is operating through space due to the formation of a noncovalent supramolecular organisation (see below). This spectrum is compatible with a radical showing three electron spin exchanges (J_{12} , J_{13} and J_{23}) in which the three spins are placed either in a symmetric triangular arrangement ($J_{12}=J_{13}=J_{23}$)[18] or in linear fashion ($J_{12}=J_{13} \neq J_{23}$).³²

Slow cooling of the aqueous solution containing CB8 and **6** from room temperature to 5 °C led to the formation of a long fibrous network with fibre lengths of the order of a few millimetres, as shown by the optical microscope image in Figure 3.8. The presence of nitroxide radicals in the fibres was demonstrated by EPR spectroscopy both in solution and in the solid state. Figure 3.6b shows the EPR spectrum obtained when dried fibres were redissolved in water containing a small amount of NaCl (1 mM) at room temperature. An excellent numerical fitting to a single species, that is, the nitroxide triradical, was obtained (>96%) for such a spectrum.

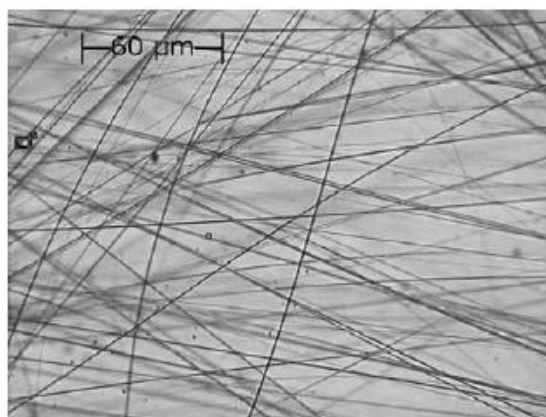


Figure 3.8: Optical microscope image of fibres containing CB8 and **6**.

The EPR spectrum of randomly oriented solid fibres recorded at 77 K (Figure 3.9) is characteristic of a polyradical since it shows a weak $|\Delta_{ms}|=2$ transition [20] and a strong $|\Delta_{ms}|=1$ line of unusually large spectral width (ca. 70 G), that is much broader than that of bulk TEMPO (13 G). Actually the $|\Delta_{ms}|=1$ transition is interpreted as the superposition of unresolved symmetrically disposed broad peaks, separated by the zero-field splitting interaction.

By using the point dipole approach and $D'=35$ G we made a crude estimate of the distance between the unpaired electrons as 9.4 Å.³³ This value is compatible with an intermolecular dipole–dipole interactions between nitroxide radicals aligned by closed molecular packing in 1D channels of cucurbituril.

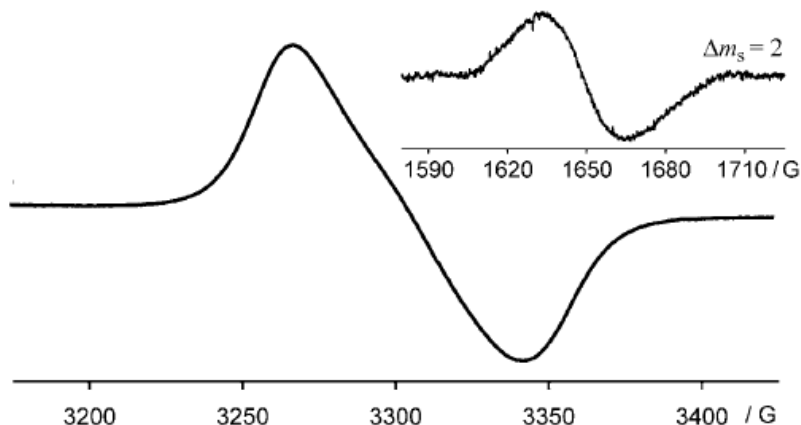


Figure 3.9: EPR spectra at 77 K of randomly oriented fibres containing CB8 and **6**.

Cucurbiturils are known to form fibres. Actually Kim and co-workers have shown that molecules of CB7 are able to aggregate through strong interactions between CB portals and hydronium ions, as well as between CB7 molecules themselves. Bardelang et al. have reported that molecules of CB8 are able to form water-filled channels consisting of one-dimensional macrocycle nanotubes.³³ In the same way, we can suppose that mixing of **6** with CB8 may lead to the formation of a supramolecular organisation of the macrocyclic hosts containing radical units that assemble into a long fibril, which in turn bundles into a thick fibre to form the fibrous network: the nitroxide behaves as glue to form a linear building unit the length of which remains to be determined.

The noncovalent and reversible nature of the triradical was evidenced by following the EPR spectral variations observed by addition of anilinium chloride in the pH range from 3 to 7, as illustrated in Figure 3.6. Around pH 3 the EPR spectrum of a solution containing CB8 (0.9 mM), **6** (1 mM) and anilinium chloride (2 mM) (Figure 3.6c) showed only the signals due to the radical dissolved in water, this being an indication that the radicals are completely displaced from the macrocyclic cavity by the aromatic ammonium cation. When increasing the basicity of the solution to pH~7 with NaOH, the signal due to the radical in water was suppressed and the spectra of the monoradical complex and of the triradical were instead observed (see Figure 3.6d). This observation strongly suggests that the deprotonated aniline ($pK_a=4.6$) is released from the cavity being replaced by the nitroxide guests.

3.5 References

1. R. Behrend, E Meyer, F Rusche *Liebigs Ann. Chem.* **1905**, 339.
2. W. A. Freeman, W. L. Mock, N-Y. Shih *J. Am. Chem. Soc.* **1981**, *103*, 7367.
3. P. Cintas *J. Incl. Phenom. Mol. Rec. Chem.* **1994**, *17*, 205.
4. H-J. Buschmann, E Cleve, E Schollmeyer *Inorg. Chim. Acta* **1992**, *193*, 93.
5. P. Germain, J. M. Letoffe, M. P. Merlin, H. J. Buschmann *Thermochim. Acta* **1998**, *315*, 87.
6. A. Flinn, G. C. Hough, J. F. Stoddart, D. J. Williams *Angew. Chem., Int. Ed. Engl.* **1992**, *31*, 1475.
7. J. Kim, I-S. Jung, S-Y. Kim, E. Lee, J-K. Kang, S. Sakamoto, K. Yamaguchi, K. Kim *J. Am. Chem. Soc.* **2000**, *122*, 540.
8. A. Day, A. P. Arnold, R. J. Blanch, B. Snushall *J. Org. Chem.* **2002**, *66*, 8094.
9. K. S. Oh, J. Yoon, K. S. Kim *J. Phys. Chem. B* **2001**, *105*, 9726.
10. K. A. Kellersberger, J. D. Anderson, S. M. Ward, K. E. Krakowiak, D. V. Dearden *J. Am. Chem. Soc.* **2001**, *123*, *11*, 316.
11. K. Jansen, H-J. Buschmann, A. Wego, D. Dopp, C. Mayer, H-J. Drexler, H-J. Holdt, E. Schollmeyer *J. Incl. Phenom. Macrocycl. Chem.* **2001**, *39*, 357.
12. H. J. Buschmann, E. Cleve, K. Jansen, A. Wego, E. Schollmeyer *J. Incl. Phenom. Macrocycl. Chem.* **2001**, *40*, 117.
13. X. X. Zhang, K. E. Krakowiak, G. P. Xue, J. S. Bradshaw, R. M. Izatt *Ind. Eng. Chem. Res.* **2000**, *39*, 3516.
14. R. Blanch, A. Arnold, A. Sleeman, T. White, A. Day, in *Proceedings of the World Chemistry Congress, Brisbane*, **2001** p. A32
15. C. Marquez, W. M. Nau *Angew. Chem., Int. Ed. Engl.* **2001**, *40*, 4387.
16. S-Y. Kim, I-S. Jung, E. Lee, J. Kim, S. Sakamoto, K. Yamaguchi, K. Kim *Angew. Chem., Int. Ed. Engl.* **2001**, *40*, 2119.
17. A. I. Day, R. J. Blanch, A. P. Arnold, S. Lorenzo, G. R. Lewis, I. Dance *Angew. Chem., Int. Ed. Engl.* **2002**, *41*, 275.
18. S. Lorenzo, A. Day, D. Craig, R. J. Blanch, A. P. Arnold, I. Dance *Cryst. Eng. Commun.* **1** **2001**
19. S. Lorenzo, A. Day, I. Dance, P. Turner, R. Blanch, A. Arnold, J. McMurtrie, in *Proceedings of the World Chemistry Congress, Brisbane*, **2001** p. OFB12
20. K-C. Zhang, T-W. Mu, L. Liu, Q-X. Guo *Chinese J. Chem.* **2001**, *19*, 558.
21. H. J. Kim, J. Heo, W. S. Jeon, E. Lee, J. Kim, S. Sakamoto, K. Yamaguchi, K. Kim *Angew. Chem., Int. Ed. Engl.* **2001**, *40*, 1526. 107. S Y Jon, Y H Ko, S H Park, H-J Kim, K Kim *Chem. Commun.* 1938 (2001)
22. J. Zhao, H-J. Kim, J. Oh, S-Y. Kim, J. W. Lee, S. Sakamoto, K. Yamaguchi, K. Kim *Angew. Chem., Int. Ed. Engl.* **2001**, *40*, 4233.
23. O. A. Gerasko, D. G. Samsonenko, V. P. Fedin *Russian Chem. Rev.* **2002**, *71* (9), 741-760.
24. For examples, see: a) R. Briere, H. Lemaire, A. Rassat, *Bull. Soc. Chim. Fr.* **1965**, 3273 – 3283; b) B. R. Knauer, J. J. Napier, *J. Am. Chem. Soc.* **1976**, *98*, 4395 – 4400. Recent review on the effect of solvent in determining the hyperfine coupling constants of free radicals: c) R. Improta, V. Barone, *Chem. Rev.* **2004**, *104*, 1231 – 1254.
25. For a review, see: P. Franchi, M. Lucarini, G. F. Pedulli, *Curr. Org. Chem.* **2004**, *8*, 1831 – 1849.
26. a) J. Martinie, J. Michon, A. Rassat, *J. Am. Chem. Soc.* **1975**, *97*, 1818 – 1823; b) M. Okazaki, K. Kuwata, *J. Chem. Phys.* **1984**, *88*, 3163 – 3165.
27. J. Lagona, P. Mukhopadhyay, S. Chakrabarti, L. Isaacs, *Angew. Chem.* **2005**, *117*, 4922 – 4949; *Angew. Chem. Int. Ed.* **2005**, *44*, 4844 – 4870.
28. M. Lucarini, B. Luppi, G. F. Pedulli, B. P. Roberts, *Chem. Eur. J.* **1999**, *5*, 2048 – 2054.
29. Preparation of **6** was performed by addition of HCl to **5**.
30. C. Marquez, R. R. Hudgins, W. M. Nau, *J. Am. Chem. Soc.* **2004**, *126*, 5806 – 5816.
31. E. Mezzina, F. Cruciani, G. F. Pedulli, M. Lucarini, *Chem. Eur. J.* **2007**, *13*, 7223 – 7233.
32. E. Sartori, C. Corvaja, S. Oancea, F. Formaggio, M. Crisma, C. Toniolo, *ChemPhysChem* **2005**, *6*, 1472 – 1475.
33. D. Bardelang, K. A. Udachin, D. M. Leek, J. A. Ripmeester, *Cryst Eng Comm* **2007**, *9*, 973 – 975.

CHAPTER 4

PARAMAGNETIC SUPRAMOLECULAR ARCHITECTURES DERIVED FROM GUANOSINE

4.1 Introduction

Nature's use of a simple genetic code to enable life's complex functions is an inspiration for supramolecular chemistry. DNA nucleobases carry the key information utilizing a variety of cooperative and non-covalent interactions such as hydrophobic, van der Waals, π - π stacking, ion-dipole and hydrogen bonding.

Guanosine analogs, with their self-complementary hydrogen-bonding edges and aromatic surfaces, are programmed to self-associate. Guanine has two hydrogen bond acceptors (N7 and O6) on its Hoogsteen face and two hydrogen bond donors (N1 amide and N2 amino) on its Watson-Crick face (Figure 4.1).

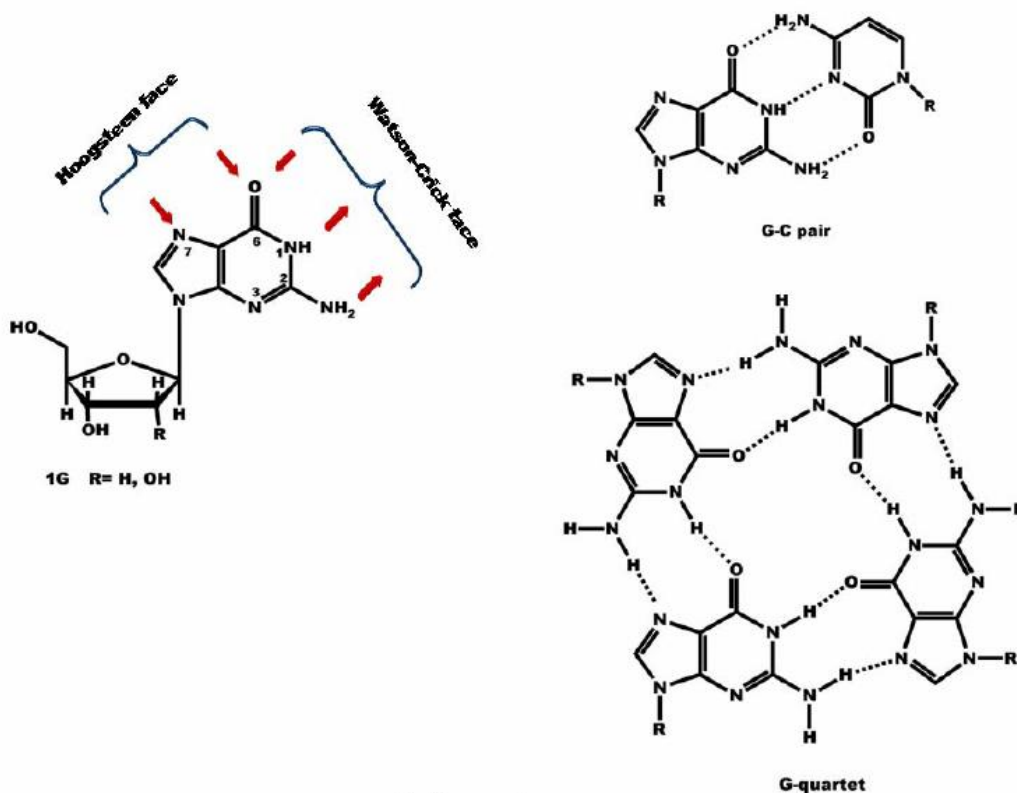


Figure 4.1

Depending on the conditions, guanosine derivatives can selfassociate into dimers, ribbons, or macrocycles. These hydrogen-bonded structures can stack in solution due to their polarized aromatic surfaces.

Based on fiber diffraction data of the 5'-GMP hydrogels, Gellert and colleagues proposed that the G-quartet was formed by 8 intermolecular hydrogen bonds between complementary Watson-Crick and Hoogsteen edges of neighboring guanines (Figure 4.1).¹ A decade later, Pinnavaia and colleagues reported that G-quartets are stabilized by Na⁺ and K⁺. These cations coordinate to the four carbonyl oxygens in each G-quartet (Figure 4.2).²

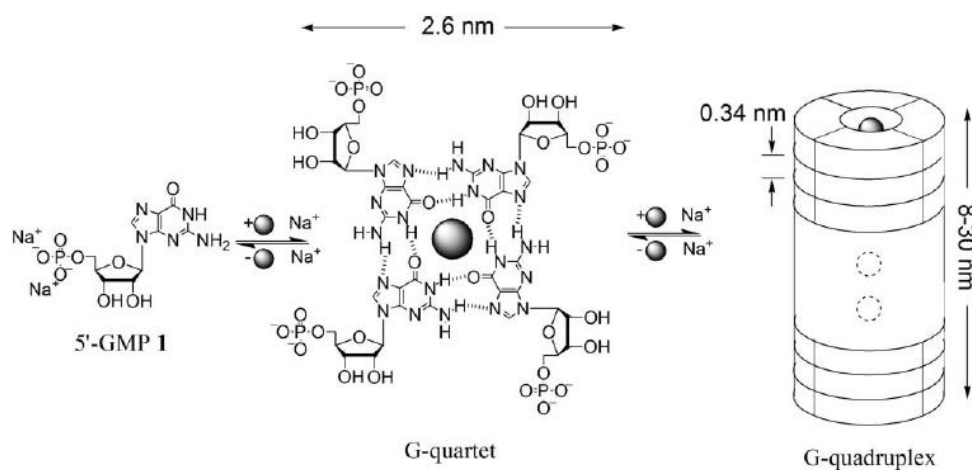


Figure 4.2: G-quadruplex cylinder formed by self-assembly of 5'-GMP 1.

4.2 Recent studies on the molecular self-assembly of lipophilic guanosine analogs

In 1995, Gottarelli, Spada and colleagues reported that 3',5'-didecanoyl-2'-dG **2** extracts K⁺ picrate from water into CDCl₃ to give a discrete octamer [dG **2**]₈•K⁺ Pic⁻.³ The K⁺ cation was essential for formation of this lipophilic octamer (Figure 4.3).

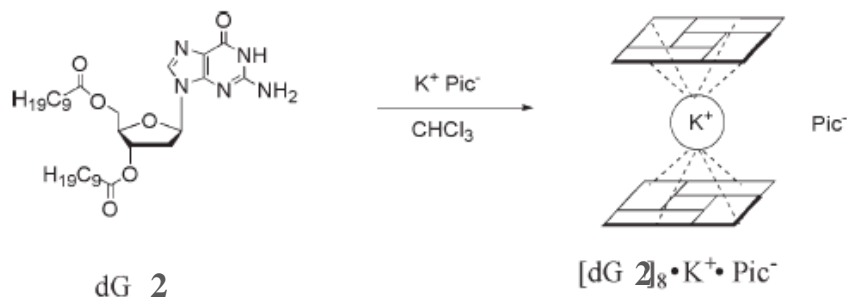


Figure 4.3: Lipophilic [dG 3]₈•K⁺ octamer formed by extraction of K⁺ picrate from water.

Without templating cations, dG **2** organized into two different hydrogen-bonded ribbons.⁴ Changing the sugar substituents or the solvent modulated the ribbon's hydrogen bonding pattern (giving ribbon A or B as in Figure 4.4).

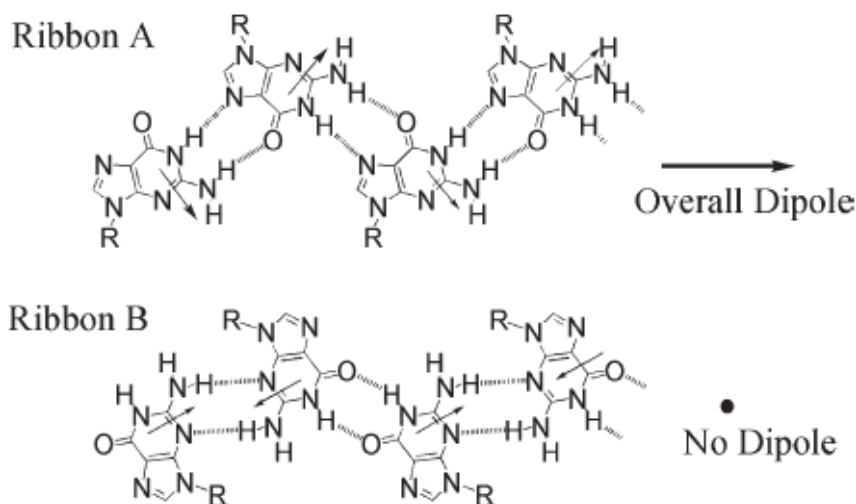


Figure 4.4: Two different H-bonded ribbons formed by self-assembly of lipophilic dG **2** in absence of cations. Ribbon A has a net dipole, whereas ribbon B contains no dipole.

To better understand how individual G-quartets organize within G-quadruplexes, the Gottarelli and Davis groups solved the NMR structure of [dG **2**]₈•KI in CDCl₃.⁵ This study showed that the octamer [dG **2**]₈•KI existed as a single diastereomer with the templating K⁺ sandwiched between an all-anti G-quartet and an all-syn G-quartet. In 2000, an X-ray structure illustrated that lipophilic G-quadruplexes are formed in high diastereoselectivity in organic solvents.⁶ The lipophilic G-quadruplex [G **3**]₁₆•3K⁺•Cs⁺•4pic⁻ consists of 4 stacked G-quartets. The complex was generated when 5'-silyl-2', 3'-isopropylidene G **3** was used to extract K⁺ picrate from water into CH₂Cl₂ (Figure 4.5). Diffraction-quality crystals of the lipophilic G-quadruplex were grown from acetonitrile. This G-quadruplex can be described as a pair of head-to-tail [G **3**]₈ octamers with each G8-octamer using its 8 carbonyl oxygens to coordinate a K⁺ ion. A third K⁺ ion holds the two [G **3**]₈ octamers together and a Cs⁺ cation caps the structure. The G-quartets within [G **3**]₁₆•3K⁺•Cs⁺•4pic⁻ showed π - π stacking separations of

3.3–3.4 Å. In addition to stabilization by cations, four picrate anions form hydrogen bonds to N2 amino groups that extend from the two “central” G-quartets.

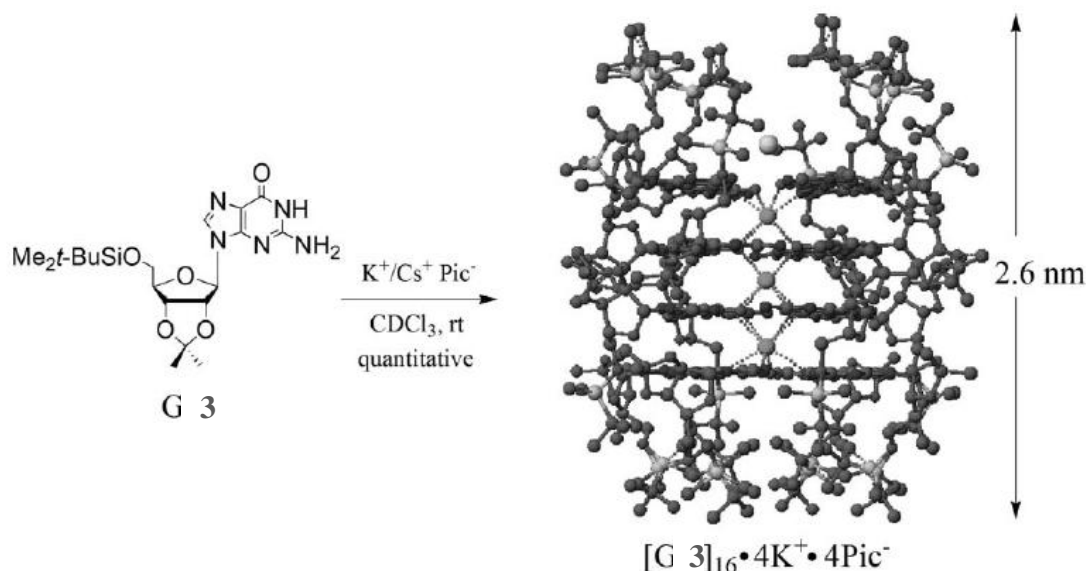


Figure 4.5: Crystal structure shows that cation-templated self-assembly of 16 equiv. of G 3 gives a lipophilic G-quadruplex $[\text{G } 3]_{16} \cdot 3\text{K}^+/\text{Cs}^+ \cdot 4\text{Pic}^-$.

The lipophilic G-quadruplex looks like a cation channel with an anionic belt wrapped around its middle. As described below, these lipophilic G-quadruplexes can be used as models for DNA G-quadruplexes and for the development of functional nanostructures.

Furthermore, the identity of the bound cations also controls the solution properties of these lipophilic G-quadruplexes. For example, G-quadruplexes containing divalent cations such as Ba^{2+} or Sr^{2+} are thermodynamically and kinetically more stable than G-quadruplexes that contain monovalent Na^+ or K^+ .⁷ Davis and colleagues attributed this enhanced stability in the presence of divalent cations to stronger ion–dipole interactions between the cations and the nucleobase oxygens, as well as to a strengthening of the G-quartet’s hydrogen bonds. The studies showed that both the cation and anion influence the stability of these lipophilic G-quadruplexes.

4.3 Lipophilic guanosine assemblies not templated by ions

As anticipated from the discussion in Section 4.2, lipophilic guanosine derivatives self-assemble into linear ribbon-like motifs in the absence of alkali cation templates (Figure 4.4). These ribbon structures in solution were identified mainly by NMR⁸ and, in the solid state, by

single crystal X-ray diffraction.⁹ Lipophilic guanosines are able to form lyotropic mesophases in several solvents. For example, dG **2** in hexadecane gives, above a critical concentration, a viscous birefringent (LC) phase. X-ray diffraction measurements gave narrow Bragg reflections whose reciprocal spacing is indicative of a two-dimensional square packing of extended hydrogen-bonded elements with the alkyl chains and solvent molecules filling the lateral gap between the tapes.⁹

4.4 Guanosine Derivatives Functionalised with Open-Shell Units

Switching of the spin-spin interactions in organic radicals is of particular interest for the development of molecular-scale magnetic devices.¹⁰ When the spin exchange occurs only through-space, complete control of this interaction can be obtained by modifying the spatial arrangement of radical centres.¹¹ As it is possible to functionalise the guanosines in the 8 position and/or at the sugar hydroxy functions, they are ideal scaffolds to locate functional units in pre-programmed positions, inside highly ordered architectures.

The ability of guanosine derivatives to self-assemble has been exploited for modulating the electron spin-spin exchange interaction of nitroxyl probes, in particular we report on a guanosine derivative functionalised with the persistent radical unit 4-carbonyl-2,2,6,6-tetramethylpiperidine-1-oxyl (**4**).

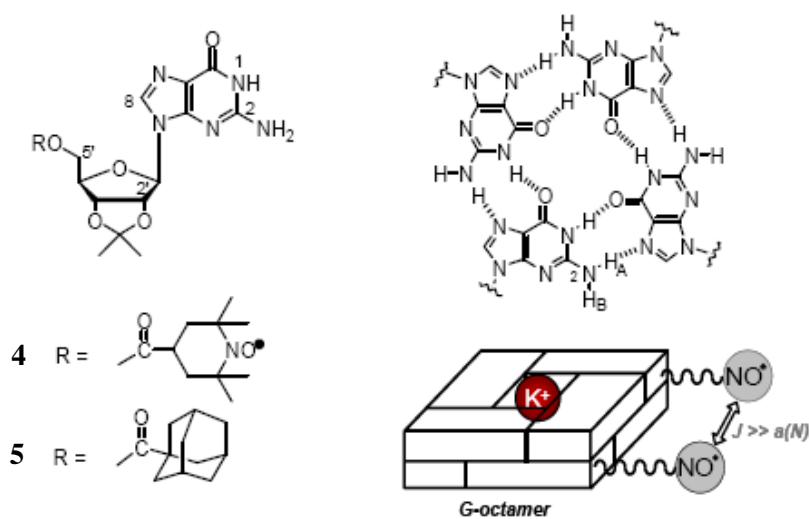


Figure 4.6: The molecular structures of guanosines **4** and **5**, the G-quartet motif and the D_4 -symmetric stacking of two G-quartets (templated by a cation).

While **4** in solution has no particular intermolecular spin-spin interactions, in the presence of potassium ions this compound can form a D_4 -symmetric octameric assembly $[\mathbf{4}_8\text{K}]^+$ in which the nitroxyl moieties show a weak electron spin-spin exchange interaction (Figure 4.6). Since the relative geometry of the radicals is the outcome of K^+ -directed self-assembly, the spin-spin interaction can be suppressed by removing the alkaline ion. To the best of our knowledge, the system described here is the first example of a reversible introduction-suppression of spin-spin exchange in a self-recognising and self-assembling molecule controlled by the addition/removal of a templating cation.

Circular dichroism (CD) was initially employed to prove the self-assembly of **4** to give quartet-based structures in CHCl_3 . Figure 4.7 shows CD spectra of solutions of **1** recorded before (trace a) and after (trace b) solid-liquid extraction of potassium picrate (K-Pic). In the presence of K-Pic an intense negative CD coupling is observed in the 250-300 nm region, this feature being diagnostic of an assembly of (at least) two G-quartets chirally rotated.^{12,13} Neither temperature (25-60°C) nor concentration (0.05-10 mM) variations do modify the intensity (and shape) of the CD spectrum, suggesting that, even in the presence of large modification of the experimental conditions, the self-assembled structure is maintained and that almost all guanosine molecules are in the assembled state.

The EPR spectrum of radical **1** (Figure 4.7, lower part) recorded in chloroform is characterised by three hyperfine lines (trace a) as normally found for a monoradical nitroxide species ($a_{\text{N}} = 15.9$ G, $g = 2.0057$). Solid-liquid extraction of potassium picrate modifies the EPR spectrum into a new spectrum containing five lines (trace b) separated by $a_{\text{N}}/2$ with the width of the second and fourth line much broader than the other ones. The observation of five equally spaced lines clearly suggests the presence in solution of an assembled species in which the nitroxyl moieties are coupled by a through-space spin-spin exchange interaction (J), with $J \gg a_{\text{N}}$. The EPR spectrum in the presence of potassium ions shows considerable narrowing of the 2nd and 4th lines when the temperature increases (Figure 4.8) this being an indication that an intramolecular motion is fast modulating the exchange interactions. However, even at 60 °C,

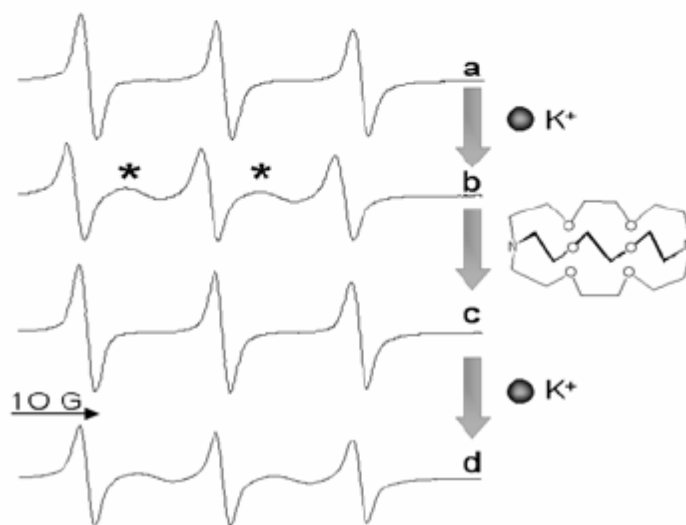
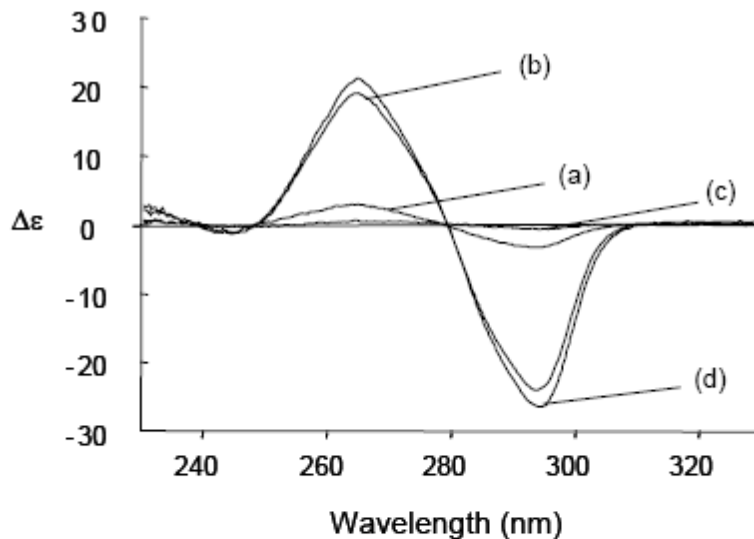


Figure 4.7: CD (top) and EPR (bottom) spectra of solutions of **4** (0.5 mM) in CHCl_3 before (a) and after (b) solid-liquid K-Pic extraction, (c) solution b after water washing and addition of [2.2.2] cryptand 0.25 mM, (d) solution c after addition of solid K-Picrate (1 mol/mol of [2.2.2] cryptand).

when the width of the 2nd and 4th lines tend to be closer to those of the outermost lines, the ratio of integrated line intensities still differs essentially from the theoretically predicted 1:2:3:2:1 ratio. The observed distribution of line intensities can be explained¹⁴ as the result of the superposition of two EPR spectra due to different paramagnetic species which are exchanging slowly in the EPR time scale: one due to a non interacting ($J = 0$) nitroxide unit while the other

is due to nitroxide fragments that can either interact ($J \gg a_N$) or not ($J = 0$) depending on their mutual orientation.¹⁵

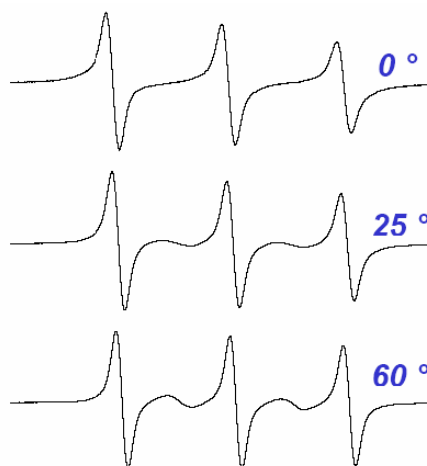


Figure 4.8: EPR spectra of **4** 0.5 mM in CHCl_3 at different temperature.

For the latter species the fast modulation of J due to the conformational freedom of the side chains carrying the nitroxide moieties is responsible of the line broadening.

Because of the presence of paramagnetic units the ^1H NMR spectra are characterised by a very low spectral resolution (see Figure 4.9, upper part). Nevertheless, some information can be inferred. In particular, after extraction of K-Pic, one amino proton N2-H_A shifts considerably from *ca.* 6.5 ppm (in DMSO $\delta = 6.6$ ppm) to 9.4 ppm (see Figure 4.9, upper part, trace b): this downfield resonance for N2-H_A is characteristic of G-quartet formation where this proton is involved in the cyclic H-bond scheme.¹⁶ The complex obtained after K-Pic extraction shows a molar ratio $1/\text{K}^+$ of 2:1 suggesting an empirical formula of $[\mathbf{1}_8\text{K}_4](\text{Pic}_4)$. On the other hand, by washing the solution with water a new species with a molar ratio $1/\text{K}^+$ of 8:1, corresponding to $[\mathbf{1}_8\text{K}](\text{Pic})$, is formed. These two 2:1 and 8:1 complexes show very similar spectral features: they have similar CD, NMR and EPR spectra (see SI).¹⁷ In spite of line broadening, both ^1H NMR spectra of the complexes with 2:1 and 8:1 molar ratio are characterised by only one set of signals: this is consistent with D_4 -symmetric octameric species (two G-quartets stacked in either a head-to-head or a tail-to tail orientation).^{18,19}

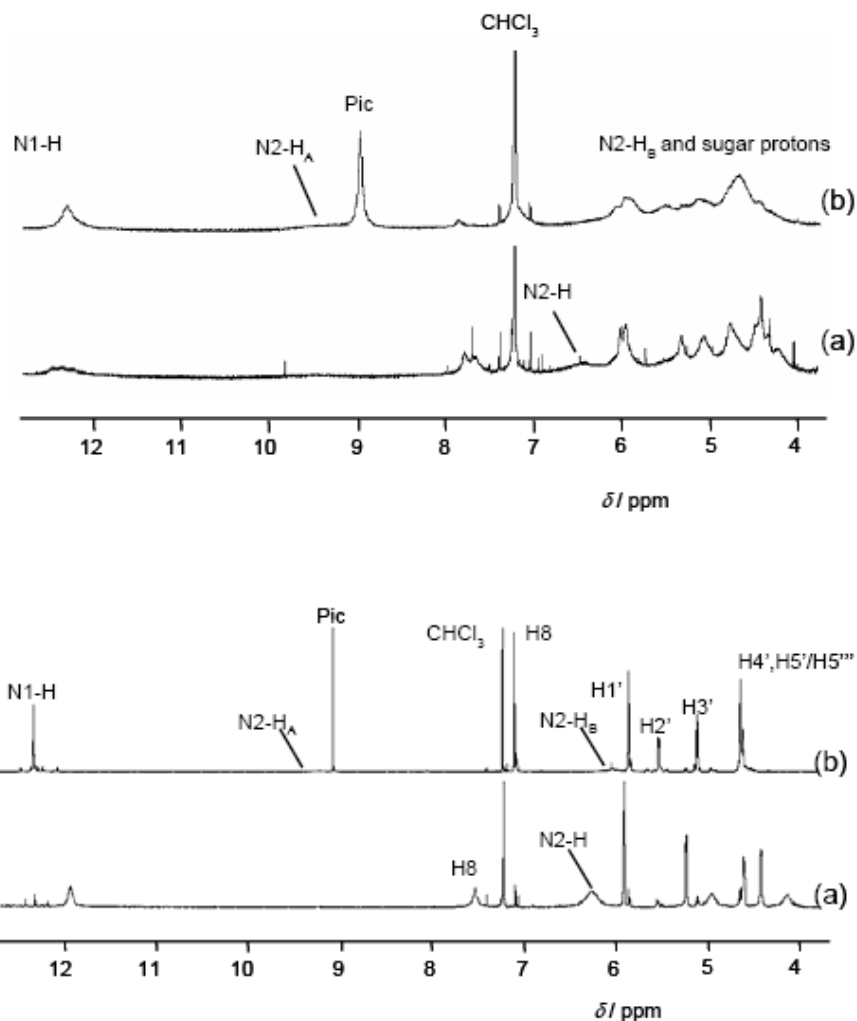


Figure 4.9: Low field portions of ^1H NMR spectra of solutions of **4**, top, and **5**, bottom (10 mM) in CDCl_3 before (a) and after (b) solid-liquid K-Pic extraction.

We also prepared and characterized compound **5** in which the paramagnetic moiety is replaced by the diamagnetic structurally related adamantyl fragment. Because of the much higher resolution of NMR spectra (Figure 4.9, lower part), a full characterisation of the assembly could be obtained for this derivative. Based on CD and NMR data we can conclude that in the presence of K^+ both derivatives **4** and **5** self associate into two stacking all-*syn* G-quartets in a tail-to-tail or head-to-head arrangement with the metal ion sitting in the central cavity, to form a D_4 -symmetric octamer. Both derivatives can associate more loosely three additional K-Pic molecules.

4.5 Self-Assembled Hexadecanitroxide

Our next challenge was to increase the spin exchange difference between the two states to obtain drastic magnetic changes before and after addition of the metal cation. We studied the self-assembly properties of derivative **7a** where two TEMPO units are connected to the guanosine deoxynucleoside at the O5' and O3' positions. This target molecule has been chosen for two reasons: (i) in the metal templated assembled species of **7a** the number of paramagnetic units doubles, possibly leading to significant enhancement of magnetic coupling; (ii) passing from ribo-guanosine (such as **6**) to 2'-deoxyguanosine derivatives, the discrete K⁺-templated assembly was expected to be C₄-symmetric (the two faces of the G-quartets are heterotopic and, in principle, the two quartets in the octamer can be arranged in three different orientations, see Figure 1, C₄-symmetric head-to-tail, and D₄-symmetric head-to-head or tail-to-tail)^{6a}, and this structural variation could originate a different (higher) spin-spin interaction.

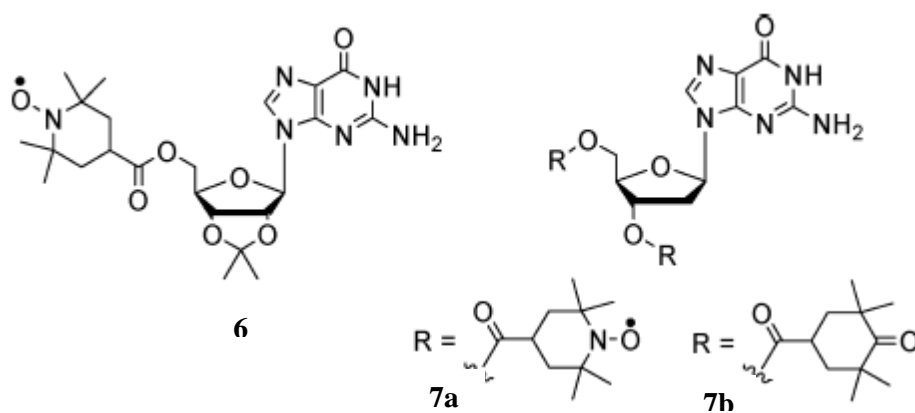


Figure 4.10

We will show that **7a**, despite the presence of two bulky substituents, forms indeed a K⁺-templated octameric assembly giving rise to very strong spin-spin interactions comparable to those observed in very concentrated monoradical solutions. This finding is consistent with the proposed structure consisting of 16 radical units confined within the complex.

Because steric hindrance potentially introduced by the double substitution in O5' and O3' could destabilize supramolecular assemblies, CD spectroscopy was initially employed to prove the self-assembly of **7a** to give quartet-based structures in CH₂Cl₂ upon K-Pic extraction.

Circular dichroism is diagnostic of either the formation of G-quartet based assemblies or the stacking polarity of two contiguous G-quartets.²⁰ In fact, the tetramers do not stack in register, but are rotated with respect to each other to give, in the 230-300 nm region, characteristic of the π - π^* transitions of guanine chromophore, a double signed exciton-like CD signal. This couplet, whose sign allows the assignment of the stacking helicity (handedness), exhibits opposite signed bands at ca. 260 and 240 nm for the head to tail (C_4 -symmetric) stacking while both bands are blue-shifted by 20-30 nm in the D_4 -symmetric stacking.²⁰ Figure 4.11 shows CD spectra of solutions of **7a** recorded before (red trace) and after (black trace) solid-liquid extraction of potassium picrate K-Pic.

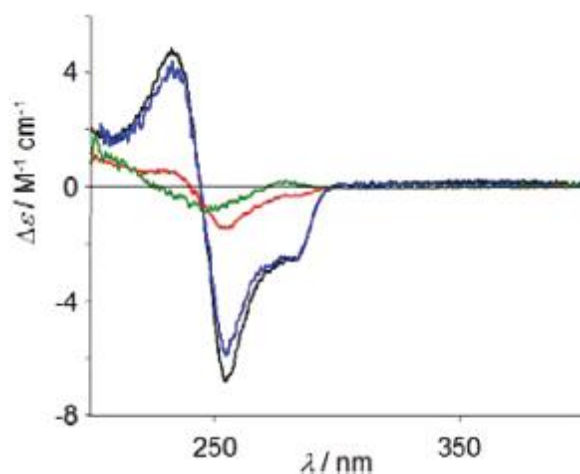


Figure 4.11: CD spectra of **7a** (5 mM) before (red line) and after (black line) K-Pic extraction. CD spectra of **2a**/K-Pic complex sample after dilution to 0.5 mM (blue line) and after addition of 4 equiv [2.2.2] cryptand (green line).

While the solution of **7a** shows a weak Cotton effect corresponding to the guanine chromophore, in the presence of K-Pic an intense negative CD coupling with the negative and positive components at around 265 and 245 nm, respectively, is observed: this feature is diagnostic of a C_4 -symmetric assembly of (at least) two G-quartets chirally rotated. Intensity and shape of the CD spectrum do not change with concentration, in the range 8-0.5 mM (see Figure 4.11, blue trace), suggesting that in these conditions the self-assembled structure is maintained. The molar ratio between **6a** and K-Pic has been determined spectrophotometrically to be >8:1. These findings suggest that the assembly is a C_4 -symmetric octamer formed by two head-to-tail stacked G-quartets.

Figure 4.12 shows ESR spectra recorded on **7a** in CH₂Cl₂ (before, trace a, and after, trace b, K-Pic extraction). In the absence of metal cations, the spectrum is characterized by three equally spaced lines with a broadening between them, this being an indication that intramolecular spin exchange is occurring.

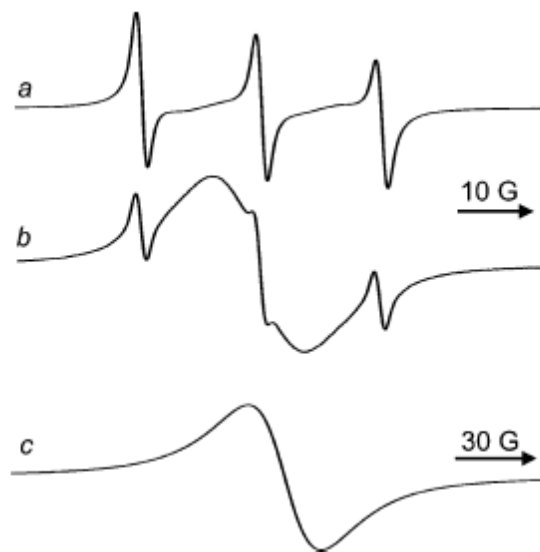


Figure 4.12: ESR spectra of **7a** (0.5 mM) before (a) and after (b) K-Pic extraction. (c) ESR spectrum recorded at 77 K in CH₂Cl₂ glass in the presence of K⁺.

In sharp contrast, the ESR spectrum recorded after solid-liquid extraction of potassium picrate shows mainly one broad signal whose integrated intensity corresponds to the initial amount of radicals. The broadening (peak to peak line width=12 G) of the signal is independent of concentration and temperature, and thus interassembly interactions and motional broadening can be discounted. This spectrum is reminiscent of those obtained from very concentrated nitroxide solutions (>0.05 M). Since the spectrum was obtained at 0.5 mM concentration, the signal broadening is ascribed to the proximity of spin centers of **7a** within the framework of the octamer. This signal may contain not only a triplet transition but also other multiplet transitions from higher spin states arising from multiple interactions between the 16 radical units. At 77 K in CH₂Cl₂ glass, the spectrum of the octamer (see Figure 4.12, trace c) showed only a featureless single peak in the $g \approx 2$ region and a weak $|\Delta ms|=2$ peak at 1660 G. The observation of a $|\Delta ms|=2$ transition also support the presence of intermolecular spin-spin interaction. However, the signal of $|\Delta ms|=2$ transition is very weak, indicating that these transition probabilities are extremely small as a result of a small D -value of the high spin-spin states from

the octamer. Accordingly to previous investigation, on symmetric tetradical, we attributed the lack of resolvable zero field splitting to the time-averaged symmetry of the complex. (Figure 4.13).

Reversible interconversion between uncomplexed and octameric forms was demonstrated by addition of four equivalents of [2.2.2] cryptand to a solution containing the assembly. Under these conditions the EPR and CD spectra returned to the original signals (see Figure 4.11, green trace). Because of the presence of two paramagnetic units, the ^1H NMR spectra of **6a** are characterized by a very low spectral resolution and their analysis turned out far more complicated than for derivative **6**. Therefore we prepared and characterized by CD and NMR compound **7b** in which the paramagnetic moiety is replaced by the closed-shell structurally related 3,3,5,5-tetramethyl-4-oxocyclohexanecarboxylate fragment. Because of the much higher resolution of NMR spectra, a full characterization of the assembly could be obtained for this derivative. The proton spectrum of a CD_2Cl_2 solution of **7b** after K-Pic extraction is characterized by the doubling of almost all of the signals. Integration of the picrate signal at 8.75 ppm and H8 signals (8.03 and 7.48 ppm) supports a 8:1 stoichiometry for the complex. The signal doubling is thus consistent with a C_4 -symmetric octamer. This is confirmed by NOESY spectra, which show the features of an octamer composed of an all-*anti* quartet stacked on top of an all-*syn* quartet in a head-to-tail relative orientation. In particular, the characteristic interquartet correlations between *syn*-H8 (7.48 ppm) and *anti*-H1' (6.43 ppm) and between *anti*-H8 (8.03 ppm) and *syn*-H5'/H5'' (4.79 and 4.53 ppm) can be observed. Shape and intensity of CD spectra of **7b** (before and after K-Pic extraction) are quite similar to those of **7a** suggesting a similar self-assembly behavior.

Based on CD and NMR data we can conclude that in the presence of K^+ both derivatives **7a** and **7b** self-associate into two stacking G-quartets in a head-to-tail arrangement with the metal ion sitting in the central cavity, to form a C_4 -symmetric octamer. To obtain a more detailed picture of the geometry of the octamer, stochastic dynamics (SD) simulations were performed by using the AMBER* force field of Macromodel 7.0 program.

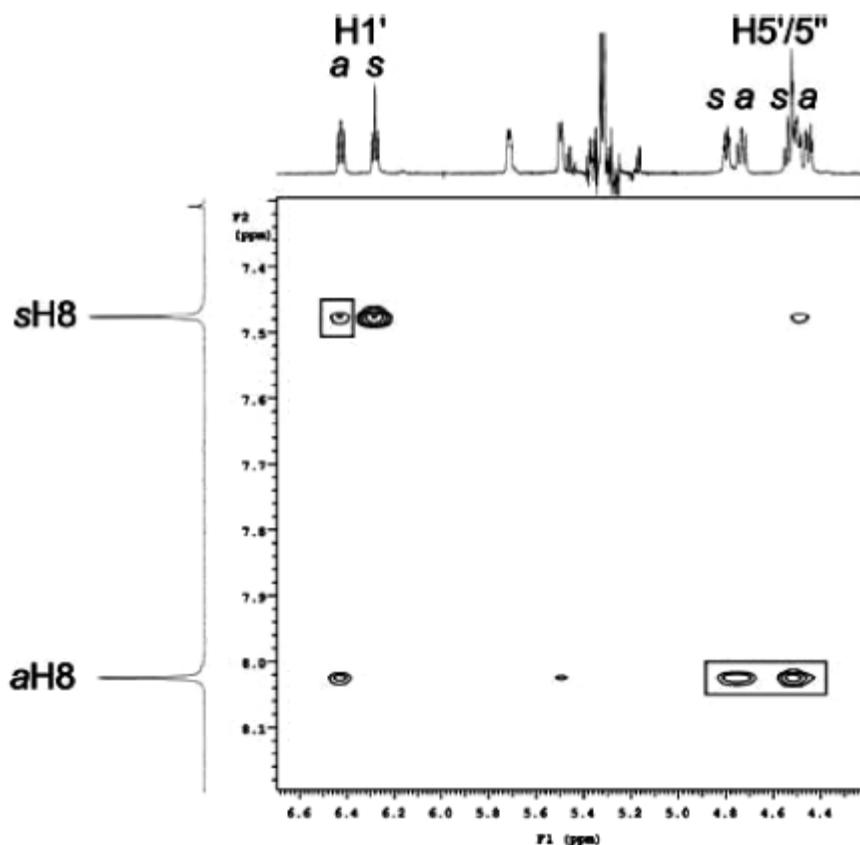


Figure 4.13: Portion of the 600 MHz NOESY spectrum of the octameric complex between **7b** and K-Pic, recorded at rt in CD₂Cl₂ (mixing time 150 ms) showing the interquartet correlations.

Initially, a Monte Carlo conformational search was carried out by rotating all rotatable bonds and by preserving all-*anti* quartet stacked on top of an all-*syn* quartet in a head-to-tail relative orientation. The most stable conformation found by this procedure was then used in the dynamic simulation. The simulations were run at 300 K with time steps of 1 fs and an equilibrium time of 500 ps before dynamic run. The total simulation time was set to 5000 ps in order to achieve full convergence. Molecular dynamics calculations (see Figure 4.14) confirm the C₄-symmetric nature of the octamer and indicate the presence of four triradical modules protruding from the two tetramers and pointing outside the assembly (in green) and a tetradical module located on top of the all-*anti* quartet (in red). In the triradical module the nitroxide are arranged in isosceles triangles. In each triangle, the distance between the oxygen atoms of the three nitroxides is in the range 9.5-10.5 and 6-7 Å, which is expected to lead to three spin-spin interactions with high *J* values. The tetradical unit is, instead, arranged in a

rombic fashion with an average distance between radical oxygen atoms of 7.5 Å, which is expected given a strong spin-spin interaction between all of them.

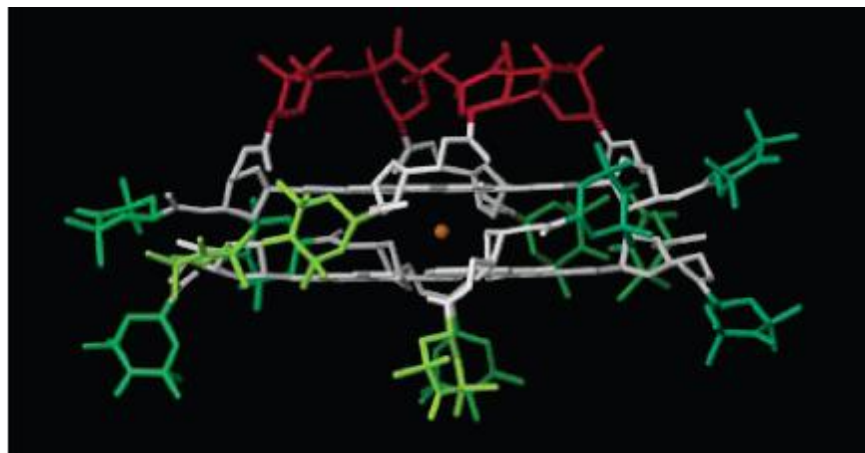


Figure 4.14: Structure of the octamer that refer to the time interval of dynamic simulation between 2000th to the 2250th ps.

Although self-assembly of a paramagnetic guanosine in the presence of alkali metal ions has already been reported, here we have shown the advantages of obtaining a supramolecular hexadecanitroxide from **7a**, a derivative with two open-shell moieties; in particular, ESR line-broadening due to dipolar and/or exchange effects is more remarkable because of increasing pathways of the radical-radical contact. The present work should be regarded as the first example of a radical-armed self-assembling scaffold showing drastic magnetic changes by addition-removal of diamagnetic alkali metal cations.²¹

4.6 References

1. M. Gellert, M. Lipsett and D. Davies, *Proc. Natl. Acad. Sci. USA* **1962**, *48*, 2013.
2. A. Wong, R. Ida, L. Spindler and G. Wu, *J. Am. Chem. Soc.* **2005**, *127*, 6990.
3. G. Gottarelli, S. Masiero and G. P. Spada, *J. Chem. Soc., Chem. Commun.*, **1995**, 2555.
4. T. Giorgi, F. Grepioni, I. Manet, P. Mariani, S. Masiero, E. Mezzina, S. Pieraccini, L. Saturni, G. P. Spada and G. Gottarelli, *Chem.–Eur. J.*, **2002**, *8*, 2143.
5. A. L. Marlow, E. Mezzina, G. P. Spada, S. Masiero, J. T. Davis and G. Gottarelli, *J. Org. Chem.*, **1999**, *64*, 5116.
6. S. L. Forman, J. C. Fettinger, S. Pieraccini, G. Gottarelli and J. T. Davis, *J. Am. Chem. Soc.*, **2000**, *122*, 4060.
7. X. D. Shi, K. M. Mullaugh, F. C. Fettinger, Y. Jiang, S. A. Hofstadler and J. T. Davis, *J. Am. Chem. Soc.*, **2003**, *125*, 10830.

8. G. Gottarelli, S. Masiero, E. Mezzina, S. Pieraccini, J. P. Rabe, P. Samorì and G. P. Spada, *Chem.–Eur. J.*, **2000**, *6*, 3242.
9. T. Giorgi, F. Grepioni, I. Manet, P. Mariani, S. Masiero, E. Mezzina, S. Pieraccini, L. Saturni, G. P. Spada and G. Gottarelli, *Chem.–Eur. J.*, **2002**, *8*, 2143.
10. Magnetism: Molecules to Materials, Miller, J. S., Drillon M., Eds.; *Wiley-VCH: Weinheim*, 2001-2003, Vols. I-IV.
11. Fujita, W.; Awaga, K. *Science* **1999**, *286*, 261. Itkis, M. E. ; Chi, X. ; Cordes, A. W.; Haddon, R. C. *Science* **2002**, *296*, 1443.
12. Kaucher, M. S.; Lam, Y.-F.; Pieraccini, S.; Gottarelli, G.; Davis, J. T. *Chem. Eur. J.* **2005**, *11*, 164.
13. Setnička, V.; Urbanová, M; Volka, K.; Nampally, S.; Lehn, J.-M *Chem. Eur. J.* **2006**, *12*, 8735. Gottarelli, G.; Lena, S.; Masiero, S.; Pieraccini, S.; Spada, G. P. *Chirality* **2008**, *20*, 471.
14. Pardon, V. N.; Kokorin, A. I.; Zhidomirov, G. M.; Zamaraev, K. I. *Molec. Phys.* **1975**, *30*, 695.
15. An estimate of interspin distance can be obtain by measuring the relative intensity of the $|\Delta m_s| = 1$ and $|\Delta m_s| = 2$ (Eaton, S. S.; More, K. M.; Sawant, B. M.; Eaton, G. R. *J. Am. Chem. Soc.* **1983**, *105*, 6560; Rohde, O.; Pong Van, S.; Kester, W. R.; Hayes Griffith, O. *J. Am. Chem. Soc.* **1974**, *96*, 5311). Unfortunately, we were not able to detect any signal for the half-field transition up to 77 K .
16. Marlow, A. L.; Mezzina, E.; Spada, G. P.; Masiero, S.; Davis, J. T.; Gottarelli, G. *J. Org. Chem.* **1999**, *64*, 5116.
17. The possibility for guanosine derivatives to extract more potassium or sodium than required by the templation in the inner cavity as well as the effect of water washing have been already described.
18. Forman, S. L.; Fettinger, J. C.; Pieraccini, S.; Gottarelli, G.; Davis, J. T. *J. Am. Chem. Soc.* **2000**, *122*, 4060.
19. Pieraccini, S.; Masiero, S.; Pandoli, O.; Samorì, P.; Spada, G. P. *Org. Lett.* **2006**, *8*, 3125.
20. (a) Gray, D. M.; Wen, J.-D.; Gray, C. W.; Repges, R.; Repges, C.; Raabe, G.; Fleishhauer, J. *Chirality* **2008**, *20*, 431–440. (b) Gottarelli, G.; Masiero, S.; Spada, G. P. *Enantiomer* **1998**, *3*, 429–438. (c) Gottarelli, G.; Lena, S.; Masiero, S.; Pieraccini, S.; Spada, G. P. *Chirality* **2008**, *20*, 471–485.
21. a) P. Neviani, E. Mileo, S. Masiero, S. Pieraccini, M. Lucarini, G. P. Spada *Org. Lett* **2009**, *11*(14), 3004. b) C. Graziano, S. Masiero, S. Pieraccini, M. Lucarini, G. P. Spada *Org. Lett* **2008**, *10*, 1739.

CHAPTER 5

RESORCINARENE MOLECULAR CAPSULES

5.1 Introduction

The easy synthesis of resorcin[4]arenes (**1**, Figure 1) developed by Högberg more than 25 years ago fostered their widespread use in studies of self-assembly and supramolecular chemistry^{1,2}. They provided the modules from which open-ended container molecules, the cavitands, were elaborated and led to the first covalent structures that completely surrounded other molecules, the carcerands³. These shallow, bowl-shaped structures have intrinsic properties as receptors for molecular recognition as introduced by Aoyama and coworkers^{4,5}. They described complexes of **1** in organic solvents with a number of guests, small diacids, alcohols, and even steroids, featuring a 1:1 stoichiometry. Intermolecular hydrogen bonding was proposed to hold the guest in the concavity of the resorcinarene host. The NMR spectra confirmed that the signals of the guest were upfield-shifted, as expected for their positions above the four aromatic units of the resorcinarene.

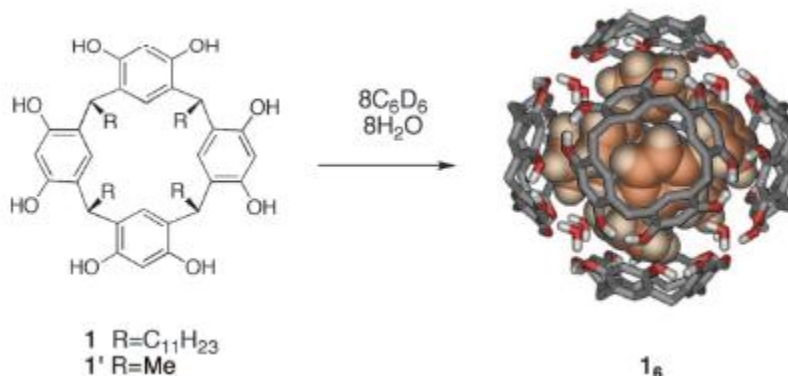


Figure 5.1: Resorcin[4]arenes assemble to give hexameric capsules. Peripheral alkyl groups (R =C₁₁H₂₃) have been removed for viewing clarity.

However, the same spectra showed an unexpected feature: guest exchange took place slowly on the NMR time scale, with separate signals for free and bound guests. The broad range of molecules recognized and the slow on-off dynamics appeared at odds with the simple structures proposed for the complexes, and raised some questions as to the extent of the intermolecular forces involved. The Rebek group examined the glutaric acid, -methyl D-glucopyranoside, and related complexes of **1** in solution through modern NMR techniques and report on them here.

They find that the unprecedented behavior can be reconciled through encapsulation complexes involving the self-assembly of six resorcinarenes in a capsular host. A blueprint to the solution structure came from the crystallographic studies of Atwood and MacGillivray⁶. They found that, unlike the many previous solid-state structures of resorcinarenes and guests that involve layered arrays of the molecules^{7, 10}, resorcin[4]arene **1**₆ crystallized from hot nitrobenzene as a rather large closed shell, a hexameric capsule surrounding a space of nearly 1,400 Å³⁶. The six resorcin[4]arene molecules appear at the sides of a notional cube, and one molecule of water is at each of the eight corners (Fig. 1). An unknown number of highly disordered solvent molecules are inside the cavity. Since that structure appeared, evidence has grown that the resorcinarene self-assembles as a capsule in solution as well¹¹⁻¹⁵. In scrupulously dry solvents such as benzene and chloroform, the molecules are rather insoluble or show slight solubility and broadened, featureless NMR spectra characteristic of multiple aggregated states. However, when small amounts of water are added, well defined host structures emerge; they show resolved signals in the NMR spectra that can be characterized by the methods described below.

5.2 Hexamer assembly in organic solvents

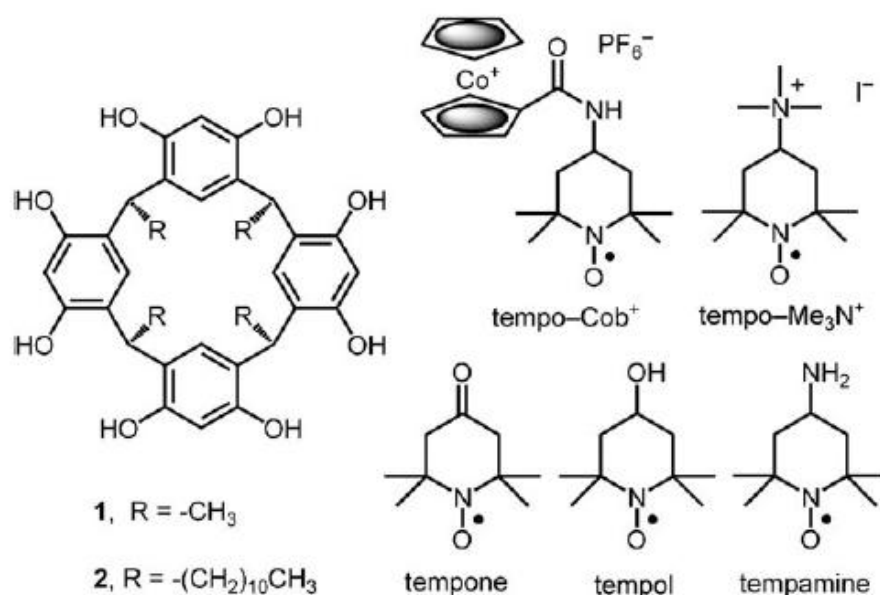
Resorcinarene **1** in wet, nondeuterated solvents encapsulates six and eight molecules of chloroform and benzene, respectively, as shown by ¹H NMR¹²⁻¹⁵. The encapsulated solvent molecules show upfield shifted resonances in their NMR spectra, separated from those of the solvents in bulk solution, indicating slow in–out exchange on the NMR time scale (up to 600 MHz). The diffusion NMR spectra in wet organic solvents show diffusion coefficients of **1** that are consistent with a hexameric assembly^{12,13}. The solvents can be the only occupants of the capsule **1**₆, or they can share it with additional guests¹⁶⁻¹⁹, when the interaction between coguests is favorable. The recent solid-state studies by Atwood and colleagues²⁰ indicate that strong host–guest interactions relative to the interactions between coencapsulated guests are also possible.

The requirement of structural water molecules and the potential for these waters to occupy part of the cavity complicates studies with other solvents. Typical solvents that compete for hydrogen bonds (e.g., methanol or DMSO) disrupt the assemblies and reduce them to their

constituent monomers^{12,14}. Many other polar solvents also interfere with capsule formation. For example, no assembly is observed in the presence of diglyme (2-methoxyethylether) or other oligo(ethylene oxide)s²¹.

5.3 Probing the inner space of resorcinarene molecular capsules with nitroxide guests

We are particularly interested in the application of EPR techniques to investigate the formation and properties of large molecular capsules that result from the self-assembly of resorcinarenes^{7,22} in nonpolar media, such as chloroform and dichloromethane solutions. Several groups have investigated this interesting selfassembly process in the solution phase by using NMR spectroscopy^{21,23}, mass spectrometry²⁴, fluorescence²⁵, fluorescence resonance energy transfer²⁶, and electrochemical techniques²⁷. Herein, we report a work on the self-assembly of resorcinarene molecular capsules in solution by using nitroxide spin probes (2,2,6,6-tetramethylpiperidine-1-oxyl (tempo) or derivatives) as potential guests for encapsulation by resorcinarene **2** (Scheme 1) in water-saturated dichloromethane solutions. The obtained experimental results add to our limited knowledge of the internal environment in these large capsular assemblies, and the interactions between the included guests and the internal walls of the capsule.



Scheme 5.1: Structure of resorcinarene and nitroxides guests used in this work.

The EPR spectra were recorded in water-saturated CH_2Cl_2 solutions in order to provide the water molecules that are necessary to complete the hydrogen-bond network required for capsule formation. The spectrum of 0.10 mM tempamine (4-amino-2,2,6,6-tetramethylpiperidine-1-oxyl) in this medium consists of three sharp peaks, which are characteristic of free nitroxide probe molecules that undergo fast motion (Figure 2a). The ^{14}N hyperfine splitting and the g factor are given in Table 1. The addition of increasing amounts of resorcinarene **2** to the tempamine/ CH_2Cl_2 solution leads to significant changes in the EPR spectra. In the region that corresponds to the high-field line, two different, superimposed signals are clearly visible: a sharp signal, which is characteristic of a free nitroxide probe that undergoes fast motion, and a much broader line (Figure 2b).

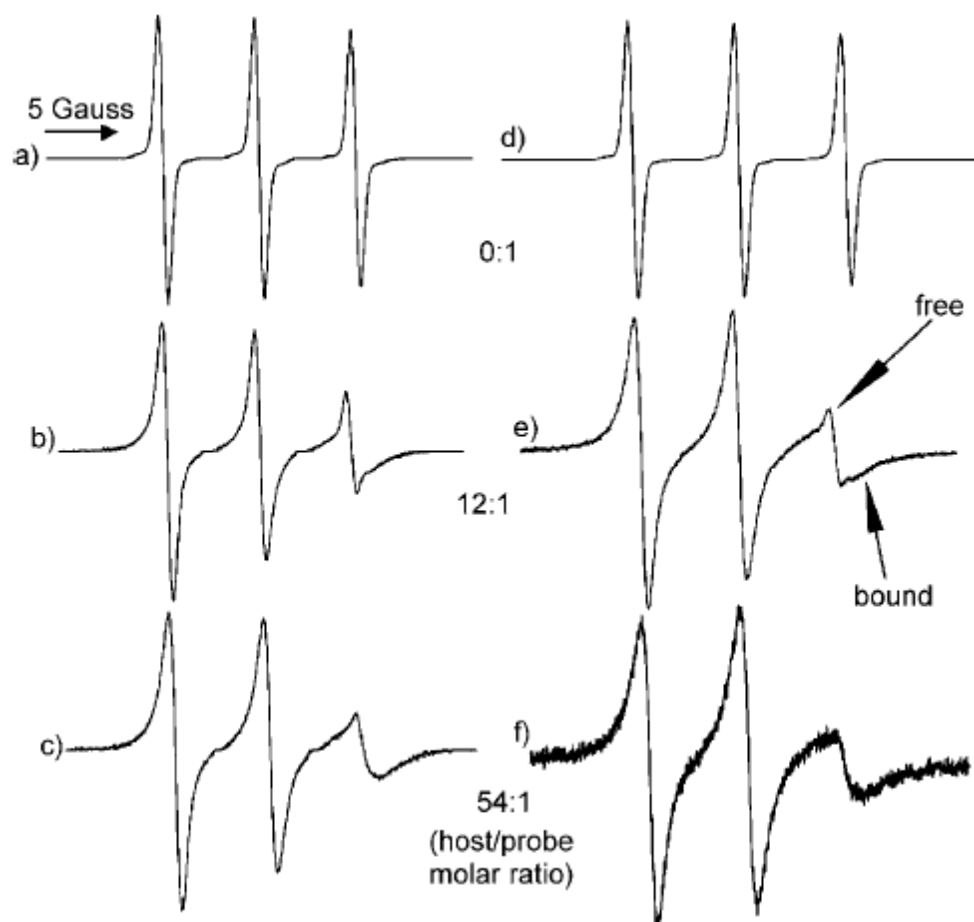


Figure 5.2: Experimental EPR spectra in water-saturated CH_2Cl_2 at 293 K. a) 0.10 mM tempamine, b) 0.10 mM tempamine + 1.20 mM **2**, c) 0.05 mM tempamine + 2.70 mM **2**, d) 0.10 mM tempo- Me_3N^+ , e) 0.10 mM tempo- Me_3N^+ + 1.20 mM **2**, f) 0.05 mM tempo- Me_3N^+ + 2.70

The formation of a complex with tempamine as the included guest is supported by the observation that an increase in the resorcinarene concentration led to gradually higher intensities for the broader signal, while the intensity of the sharp signal that arises from the free-spin probe decreased. When the concentration of resorcinarene was increased to 2.7 mM and the [resorcinarene]/[spin probe] ratio was 54:1, the spectrum of the complexed radical became dominant (Figure 2c), and the spectroscopic parameters for the included nitroxide guest could be measured. The addition of excess resorcinarene led to an EPR spectrum in which the increased linewidth of all the lines (and especially the high-field line) reflects the reduction of the probe's tumbling rate. The observed increase of the tempamine rotational correlation time²⁸ τ_r from 1.2×10^{-11} s (in the absence of **2**) to 1.3×10^{-9} s (in the presence of excess **2**, see Table 1) is consistent with the encapsulation of the spin probe. The a_N value measured for encapsulated tempamine is slightly larger than that of the free nitroxide probe (Table 1), thus indicating a small increase in the polarity of the microenvironment around the spin probe upon encapsulation.

Guest	Tempamine	Tempo–Me ₃ N ⁺	Tempo–Cob ⁺
$a_{N \text{ free}}$ [G]	15.83	15.51	15.82
$a_{N \text{ bound}}$ [G]	16.16	15.73	16.1 ± 0.5
g_{free}	2.0060	2.0062	2.0060
g_{bound}	2.0058	2.0058	2.0058
$\tau_{r \text{ free}}$ [s] ^[b]	1.2×10^{-11}	4.2×10^{-11}	3.4×10^{-11}
$\tau_{r \text{ bound}}$ [s] ^[b]	1.3×10^{-9}	2.0×10^{-9}	$(4 \pm 1) \times 10^{-9}$

Table 1: Hyperfine splitting constants a_N , g factors, and rotational correlation times τ_r obtained from the EPR spectra of various nitroxide spin probes in water-saturated CH₂Cl₂ solution, before (free) and after encapsulation (bound) inside **26**. [a] Unless otherwise specified, the error margins were ± 0.01 for the a_N values, ± 0.0001 for the g factors, and $\pm 10\%$ for the τ_r values. [b] Calculated using the equation in Ref. 28

A similar conclusion can be derived from the small decrease observed in the g factor. These results are consistent with the expected behavior, as the large internal volume (ca. 1.375 \AA^3) of the hexameric resorcinarene capsule (**26**) guarantees that a large number of solvent molecules can be included together with the nitroxide guest, but the resorcinarene OH groups and water

molecules involved in the hydrogen bonds that keep the capsule together exert a measurable effect on the polarity of the inner space of the hexameric capsule.

In light of the reported selectivity of **2**₆ capsules for cationic species²³, we decided to use cationic nitroxide derivatives as guests. Initially, we selected tempo–Me₃N⁺ (4-trimethylammonium-2,2,6,6-tetramethylpiperidine-1-oxyl) and examined its interactions with resorcinarene **2** in watersaturated CH₂Cl₂ solution. In analogy with the results obtained with tempamine, the evolution of the EPR spectral patterns (Figure 2d–f), as well as the a_N and the g factor values (Table 1) obtained as the concentration of host **2** increased show that tempo–Me₃N⁺ is sequestered inside a molecular capsule formed by the resorcinarene. Interestingly, we found that the τ_r value for tempo–Me₃N⁺ included in the capsule is 2.0×10^{-9} s, that is, its tumbling rate is slightly slower than that of encapsulated tempamine. However, the free cationic nitroxide derivative in solution also exhibits a slower tumbling rate than that of neutral tempamine. Therefore, the possible presence of cation– π interactions between the positively charged trimethylammonium residue in tempo–Me₃N⁺ and the aromatic inner walls of the capsule is not unequivocally substantiated by these data. Although a considerable excess of host **2** is necessary to fully encapsulate tempamine and tempo–Me₃N⁺, it is clear from Figure 1 that the encapsulation of the latter probe is easier to achieve. This result is consistent with the known selectivity of hexameric capsules of host **2** for cationic compounds. Pulse gradient stimulated echo (PGSE) NMR measurements²⁹ of the diffusion coefficient (D_o) of resorcinarene **2** (3 mM) in water-saturated CD₂Cl₂ yield a value of $(3.05 \pm 0.11) \times 10^{-6} \text{ cm}^2 \text{ s}^{-1}$. In the presence of 0.5 mM tempamine, the D_o value was determined as $(3.07 \pm 0.05) \times 10^{-6} \text{ cm}^2 \text{ s}^{-1}$. This value is in excellent agreement with our previously reported D_o values for these **2**₆ molecular capsules in the same medium²⁷, thus indicating that the presence of nitroxide probes does not disrupt the self-assembly of the resorcinarene host. While the NMR measurements require concentrations above 1 mM, EPR measurements are best performed at nitroxide probe concentrations around 0.1 mM (to minimize spin-exchange broadening effects). The lower overall resorcinarene concentrations in the EPR experiments may explain why the addition of a substantial host excess is required to complete the encapsulation of the nitroxide probe. At the beginning of the titration of tempamine (or tempo–Me₃N⁺) with host **2**, its concentration is so

low that capsule formation might not be quantitative. In addition to this possibility, lower absolute concentrations of probes and molecular capsules are expected to shift the complexation equilibrium away from encapsulation (see Figure 3) for any given value of the corresponding equilibrium association constant.

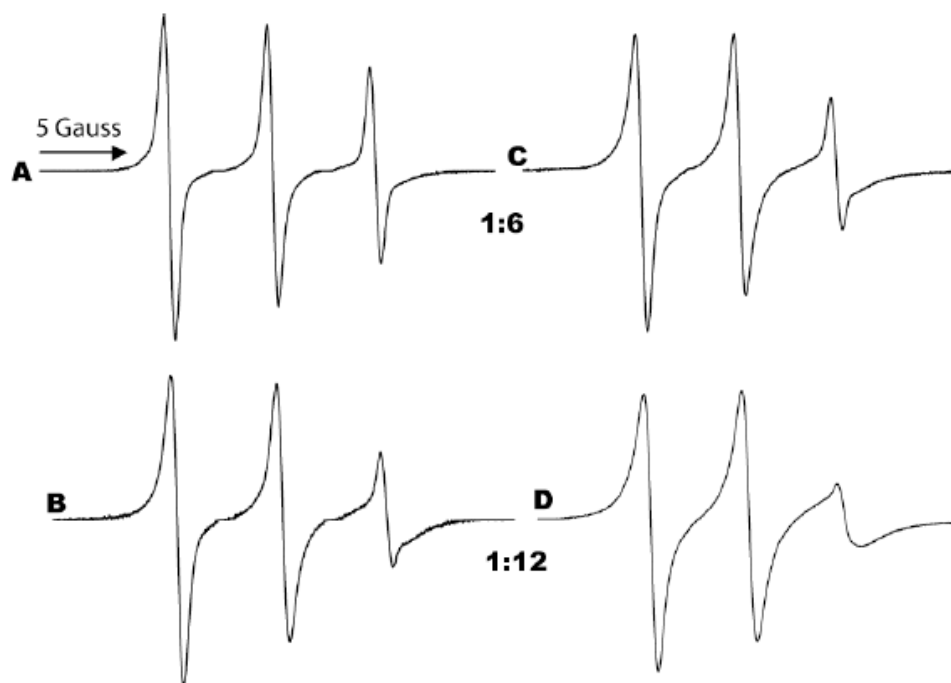


Figure 5.3: Effect of the absolute concentrations of nitroxide probe and host on the relative degree of encapsulation as reflected in the experimental EPR spectra in water-saturated CH_2Cl_2 at 293 K. (A) 0.10 tempamine + 0.60 mM **2**, (B) 0.10 mM tempamine + 1.20 mM **2**, (C) 0.45 mM tempamine + 2.70 mM **2**, and (D) 0.45 mM tempamine + 5.40 mM **2**. Spectra A and C were recorded with 1:6 [tempamine]/[**2**] ratios, while spectra B and D were recorded with 1:12 [tempamine]/[**2**] ratios. Spectra C and D were recorded with higher absolute concentrations and show larger relative fractions of encapsulated probe than their A and B counterparts.

Nonetheless, at the end of the nitroxide probe titrations with resorcinarene, the probe is undoubtedly encapsulated inside a large capsular assembly, as the measured rotational correlation times indicate a considerable deceleration of the probe's tumbling rate (ca. 100-fold for tempamine and 50-fold for $\text{tempo-Me}_3\text{N}^+$, Table 1). These substantial changes in τ_r values can only be explained by the incorporation of the nitroxide probe inside a large supramolecular assembly, such as **2**₆.

Previous voltammetric experiments have shown that the encapsulation of the organometallic cation cobaltocenium is highly favored by **2**₆ capsules. In fact, cobaltocenium is selectively complexed by the capsules, even in the presence of a large excess of tetrabutylammonium

ions²⁷. We exposed **2**₆ capsules filled with either tempo–Me₃N⁺ or tempamine to cobaltocenium, and observed the release of the nitroxide probe from the molecular capsules. The EPR experiments therefore show that the **2**₆ capsules show selectivity for cobaltocenium in competition with either tempamine or tempo–Me₃N⁺. As a result, we decided to prepare a novel cobaltocenium derivative tempo–Cob⁺, which combines the organometallic cationic residue with a nitroxide probe in the same molecule (see the Experimental Section for synthetic details). The EPR spectrum of 0.10 mM tempo–Cob⁺ in watersaturated CH₂Cl₂ shows the expected three sharp lines that correspond to the fast tumbling nitroxide residue (Figure 4a).

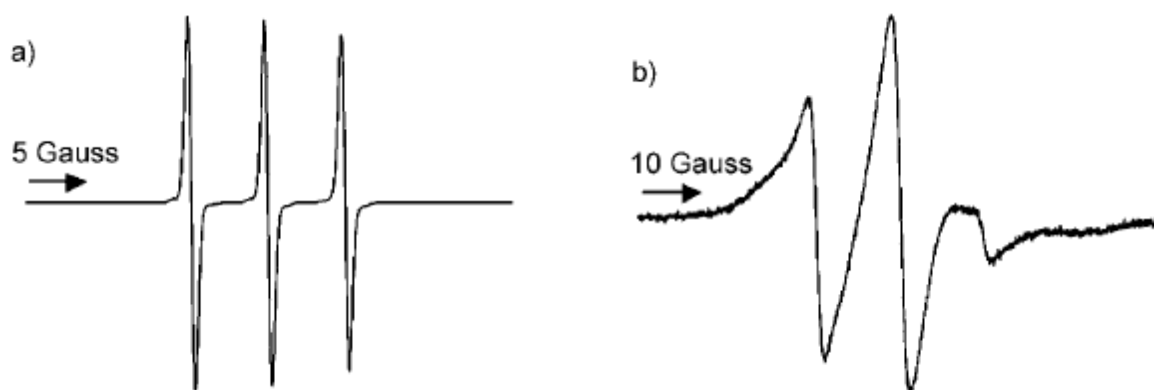


Figure 5.4: Experimental EPR spectra in water-saturated CH₂Cl₂ at 293 K. a) 0.10 mM tempo–Cob⁺, b) 0.10 mM tempo–Cob⁺ + 4.0 mM **2**.

However, the addition of excess resorcinarene host led to a considerably broadened spectrum that clearly suggests the incorporation of the tempo–Cob⁺ guest into the **2**₆ capsular assembly (Figure 2b). This spectrum is severely broadened and its shape indicates that the probe's tumbling motion falls in an intermediate region between the fast and slow motional regimes. We also investigated tempone (4-oxo-2,2,6,6-tetramethylpiperidine-1-oxyl) and tempol (4-hydroxy-2,2,6,6-tetramethylpiperidine-1-oxyl) as spin probe guests. The EPR spectrum of tempone was essentially unaffected by the presence of resorcinarene, and shows only the typical signals that arise from the free nitroxide probe in solution ($a_N=14.76$ Gauss, $g=2.0059$, and $\tau_r=1.3 \times 10^{-11}$ s). This finding suggests that this nitroxide probe is not included at all into the supramolecular assembly. Experiments with tempol showed that, although this probe is partially encapsulated inside the **2**₆ assembly, its complexation is much less favorable than that of tempamine.

The EPR spectroscopic data collected in this work clearly support the hypothesis that encapsulation of guests with $\mathbf{2}_6$ is affected by the electrostatic nature of the guests involved.

Electrostatic surface potential plots of the nitroxide probes surveyed here (see Figure 5) reveal that their encapsulation is enhanced by surfaces with positive charge density, such as those of tempamine, tempo-Me₃N⁺, and tempo-Cob⁺. In contrast, a probe such as tempone, whose surface is predominantly laced with negative charge density, fails to undergo encapsulation. This failure is probably due to the electrostatic complementarity between positively charged guests and the mostly aromatic, inner walls of the resorcinarene capsules.

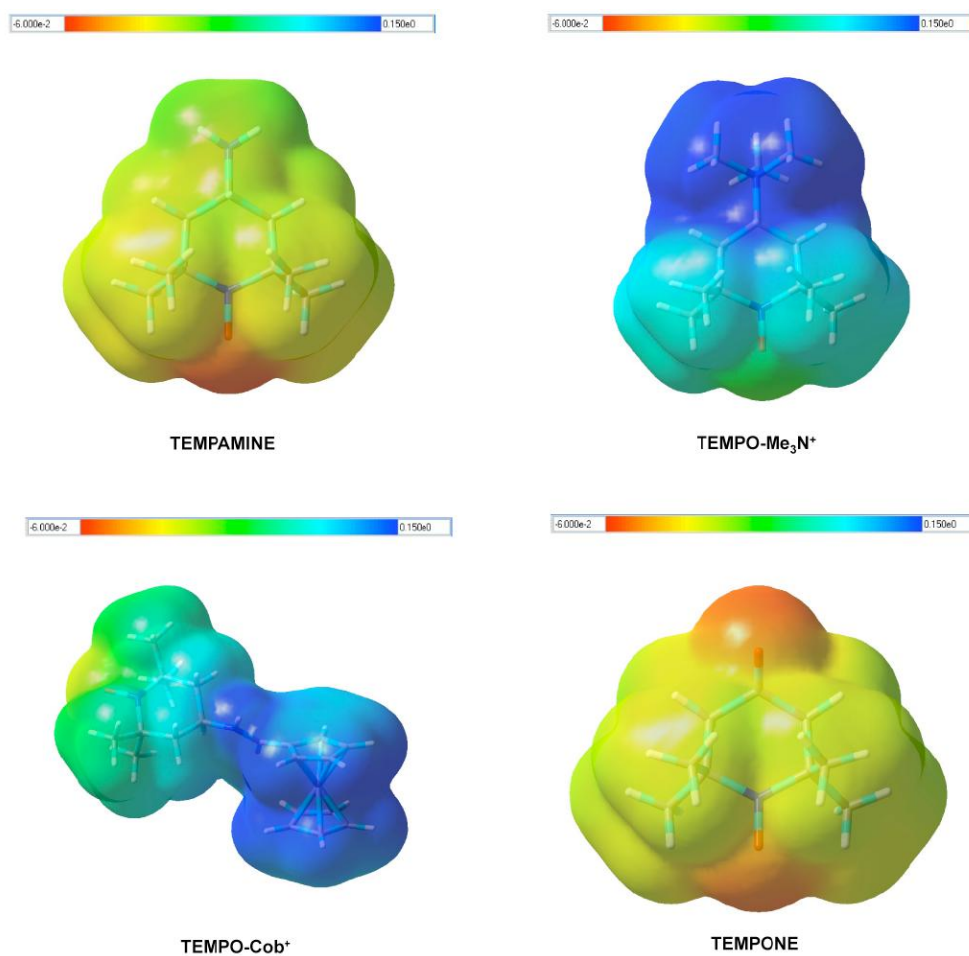


Figure 5.5: Calculated (B3LYP/3-21G*) electrostatic surface potentials for tempamine, tempo-Me₃N⁺, tempo-Cob⁺ and tempone.

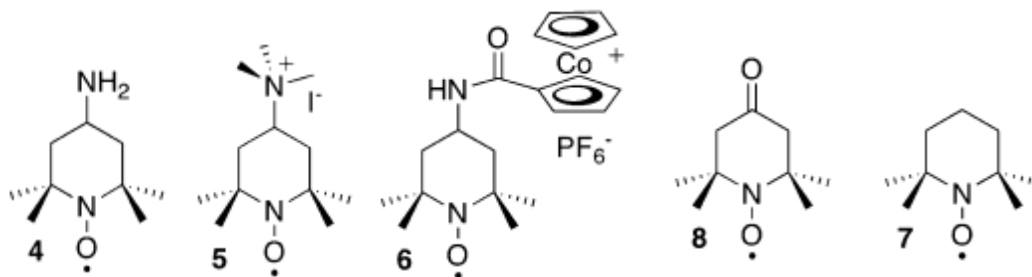
It is instructive to calculate the approximate molecular volumes from the rotational correlation times for the encapsulated nitroxide probes, in order to assess to what extent the motion of the trapped probes may reflect the overall motion of the entire assembly. By using

standard equations for this purpose^{30,31}, we estimated molecular volumes of 4700, 19000, and 39000 Å³ for encapsulated tempamine, tempo–Me₃N⁺, and tempo–Cob⁺, respectively.

Since the overall volume of the hexameric molecular capsule is expected to remain constant³² regardless of the sequestered guest, these values reflect the relative levels of probe motion inside the capsule. In other words, while tempamine appears to have a fair degree of motion that is uncoupled to the overall motion of the supramolecular assembly, the motion of tempo–Cob⁺ seems to reflect the motion of the assembly much more closely, with tempo–Me₃N⁺ as an intermediate case. It can be argued that this effect may result from cation–π interactions between the guest and the inner walls of the capsule. However, as the molecular volume of the guest increases, its motional freedom inside the capsule will be reduced because of steric hindrance.

5.4 NMR investigation on the interactions of nitroxide probes with resorcinarene molecular capsules

As we have previously reported,⁵ our EPR experiments clearly reveal that the nitroxide probes shown in Scheme X.1 can be classified into two distinct groups in terms of their interactions with resorcinarene **2**.



Scheme 5.2: Structure of nitroxides used in the work

The first group is composed of nitroxides **4-6**, which are incorporated inside hexameric capsules of **2**, as evidenced by the broadening of the highfield peak in the EPR spectrum of the corresponding nitroxide when excess **2** is added to the solution. This reflects the decreasing tumbling rate of the nitroxide probe upon encapsulation inside the hexameric assembly. In

striking contrast, the EPR spectrum of the two remaining nitroxides (compounds **7** and **8**) are little affected by the presence of excess resorcinarene **2**.

During the course of this investigation, we ran parallel NMR spectroscopic experiments with the goal of gathering further information on the location of the nitroxide spin probes inside the molecular capsules of **2**. A set of typical results is shown in Figure 5.6, which depicts the ^1H NMR spectra recorded for resorcinarene **2** in water-saturated CD_2Cl_2 solution as a function of the added concentration of nitroxide **5**.

Clearly, the presence of this nitroxide broadens many of the resonances of the resorcinarene protons. Specifically, the peaks corresponding to the resorcinarene core, that is the hydroxide protons, the aromatic protons (b and c, see Figure 5.6 for proton labels), the bridge protons (a) and the directly attached methylene protons (1) on the pendant aliphatic chains are all substantially broadened by the spin probe. Notice, however, that the rest of the protons on the pendant undecyl chains (resonating at $\delta < 1.7$ ppm) do not undergo any significant broadening. These findings are consistent with the EPR data and unequivocally reveal that the cationic spin probe is encapsulated within the central cavity of the hexameric assembly of **2**, thus affecting and broadening the core protons and leaving the outside protons on the host side chains unaffected.

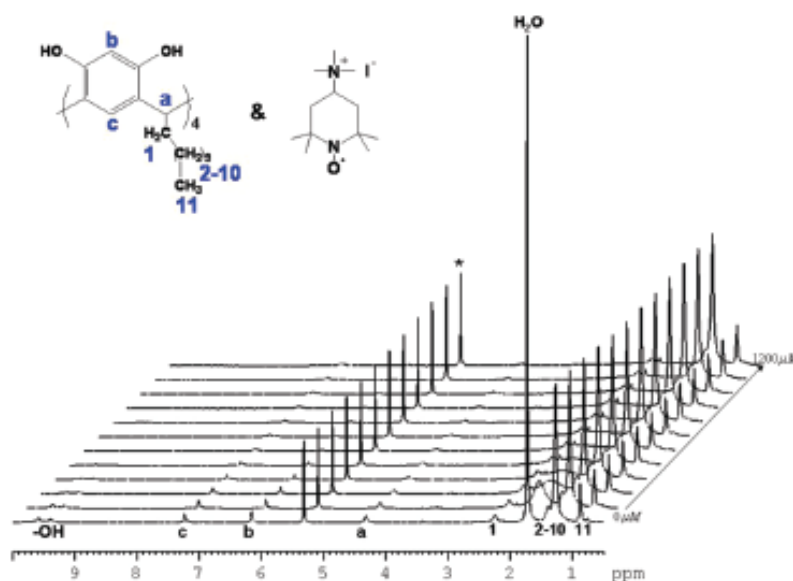


Figure 5.6: ^1H NMR spectra (400 MHz, water-saturated CD_2Cl_2) of resorcinarene **2** as a function of the added concentration of spin probe **5**.

All EPR and NMR experiments were conducted in water saturated CH_2Cl_2 (or CD_2Cl_2) as it is well established that water molecules are necessary to complete the network of hydrogen bonds that glue together the six molecules of host **2** into a capsular assembly. The peak for the water protons, clearly visible at 1.7 ppm in Figure 5.6, also undergoes extensive and effective broadening upon addition of the spin probe. Since there is a large excess of water molecules in the solution, this finding indicates that they exchange quickly between the bulk solution and the hydrogen bound positions on the capsule's surface, leading to the observed broadening of the water peak.

Similar NMR spectroscopic experiments with nitroxides **4** and **6** yield basically the same results; that is, the nitroxide causes substantial broadening of the peaks corresponding to the core protons on the host and the water protons, while the outer aliphatic protons on the host side chains remain unaffected. As in the case of nitroxide **5**, this is consistent with the EPR spectroscopic data and the proposed encapsulation of nitroxides **4-6** by the hexameric resorcinarene capsules. Using nitroxide **8** (oxotempo) led to the NMR spectroscopic data shown in Figure 4. The presence of oxotempo has a much smaller effect on the proton resonances of the resorcinarene core as compared to what we observed with nitroxides **4-6**.

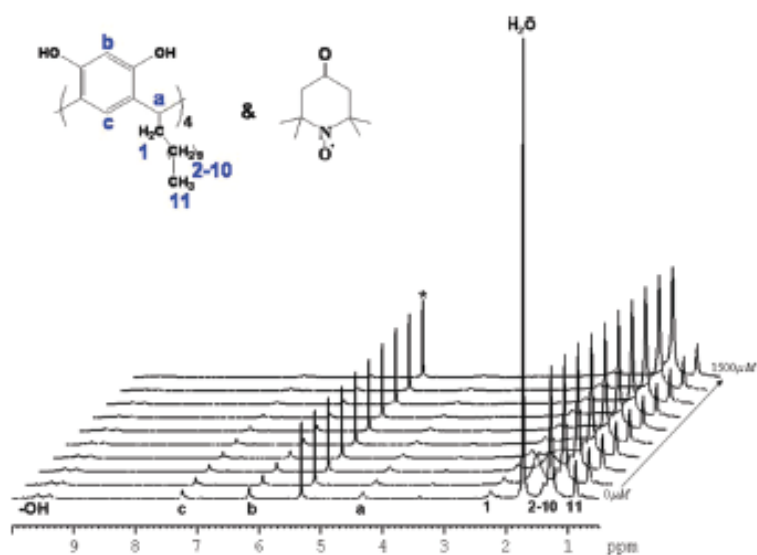


Figure 5.7: ^1H NMR spectra (400 MHz, water-saturated CD_2Cl_2) of resorcinarene **2** as a function of the added concentration of spin probe **8**.

As always, the aliphatic protons on the side chains are not broadened at all. These findings are consistent with the EPR spectroscopic evidence that provides unequivocal support against encapsulation of **8**. However, the peak corresponding to the water protons undergoes substantial and effective broadening in the presence of **8**. In order to shine some light on this unexpected finding, we also run similar experiments with unfunctionalized tempo (compound **7**). In this case, the NMR spectroscopic data show minimal broadening of the signals for the core protons of the resorcinarene and no broadening for the signals of the aliphatic chain protons, while the water peak experiences some broadening, but its magnitude is considerably less pronounced than in the case of **8**.

Obviously intrigued by the pronounced and rather unexpected broadening of the water proton resonance caused by oxotempo, we ran several control experiments. For instance, in the absence of resorcinarene **2**, similar concentrations of oxotempo cause very little broadening of the water peak in water-saturated CD₂Cl₂. This finding clearly demonstrates that preferential solvation of **8** by H₂O over CD₂Cl₂ is not a factor in the observed results. We also took advantage of the well-known fact that pyrogallolarene (host **3**) does not require any water molecules to form the corresponding hexameric capsular assembly (**36**); that is, in water-saturated CD₂Cl₂ solutions of host **3**, there are no water molecules hydrogen bound to the capsule. Interestingly, in the presence of host **3**, nitroxide **8** also fails at broadening the water peak in water-saturated CD₂Cl₂ solution (Figure S12, Supporting Information). From the results of these control experiments (see also Figure S14, Supporting Information), we conclude that the broadening of the water resonance by oxotempo requires the presence of water molecules interacting with the hexameric capsule of **2** via hydrogen bonding.

The fact that oxotempo (**8**) is considerably more effective than tempo (**7**) at broadening the NMR resonance of the water molecules in the presence of capsules of **2** led us to hypothesize that the carbonyl oxygen in the former compound may be important. We reasoned that if the carbonyl oxygens engage in hydrogen bonding interactions with the water molecules, large concentrations of molecules with structure similar to **8** may disrupt the molecular interactions and thus decrease or eliminate the observed effect on the NMR water peak. Therefore, we used 1,4-cyclohexanedione (CHD) for this purpose. Figure 5 shows some interesting NMR data in

this regard. Addition of 100 mM CHD to a solution containing 3.0 mM host **2** and 0.08 mM nitroxide **5** has very little effect on the NMR spectra (Figures 5A and 5B), beyond the expected appearance of a large resonance for the protons of CHD at 2.7 ppm. Our previous EPR and NMR experiments demonstrate that, in this case, the nitroxide is encapsulated in the central cavity of the hexameric assembly. Therefore, the presence of CHD does not affect capsule formation or the encapsulation of **5**. The degree of broadening of the water resonance remains unchanged, because the broadening is largely due to the proximity between the capsule-attached, hydrogen bound water molecules (in fast exchange with bulk water molecules) and the capsule-trapped spin probe.

A very different picture develops when oxotempo is used as the spin probe. As shown in Parts C and D of Figure 5, addition of 100 mM CHD to a solution containing 3 mM resorcinarene **2** and 0.1 mM **8** leads to a considerable narrowing of the water peak. This finding indicates that CHD interferes with the interaction between oxotempo and the water molecules. Since this interaction must take place outside the hexameric capsule, as our experimental evidence indicates that oxotempo is not encapsulated, it is reasonable to conclude that CHD competes with oxotempo for hydrogen bonding sites on the water molecules, leading to a sharper water peak.

While the correlation between EPR and NMR spectroscopic data is generally very good, a puzzling aspect of these results is the need to reconcile our observation (NMR spectroscopic data) on the hydrogen bonding of **8** to water molecules, which takes place to a measurable extent only in the presence of capsules of **2**, with our observation on the relatively small effect of the same capsules on the tumbling rate of this nitroxide probe in solution (EPR spectroscopic data). The necessary presence of the capsules clearly suggests

that only water molecules hydrogen-bound to the assemblies (or in their immediate vicinity) may interact effectively with nitroxide **8** and these interactions slow down in a detectable way the tumbling of the nitroxide in solution. The tumbling rate of **8** does not decrease nearly as much as the tumbling rates of nitroxides **4-6**, as the latter are fully encapsulated.

We can only rationalize these results by assuming that oxotempo only hydrogen binds to water molecules which are partially dislodged from the capsular assembly, that is, not reaching

their full capacity for hydrogen bonding to the assembly. In this way, the hydrogen bond between water and oxotempo would be extremely labile and would keep the nitroxide free from attachment to the large capsular assembly, preserving a relatively fast tumbling rate. Alternatively, the water molecules may accumulate in the vicinity of the hexameric capsular assembly, where their enhanced local concentration may lead to more effective hydrogen bonding with nitroxide **8**.

In conclusion, we have shown here that nitroxide spin probes can be used as guests for hexameric resorcinarene molecular capsules. EPR spectroscopic data show that the spin probe is more easily encapsulated as positive charge density accumulates on its surface. The motional regime of the spin probe upon encapsulation is partially decoupled from the slower motions of the supramolecular capsule for relatively small probes such as tempamine. However, as the molecular volume of the probe increases and fills a larger fraction of the capsule's cavity, the tumbling rate of the probe more closely reflects the overall tumbling rate of the entire supramolecular assembly. Moreover, this work shows that the combination of EPR and NMR spectroscopies constitutes a powerful tool for the investigation of the complex resorcinarene self-assembling system in solvents of low polarity.

5.5 Experimental Section

Commercially available nitroxide probes were used without further purification. Resorcinarene **2** was synthesized by following a reported procedure⁷. Carboxycobaltocenium hexafluorophosphate (CobCOOH(PF₆)) was prepared as reported by Sheats and Rausch³³. Pure compound was obtained by repeated washing with hot acetone and recrystallization from a mixture of acetone/hexane. 1-Chlorocarbonylcobaltocenium hexafluorophosphate (CobCOCl(PF₆)) was prepared by dissolving carboxycobaltocenium (50 mg, 0.13 mmol) in anhydrous CH₃CN (10 mL). Sulfonyl chloride (40 mL) was then added and the resulting solution was heated at reflux for 24 h. After completion of the reaction, the solvents were removed under vacuum. Approximately 50 mg of CobCOCl(PF₆) was obtained as a yellow solid and used in the next step without further purification.

Tempo–Cob(PF₆): A solution containing tempamine (22.5 mg, 0.13 mmol) and triethylamine (15.9 mg, 0.16 mmol) in anhydrous CH₃CN (2 mL) was added dropwise to a solution of CobCOCl(PF₆)

(ca. 50 mg) in CH₃CN (8 mL) under N₂. The reaction mixture was stirred for 2 days at room temperature and then concentrated and cooled to -25 °C in order to precipitate the triethylammonium salt that occurred as a by-product. After filtration, the solvent was removed under vacuum, and the resulting residue was subjected to column chromatography on Sephadex LH-20, using CH₃CN as eluent. The appropriate fraction was collected and dried under vacuum to

afford a mixture of tempo–Cob⁺ salts (Cl⁻/PF₆⁻) as a highly viscous yellow liquid. This liquid was then dissolved in a small amount of water and a solution of saturated NH₄PF₆ was added dropwise.

Tempo–Cob(PF₆) (ca. 25 mg) precipitated as an orange solid. The solid was further purified by recrystallization from hot water/methanol, and the final product was obtained as red, needle-shaped

crystals (13 mg, 18% yield). MS (FAB): m/z 387 [M⁺], 388; elemental analysis calcd (%) for C₂₀H₂₇N₂O₂CoPF₆ : C 45.19, H 5.12, N 5.27; found: C 44.98, H 5.12, N 5.32.

EPR spectra were recorded on a Bruker EMX 200D spectrometer. The instrument settings were as follows: microwave power 0.63 mW, modulation amplitude 0.9 G, modulation frequency 100 kHz, scan time 180 s. Determination of g factors was done by using polycrystalline DPPH (g=2.0036) as the reference.

5.6 References:

1. Högberg, A. G. S. *J. Org. Chem.* **1980**, *45*, 4498–4500.
2. Timmerman, P., Verboom, W. & Reinhoudt, D. N. *Tetrahedron* **1996**, *52*, 2663–2704.
3. Sherman, J. C., Knobler, C. B. & Cram, D. J. *J. Am. Chem. Soc.* **1991**, *113*, 2194–2204.
4. Aoyama, Y., Tanaka, Y., Toi, H. & Ogoshi, H. *J. Am. Chem. Soc.* **1988**, *110*, 634–635.
5. Aoyama, Y., Nonaka, Y., Tanaka, Y., Toi, H. & Ogoshi, H. *J. Chem. Soc. Perkin Trans. 2*, **1989**, 1025–1029.
6. MacGillivray, L. R. & Atwood, J. L. *Nature*, **1997**, *389*, 469–472.

7. Tunstad, L. M., Tucker, J. A., Dalcanale, E., Weiser, J., Bryant, J. A., Sherman, J. C., Helgeson, R. C., Knobler, C. B. & Cram, D. J. *J. Org. Chem.* **1989**, *54*, 1305–1312.
8. MacGillivray, L. R. & Atwood, J. L. *J. Am. Chem. Soc.* **1997**, *119*, 6931–6932.
9. Shivanyuk, A., Friese, J. C., Döring, S. & Rebek, J., Jr. *J. Org. Chem.* **2003**, *68*, 6489–6496.
10. Ma, B.-Q. & Coppens, P. *Chem. Commun.* **2002**, 424–425.
11. Wilson, C. F., Eastman, M. P. & Hartzell, C. J. *J. Phys. Chem. B* **1997**, *101*, 9309–9313.
12. Avram, L. & Cohen, Y. *J. Am. Chem. Soc.* **2002**, *124*, 15148–15149.
13. Avram, L. & Cohen, Y. *Org. Lett.* **2002**, *4*, 4365–4368.
14. Avram, L. & Cohen, Y. *J. Am. Chem. Soc.* **2004**, *126*, 11556–11563.
15. Shivanyuk, A. & Rebek, J., Jr. *J. Am. Chem. Soc.* **2003**, *125*, 3432–3433.
16. Shivanyuk, A. & Rebek, J., Jr. *Proc. Natl. Acad. Sci. USA* **2001**, *98*, 7662–7665.
17. Philip, I. E. & Kaifer, A. E. *J. Am. Chem. Soc.* **2002**, *124*, 12678–12679.
18. Yamanaka, M., Shivanyuk, A. & Rebek, J., Jr. *J. Am. Chem. Soc.* **2004**, *126*, 2939–2943.
19. Palmer, L. C., Shivanyuk, A., Yamanaka, M. & Rebek, J., Jr. *Chem. Commun.* **2005**, 857–858.
20. Dalgarno, S. J., Tucker, S. A., Bassil, D. B. & Atwood, J. L. *Science*, **2005**, *309*, 2037–2039.
21. Evan-Salem, T., Baruch, I., Avram, L., Cohen, Y., Palmer, L. C., Rebek, J. Jr. *PNAS*, **2006**, *103*(33), 12296–12300.
22. P. Timmerman, W. Verboom, D. N. Reinhoudt, *Tetrahedron* **1996**, *52*, 2663 – 2704.
23. a) A. Shivanyuk, J. Rebek, Jr., *Proc. Natl. Acad. Sci. USA* **2001**, *98*, 7662 – 7665; b) L. Avram, Y. Cohen, *Org. Lett.* **2003**, *5*, 1099 – 1102.
24. N. K. Beyeh, M. Kogej, A. Aahman, K. Rissanen, C. A. Schalley, *Angew. Chem.* **2006**, *118*, 5339 – 5342; *Angew. Chem. Int. Ed.* **2006**, *45*, 5214 – 5218.
25. a) S. J. Dalgarno, S. A. Tucker, D. B. Bassil, J. L. Atwood, *Science* **2005**, *309*, 2037 – 2039; b) S. J. Dalgarno, D. B. Bassil, S. A. Tucker, J. L. Atwood, *Angew. Chem.* **2006**, *118*, 7177 – 7180; *Angew. Chem. Int. Ed.* **2006**, *45*, 7019 – 7022.
26. E. Barrett, T. J. Dale, J. Rebek, Jr., *J. Am. Chem. Soc.* **2008**, *130*, 2344 – 2350.
- 27 I. Philip, A. E. Kaifer, *J. Org. Chem.* **2005**, *70*, 1558 – 1564.
28. The rotational correlation time τ_r (s) was determined using the following equation:

$$\tau_r = 6.5 \times 10^{-10} x \Delta H \left[\sqrt{\frac{h_0}{h_{-1}}} + \sqrt{\frac{h_0}{h_{+1}}} - 2 \right]$$

where ΔH is the peak-to-peak width (in Gauss) of the central line; h_{-1} , h_0 , and h_{+1} are the intensities of the low-, center- and high-field lines, respectively.

29. Y. Cohen, L. Avram, L. Frish, *Angew. Chem.* **2005**, *117*, 524 –560; *Angew. Chem. Int. Ed.* **2005**, *44*, 520 – 554.
30. P. C. Griffiths, C. C. Rowlands, P. Goyffon, A. M. Howe, B. L. Bales, *J. Chem. Soc. Perkin Trans. 2* **1997**, 2473 – 2477.
31. P. P. Borbat, A. J. Costa-Filho, K. A. Earle, J. K. Moscicki, J. H. Freed, *Science* **2001**, *291*, 266 – 269.
32. The volume of the 2_6 supramolecular assembly was calculated by molecular modeling studies to be in the range 42000–51000 Å³.
33. J. E. Sheats, M. D. J. Rausch, *J. Org. Chem.* **1970**, *35*, 3245.